Supplementary information files for Mechanistic insight into Pd-catalyzed asymmetric alkylation of indoles with diazoesters employing bipyridine-N,N'-dioxides as chiral controllers

Advanced Synthesis & Catalysis

Supporting Information

Mechanistic Insight into Palladium-Catalyzed Asymmetric Alkylation of Indoles with Diazoesters Employing Bipyridine-*N*,*N*'-dioxides as Chiral Controllers

Yasuaki Fukazawa, Vladimir Yu. Vaganov, Julia V. Burykina, Artem N. Fakhrutdinov, Ruslan I. Safiullin, Felix Plasser, Aleksandr E. Rubtsov, Valentine P. Ananikov,* and Andrei V. Malkov*

SUPPORTING INFORMATION

Mechanistic Insight into Pd-Catalyzed Asymmetric Alkylation of Indoles with Diazoesters Employing Bipyridine-*N,N'*-dioxides as Chiral Controllers.

Yasuaki Fukazawa, Vladimir Yu. Vaganov, Julia V. Burykina, Artem N. Fakhrutdinov, , Ruslan I. Safiullin, Felix Plasser, Aleksandr E. Rubtsov, Valentine P. Ananikov, and Andrei V. Malkov

1. General Methods

Yields are given for isolated products showing one spot on a TLC plate and no impurities detectable in the NMR spectrum. The identity of the products prepared by different methods was checked by comparison of their NMR spectra.

^{1}H and ^{13}C NMR spectra were recorded at 400 MHz for ^{1}H and 100 MHz for ^{13}C NMR at room temperature; the chemical shifts (δ) were measured in ppm relative to the solvent ($CDCl_3$: ^{1}H: δ = 7.26 ppm, ^{13}C: δ = 77.16 ppm, C_6D_6: ^{1}H δ = 7.16 ppm, ^{13}C: δ = 128.06 ppm). Coupling constants (*J*) are given in Hertz. Splitting patterns of apparent multiplets associated with an averaged coupling constants were designated as s (singlet), d (doublet), t (triplet), q (quartet), sept (septet), m (multiplet), dd (doublet of doublets) and br (broadened). Various 2D techniques and DEPT experiments were used to establish the structures and to assign the signals. The mass spectra were measured on a Thermo Exactive (Orbi), where the spectra were recorded in a positive or negative ion mode using electrospray ionization (ESI) from methanol or acetonitrile. UV-Vis kinetic measurements were recorded on LEKI SS2109UV spectrophotometer with standard 10×10×45 mm quartz cuvettes. Enantiomeric excess (ee) was determined by GC or HPLC on columns with chiral sorbents. All chromatographic manipulations used silica gel (40-63 μm) as the adsorbent.

Reaction progress was monitored by GC/MS, LC/MS, GC-FID analysis and thin layer chromatography (TLC) on aluminum-backed plates with Merck Kiesel 60 F254 silica gel. TLCs were either visualized by UV radiation at a wavelength of 254 nm, or stained by exposure to an ethanolic solution of phosphomolybdic acid. All solvents and reagents for the reactions were of reagent grade and were dried and distilled under nitrogen before use. Indoles **2a**, **2c**, **2d**, and **2e**, were acquired from commercial sources and were used as received. Other substituted indoles are known compounds (**2b**,[S1] **2f**,[S2] **2g**,[S3] **2h**[S4]) were synthesized following the literature method.[S2] All α-aryl-α-diazoactates are known compounds: (**1a**, **1b**, **1f**, **1h**, **1i**, **1j**;[S5] **1c, 1d**;[S6] **1e**;[S7] **1g;**[S8] **1k**[S6]) and were synthesized from commercially available aryl acetates according to standard protocol.[S5] Bipyridine-dioxide ligands were obtained from the previous work.[S9]

2. NMR and Mass Spectrometry studies

NMR studies. General considerations.

^{1}H NMR spectra were registered on a spectrometer Bruker Avance III 400 NMR at operating frequencies 400.1 MHz for nuclei ^{1}H. As an internal reference for the ^{1}H NMR spectrum, residual solvent signals (δ 5.32 ppm for DCM-d_2) were used. All spectra were processed with Bruker Topspin 3.2 software package. The DOSY spectra were recorded using 16 steps with linear increasing of gradient pulse strength (from 5 to 95% of maximum gradient coil current). The Little Delta (δ) was set to 2 ms and the Big Delta (Δ) was set to 50 msec. 2D DOSY spectra were generated using Bruker Topspin 3.2 software and the diffusion coefficients were calculated using Topspin T1/T2 relaxation module.

Mass spectrometry studies. General considerations.

Mass spectra were measured using Bruker maXis instrument equipped with an electrospray ionization source and spectra were recorded in positive ion mode with *m/z* 100 – 1500 range. Capillary Voltage was 4.5 kV, applied Spray Shield Offset was set to – 0.5 kV. For calibration of the mass spectra, a low-concentration tuning mix solution by Agilent Technologies was utilized. Nitrogen was applied as a nebulizer gas (1 bar) and dry gas (4.0 L × min^{-1}, 200 °C). Bruker Data Analysis 5.0 software package was used. Online reaction monitoring was performed for the reaction mixture in dichloromethane (argon double balloon pressurized injection). Ultrahigh-resolution mass spectra were acquired on a Bruker SolariX XR ion cyclotron resonance Fourier transform MS (Bremen, Germany) equipped with a 15 Tesla superconducting magnet and an Apollo II source in positive electrospray ionization mode. The sample was injected with a constant flow rate of 120 µl h−1, a nebulizer gas pressure of 1 bar and drying gas (200 °C, 4.0 L min^{-1}). The accumulation time was 0.1 s, the number of scans was 32 with 2 M data points, and the m/z range was 150–3000. The applied ESI voltage was 3.6 kV capillary voltage and −0.5 kV end plate offset. Transfer optic parameters were therefore ToF 0.6 ms, frequency 6 MHz and RF amplitude 350 Vpp. The spectra were processed using Bruker Data Analysis 5.1 software.

ESI-MS online monitoring of reaction mixture

A solution of ligand **7g** (5.3 mg, 0.01 mmol), $Pd(PhCN)_2Cl_2$ (3.8 mg, 0.01 mmol) and $NaBAr_F$ (21.3 mg, 0.024 mmol) in DCM (3 mL) was stirred at room temperature for 1 hour under Ar. The color of the suspension turned black. Mass spectra and ^1H NMR spectra were recorded from this mixture. After that, indole **2a** (34.8 mg, 0.24 mmol) and diazo compound **1a** (51.0 mg, 0. mmol) in DCM (3 mL) were added into a Schleck tube equipped with a magnetic stir bar under argon backflush. One neck was closed with a silicon septum and the side tap was connected with a double-walled argon balloon. PEEK capillary was pushed into the flask through the septum and immersed into the reaction mixture. After stirring for ca. 2 min (500 RPM) at room temperature, the solution of ([Pd]/**7g**/NaBArF) prepared earlier was injected into this Schleck tube through the septum by a syringe, and the reaction was monitored for 15 min. After that, the yield was measured by ^1H NMR. The same protocol was used for the reaction with ligand **7a**.

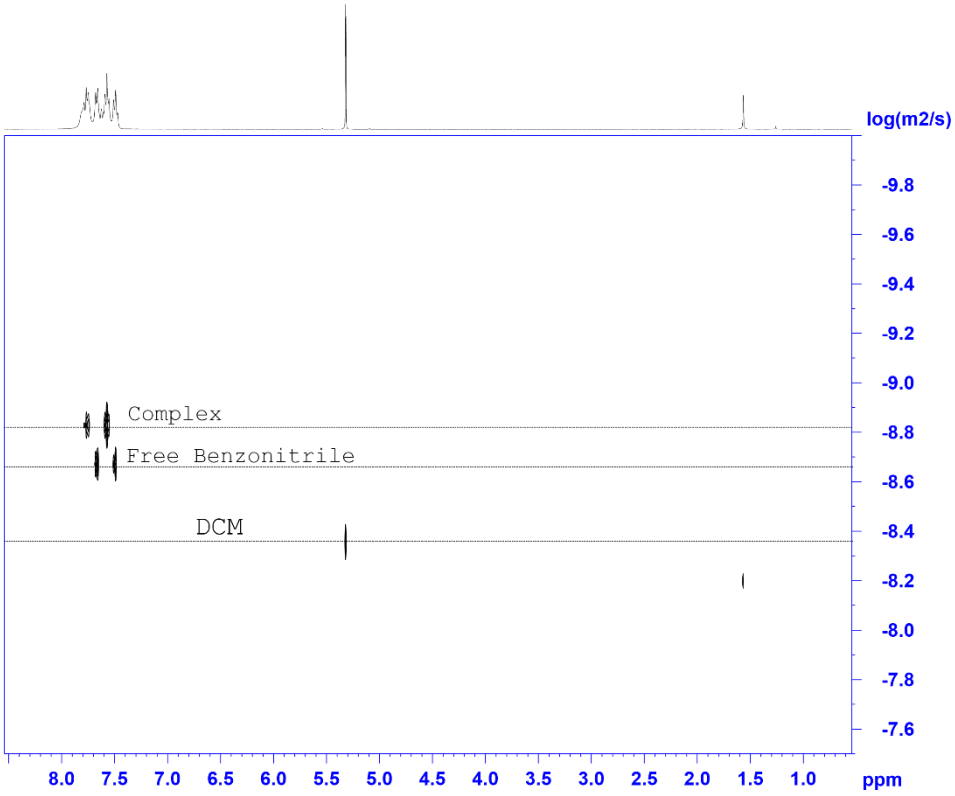

Figure S1. ^1H NMR DOSY spectrum of commercial $Pd(PhCN)_2Cl_2$

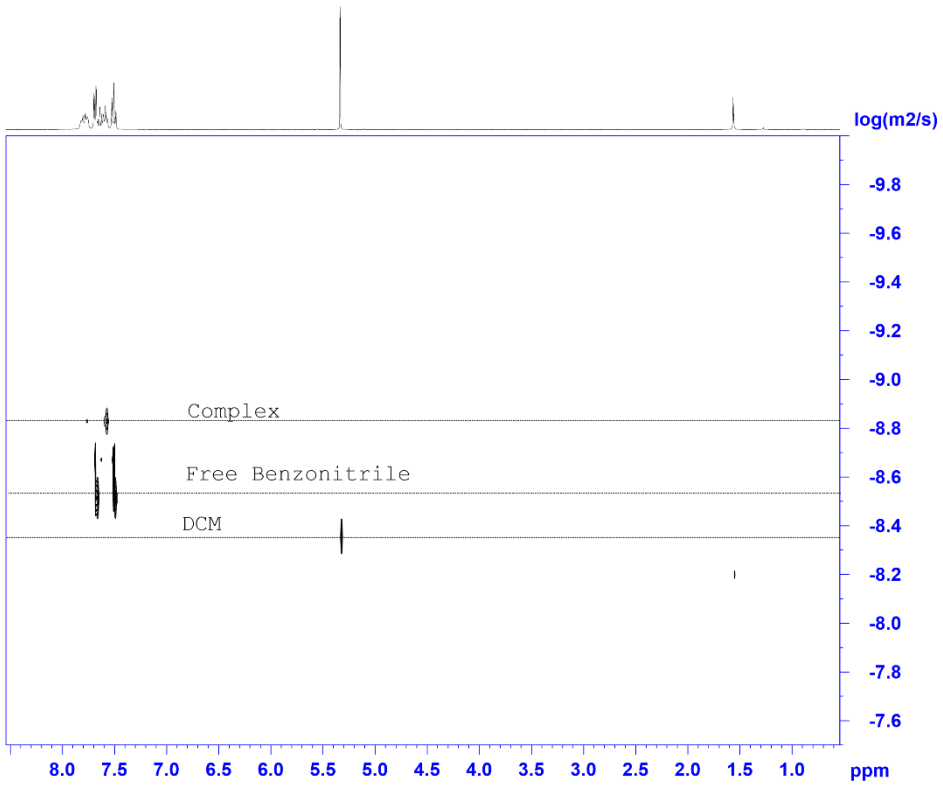

Figure S2.[1]H NMR DOSY spectrum of freshly synthesized $Pd(PhCN)_2Cl_2$

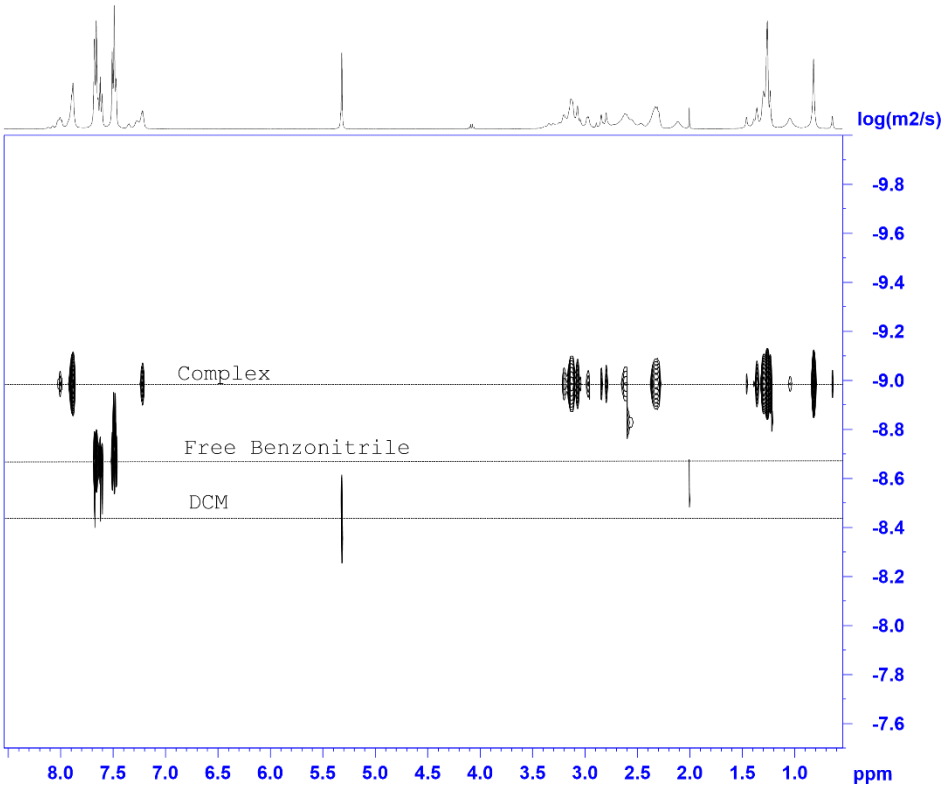

Figure S3. [1]H NMR DOSY spectrum of *freshly synthesized* $Pd(PhCN)_2Cl_2$/ligand **7g**

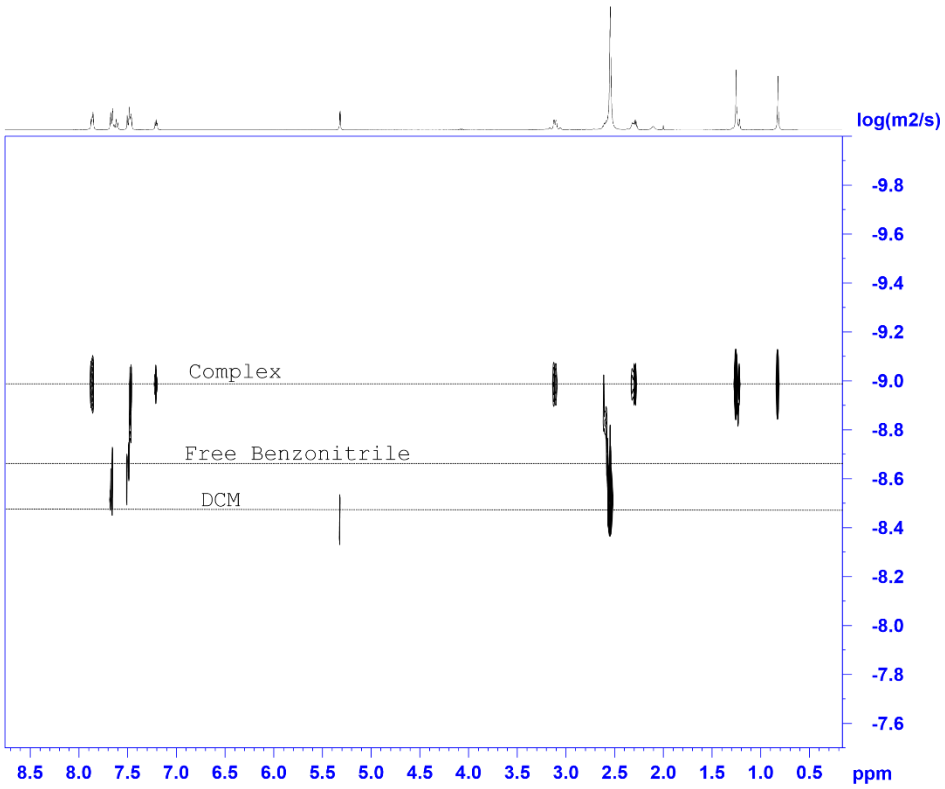

Figure S4. ^{1}H NMR DOSY spectrum of commercial $Pd(PhCN)_2Cl_2$/ligand **7g**

ESI-MS online monitoring

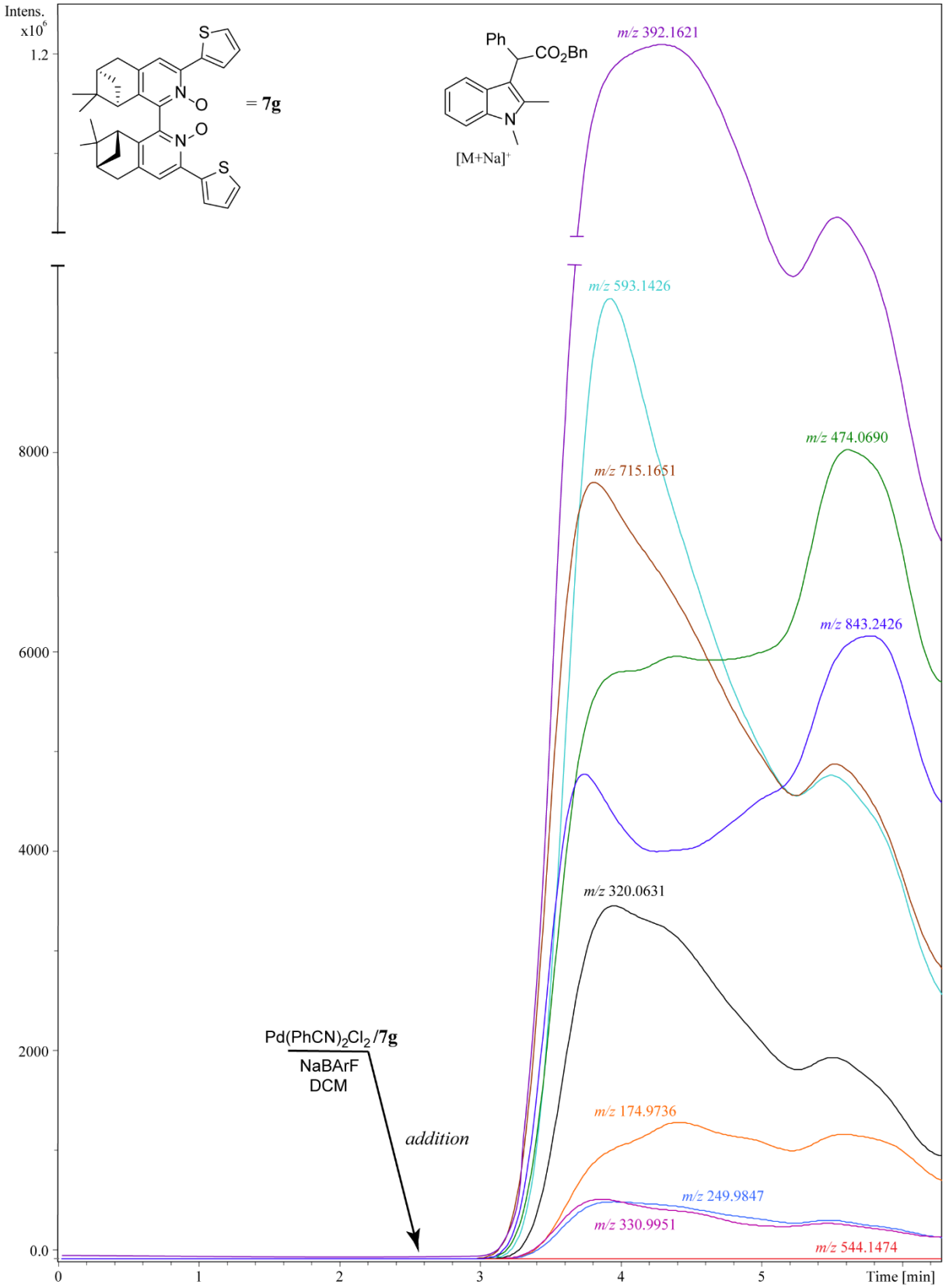

Figure S5. The real-time abundance of product and main palladium-containing complexes in Pd-catalyzed C-H functionalization of indoles. The ions of Pd complexes appeared in the spectrum only after injection of a DCM solution containing [Pd]+L(**7g**)+$NaBAr_F$.

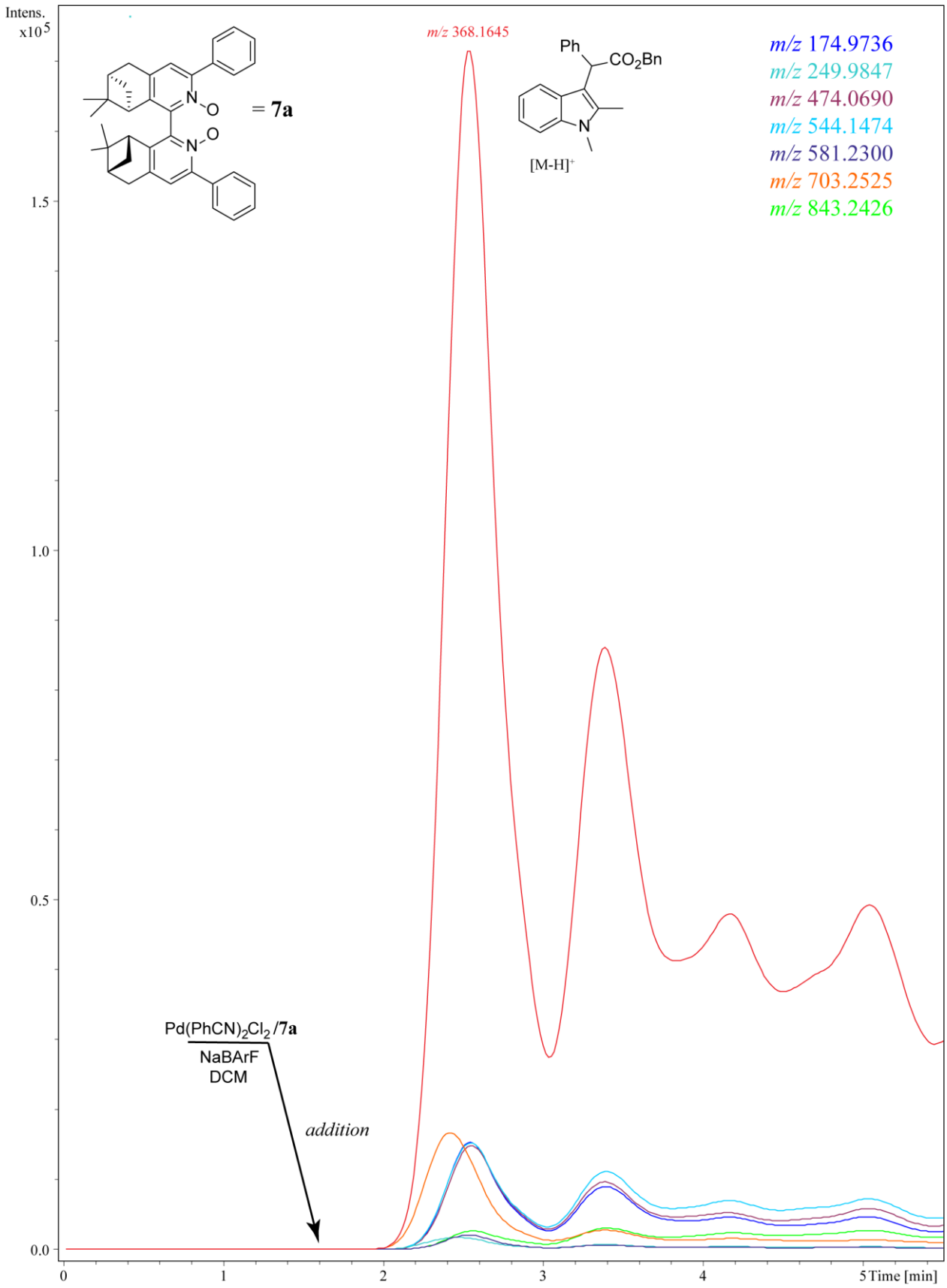

Figure S6. The real-time abundance of product and main palladium-containing complexes of palladium-catalyzed C-H functionalization of indoles. The ions of Pd-complexes appeared in a spectrum only after injection of freshly synthesized [Pd]+L(**7a**)+NaBAr$_F$+DCM solution.

Table S1. Pd-containing ions observed during ESI-HRMS monitoring of the reaction mixture with ligand **7a**.[a]

entry	calcd m/z [M]+	structure	intermediate	composition
1	174.9736	Pd(C_5H_9)		$Pd_1C_5H_9$
2	249.9847	Pd(**2**)	**E**	$Pd_1C_{10}H_{10}N$
3	474.0690	Pd(**3**)	**B'** or **C**	Pd($C_{25}H_{22}NO_2$)
4	544.1474	Pd(**3**)(C_5H_9)		Pd($C_{25}H_{23}NO_2$)(C_5H_9)
5	581.2300	$[Pd(\mathbf{7a})_2]^{2+}$		$Pd_1(C_{36}H_{36}N_2O_2)_2$
6	703.2525	Pd(**7a**)(C_5H_9)		$Pd_1(C_{36}H_{36}N_2O_2)(C_5H_9)$
7	843.2426	$Pd(\mathbf{3})_2 - H^+$		$Pd_1(C_{25}H_{23}NO_2)_2 - H^+$

[a] The reaction was performed in a Schlenk tube with freshly synthesized $Pd(PhCN)_2Cl_2$ (5 mol%), ligand (5 mol%), $NaBAr_F$ (12 mol%), **1a** (0.2 mmol, 1 equiv) and **2a** (0.24 mmol, 1.2 equiv) in 6 mL of CH_2Cl_2 at rt. The reaction was monitored for 15 min.

3. SEM and EDX data

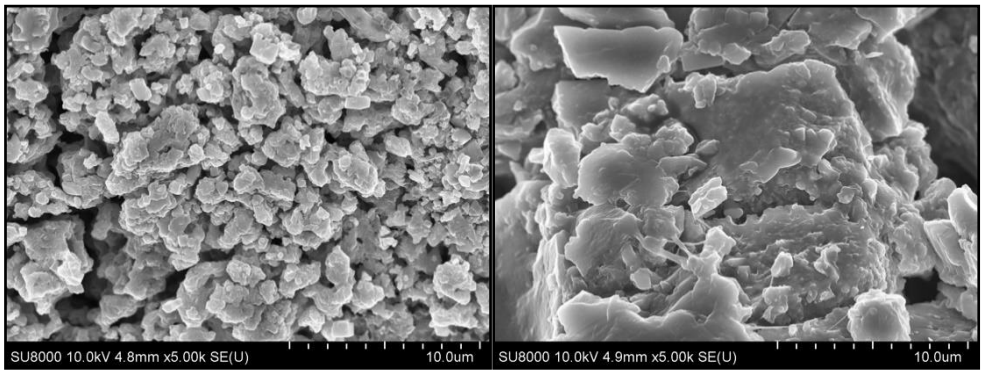

Figure S7. FE-SEM images for the precipitates formed in the solutions of commercial $Pd(PhCN)_2Cl_2$/ **7g**/ $NaBAr_F$ (left) and freshly synthesized $Pd(PhCN)_2Cl_2$/ **7g**/ NaBArF (right).

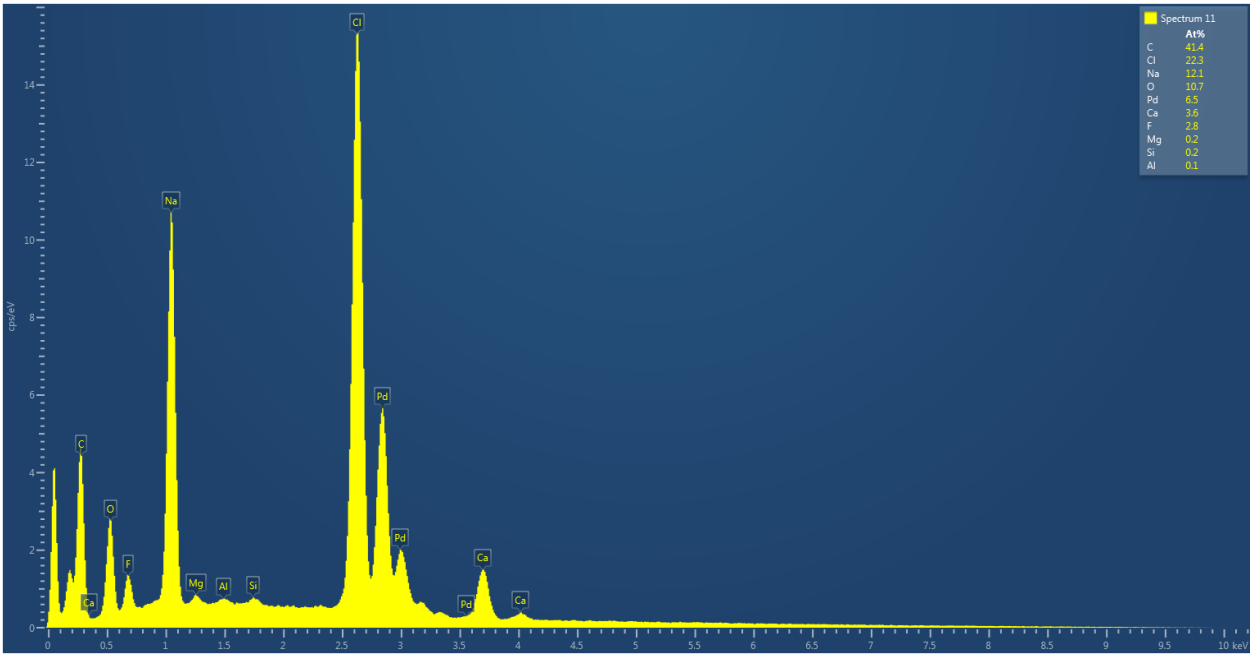

Figure S8. EDX spectrum for the precipitate formed in the solution of the mixture of commercial $Pd(PhCN)_2Cl_2$/ligand **7g**/$NaBAr_F$.

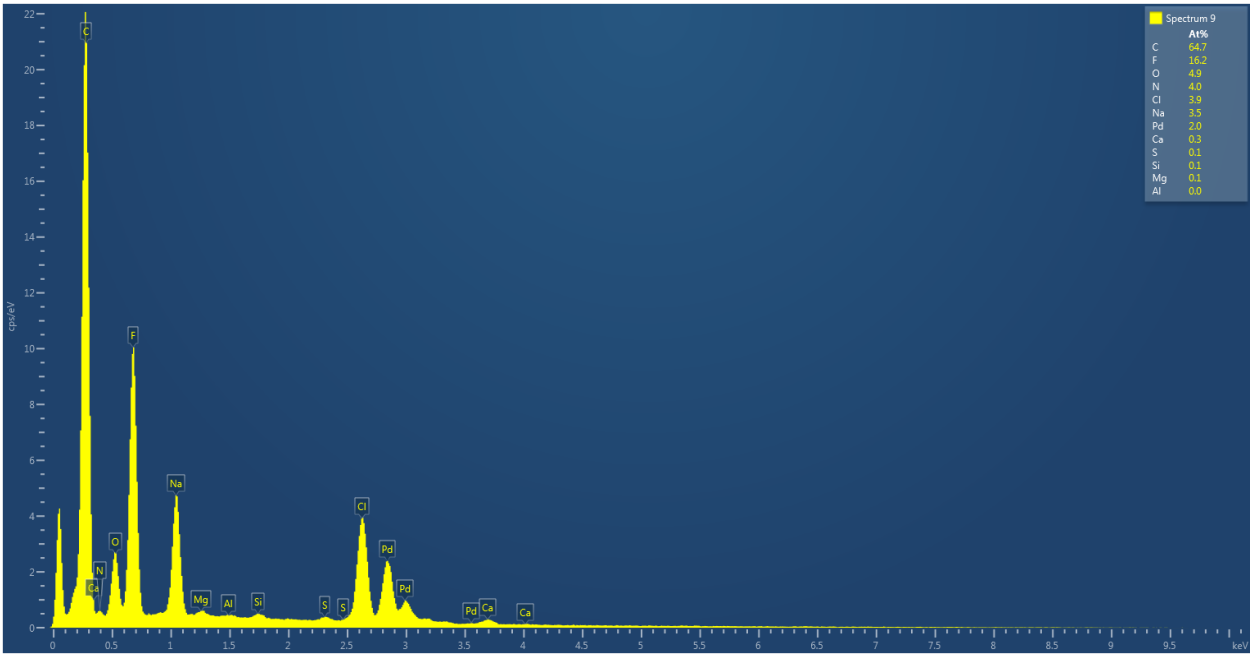

Figure S9. EDX spectrum for the precipitate formed in the solution of the mixture of freshly synthesized $Pd(PhCN)_2Cl_2$/ **7g**/ $NaBAr_F$.

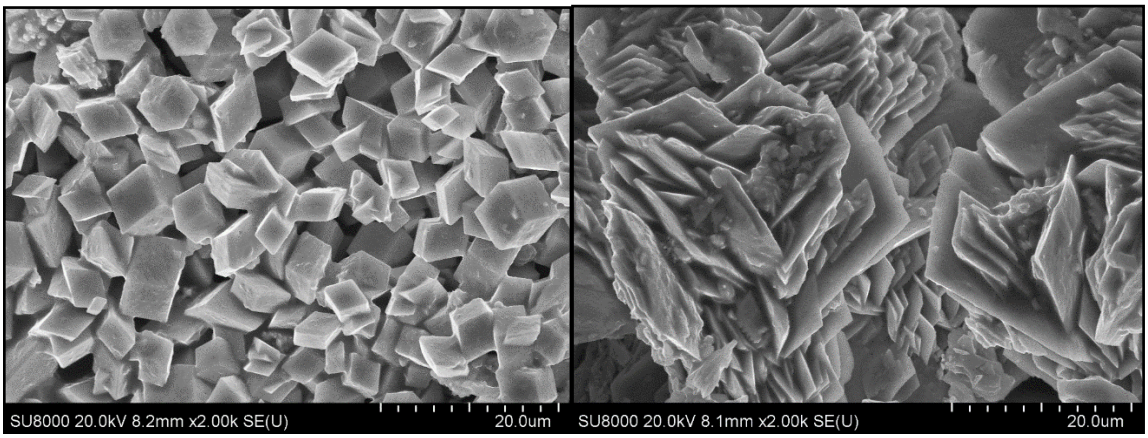

Figure S10. Scanning electron microscopy (SEM) images of precipitates of $PdCl_2$ formed upon dissolution and $Pd(PhCN)_2Cl_2$ in CH_2Cl_2: left - freshly made sample, right – aged sample.

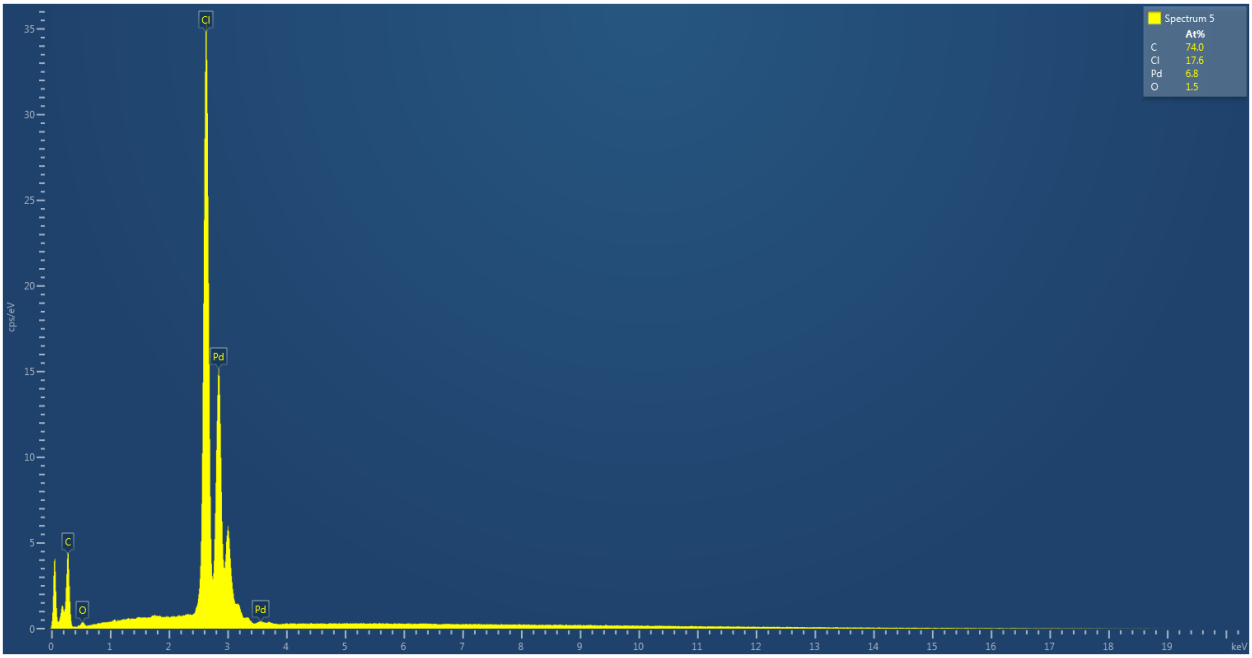

Figure S11. EDX spectrum for the precipitate formed from commercial $Pd(PhCN)_2Cl_2$.

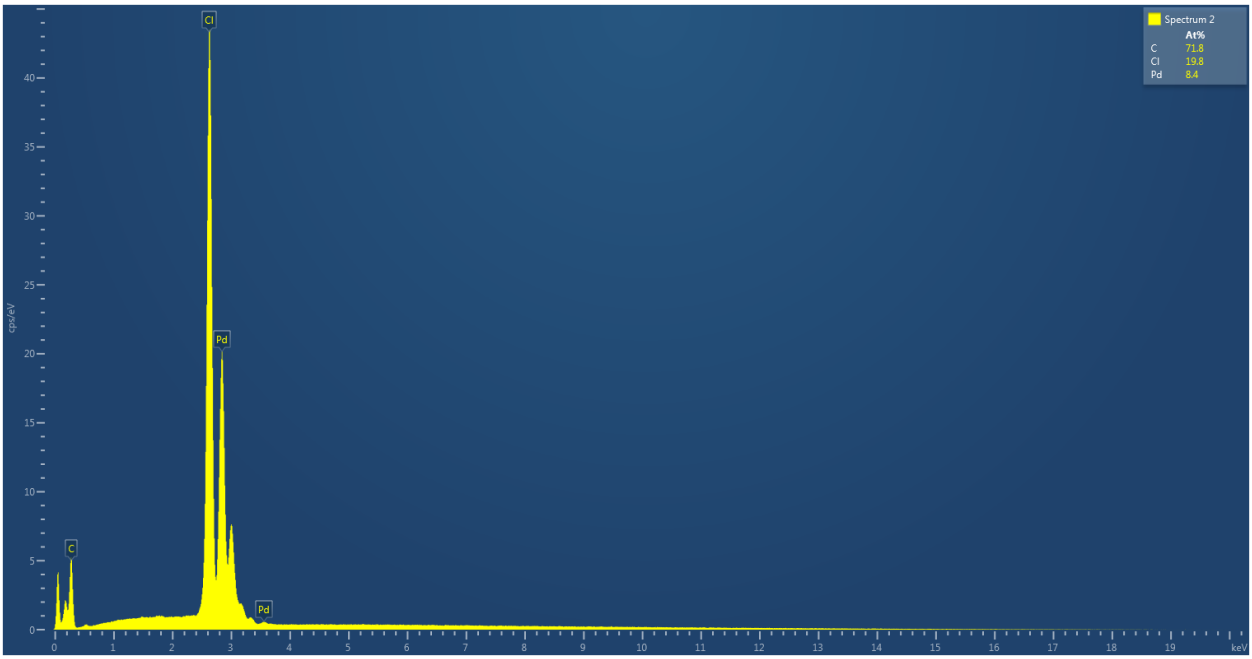

Figure S12. EDX spectrum for the precipitate formed from freshly synthesized $Pd(PhCN)_2Cl_2$.

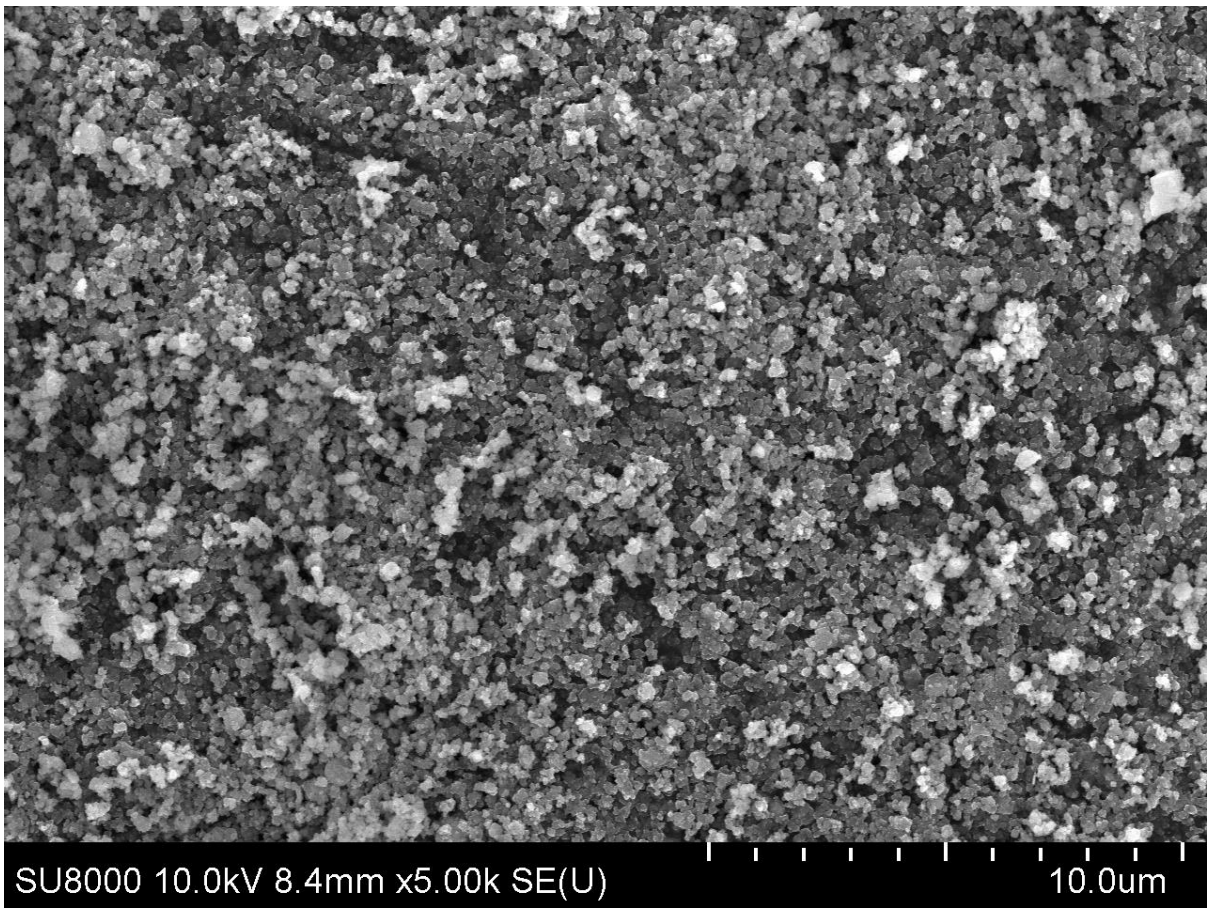

Figure S13 FE-SEM images for the precipitate formed in the solution of freshly synthesized $Pd(PhCN)_2Cl_2$/ **7g**/ NaBArF/reagents.

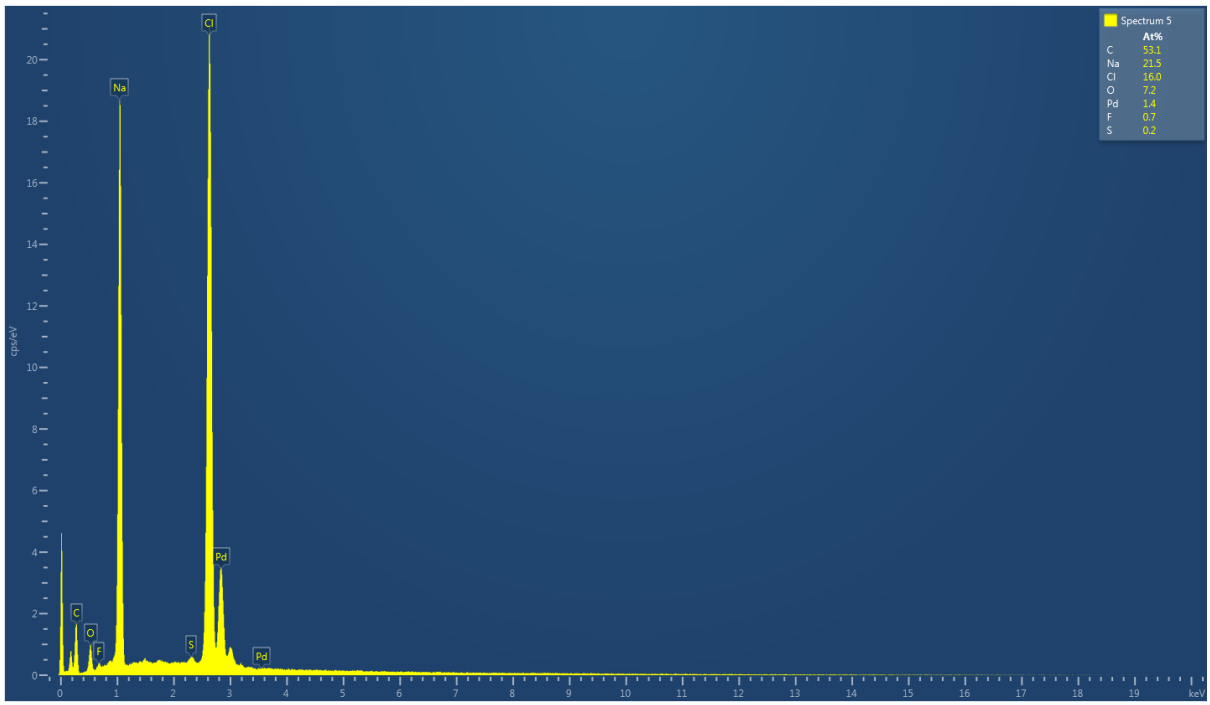

Figure S14. EDX spectrum for the precipitate formed in the solution of the mixture of commercial $Pd(PhCN)_2Cl_2$/ **7g**/ NaBArF/reagents.

4. UV kinetic studies

General considerations

All reactions were carried out in DCM at 25 °C in standard 10x10x45 quartz cuvettes with a Teflon cap in a spectrophotometer unit. The data were recorded in a kinetic mode at 251 nm with a 2 seconds scan step using the Leki ScanPro software. Kinetic curves were obtained by plotting the decrease in absorption of the diazo compound over time using Sigma Plot software. Stock solutions of reactants were prepared prior to use by dissolving an appropriate amount of each reagent in dry freshly distilled DCM in a concentration range from $2.5*10^{-3}$M to $5*10^{-3}$M for indole **2a** and diazoester **1a** and $4*10^{-4}$M to $6*10^{-4}$M for $NaBAr_F$, ligand **7g (8g)** and Pd-precatalyst. Each experiment was performed in triplicate (5 times for the experiments with the excess of H_2O and D_2O). The procedure for the preparation of precipitated $PdCl_2$ is described further (see section S5).

Experiment procedure

Measured aliquots of stock solutions of $NaBAr_F$, ligand (if required), Pd-precatalyst and indole **2a** were pippeted in sequence to a 10x10x45 quartz cuvette containing the exact volume of DCM so that further addition of stock solution of **1a** would yield the concentrations of $1.2*10^{-5}$M for $NaBAr_F$, $5*10^{-6}$ M for Pd-source and ligand **7g** or **8g**, $1.2*10^{-4}$M for indole **2a** and $1*10^{-4}$M for diazoester **1a.** The solution was thoroughly mixed using lab shaker and used as blank for baseline correction. After recording the initial absorption of the mixture, an aliquot of diazoester **1a** was added to the cuvette, quickly mixed and the decrease in absorption monitored until it reaches the plateau (for 20 minutes typically). The resulting absorption data were processed with Sigma Plot.

Typical experiment

$NaBAr_F$ (43 µl, $4.18*10^{-4}$M solution in DCM, 12 mol%), **7g** (14 µl, $5.4*10^{-4}$M solution in DCM, 5mol%), $Pd(PhCN)_2Cl_2$ (14 µl, $5.4*10^{-4}$M solution in DCM, 5mol%) and **2a** (34 µl, $4.9*10^{-3}$M solution in DCM, 1.2 equiv) were added to a 10x10x45 quartz cuvette containing 1.34 mL DCM. The cuvette was transferred to the spectrophotometer after carefully shacking and the absorbance spectrum of the resulting mixture was recorded as blank. Next, diazoester **1a** (56 µl, $2.66*10^{-3}$M solution in DCM, 1 equiv) was added to the cuvette, which was quickly shacked and transferred back to the spectrophotometer unit to begin measurements.

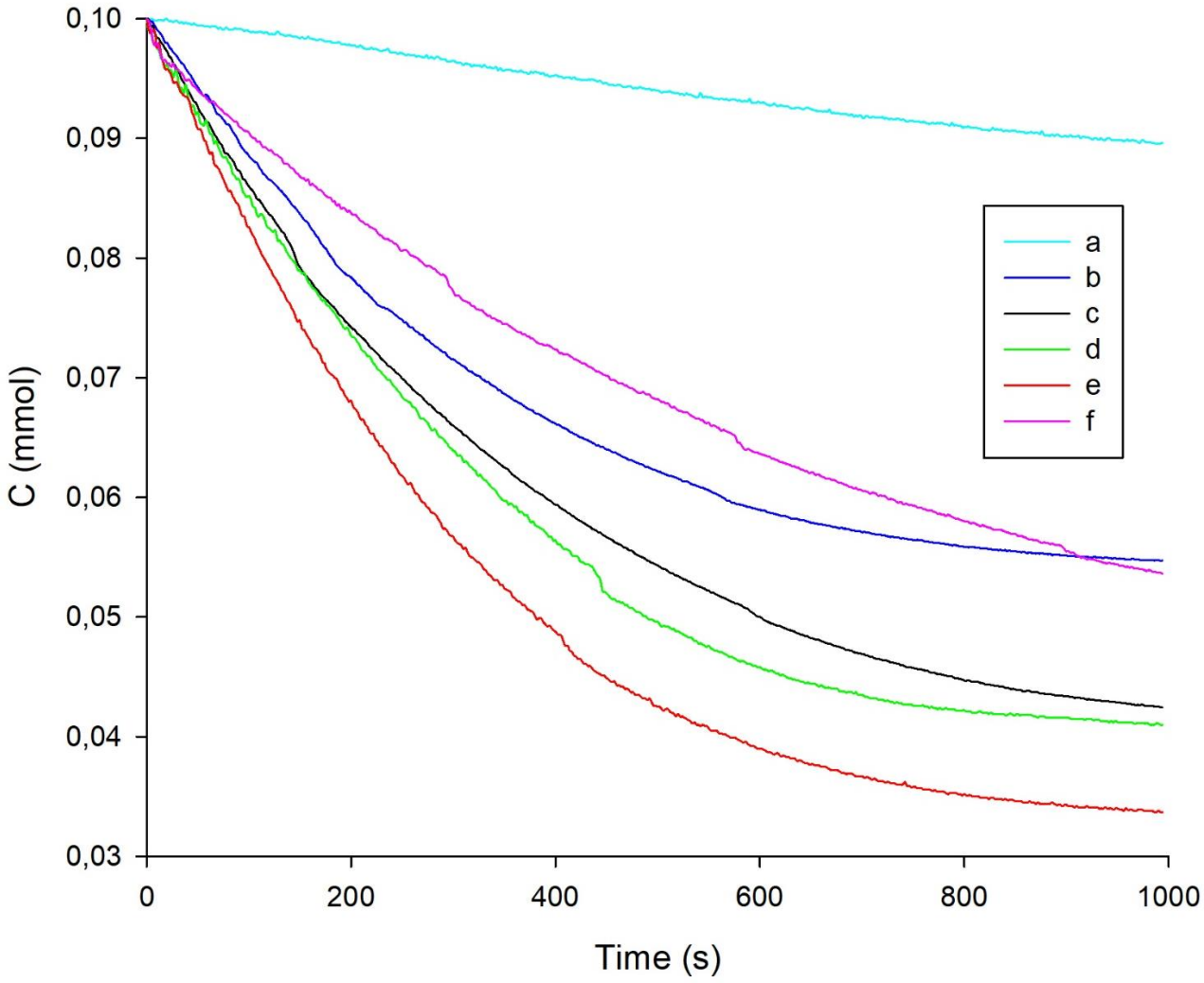

Figure S 15. A plot of [**1a**] versus time. Curve **a**: precipitated $PdCl_2$ (5 mol%), 7**g** (5 mol%); curve **b**: fresh $Pd(PhCN)_2Cl_2$ (5 mol%) without ligand; curve **c**: fresh $Pd(PhCN)_2Cl_2$ (5 mol%), 7**g** (5 mol%); curve **d**: fresh $Pd(PhCN)_2Cl_2$ (5 mol%), 7**g** (5 mol%), H_2O (20 equiv with respect to **1a**); curve **e**: fresh $Pd(PhCN)_2Cl_2$ (5 mol%), 7**g** (5 mol%), D_2O (20 equiv with respect to **1a**), curve **f**: fresh $Pd(PhCN)_2Cl_2$ (5 mol%), 8**g** (5 mol%).

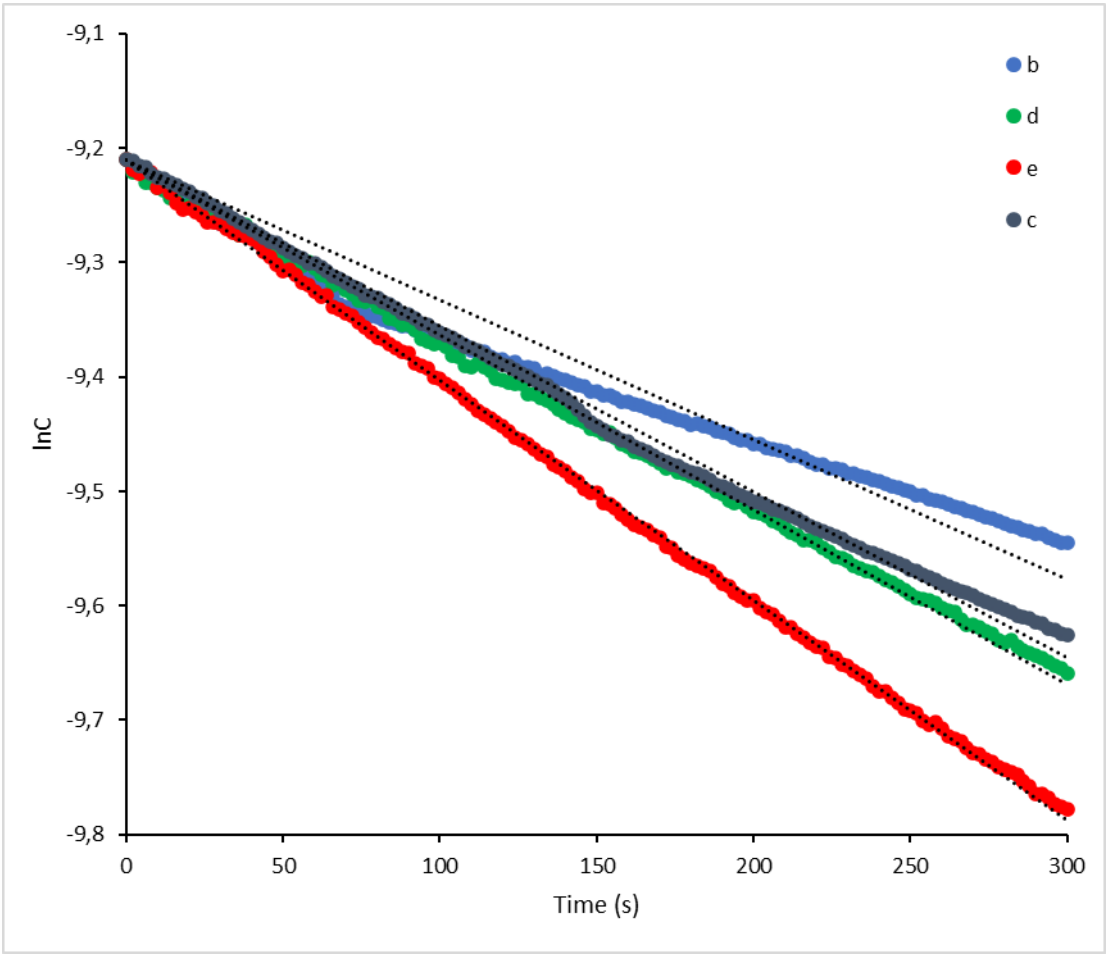

Figure S 16. A plot of ln[**1a**] versus time (dotted line - linear regression). Curve **b**: fresh $Pd(PhCN)_2Cl_2$ (5 mol%) without ligand, linear regression -ln[**1a**] = 9.2103 + 0.00121*t (R^2=0.9802); curve **c**: fresh $Pd(PhCN)_2Cl_2$ (5 mol%), 7**g** (5 mol%), linear regression -ln[**1a**] = 9.2103 + 0.00145*t (R^2=0.9861); curve **d**: fresh $Pd(PhCN)_2Cl_2$ (5 mol%), 7**g** (5 mol%), H_2O (20 equiv with respect to **1a**), linear regression -ln[**1a**] = 9.2103 + 0.00147**t* (R^2=0.9996); curve **e**: fresh $Pd(PhCN)_2Cl_2$ (5 mol%), 7**g** (5 mol%), D_2O (20 equiv with respect to **1a**) linear regression -ln[**1a**] = 9.2103 + 0.00192**t* (R^2=0.9998).

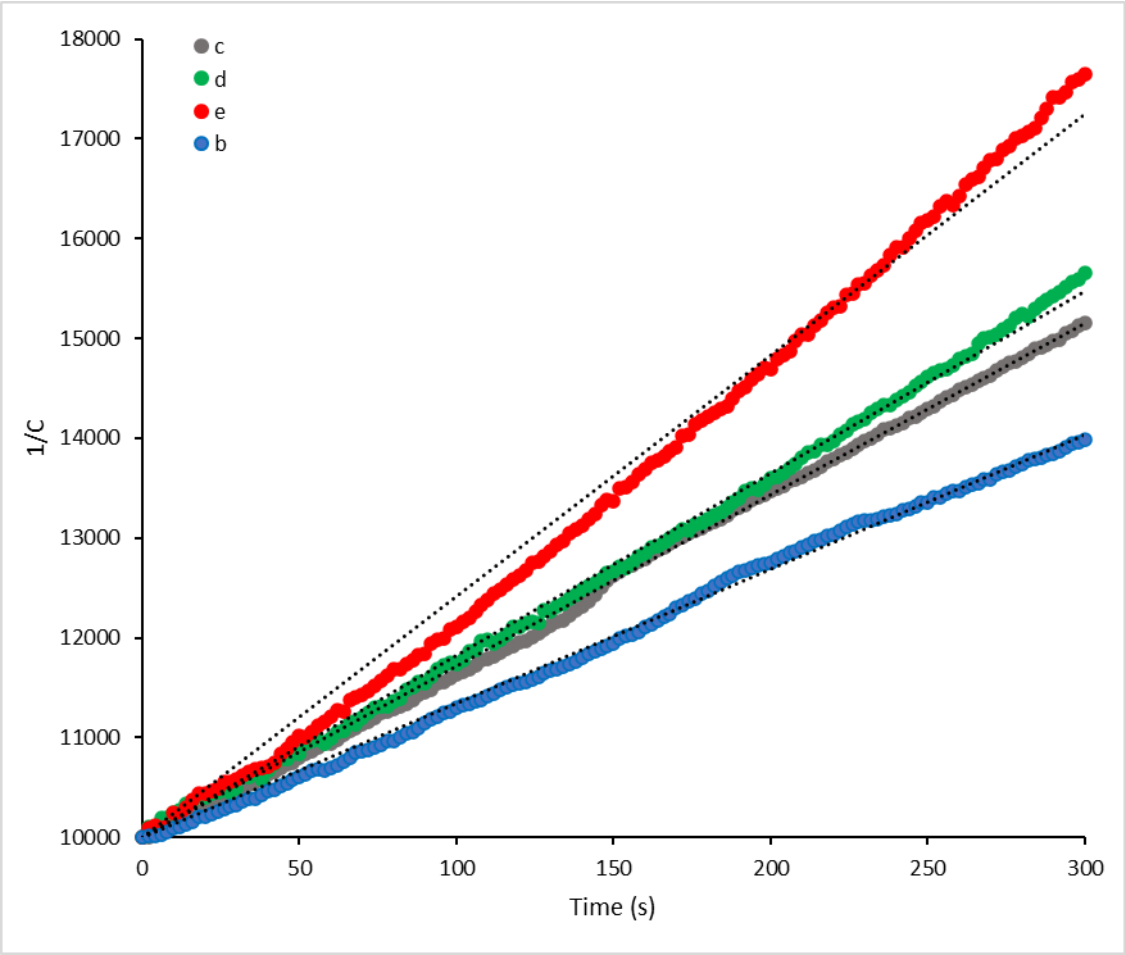

Figure S 17. A plot of $[\mathbf{1a}]^{-1}$ versus time (dotted line - linear regression). Curve **b**: fresh $Pd(PhCN)_2Cl_2$ (5 mol%) without ligand, linear regression $[\mathbf{1a}]^{-1} = 10000 + 13.825*t$ (R^2=0.9989); curve **c**: fresh $Pd(PhCN)_2Cl_2$ (5 mol%), 7**g** (5 mol%) linear regression $[\mathbf{1a}]^{-1} = 10000 + 17.143*t$ (R^2=0.9989); curve **d**: fresh $Pd(PhCN)_2Cl_2$ (5 mol%), 7**g** (5 mol%), H_2O (20 equiv with respect to **1a**), linear regression $[\mathbf{1a}]^{-1} = 10000 + 18.237*t$ (R^2=0.9695); curve **e**: fresh $Pd(PhCN)_2Cl_2$ (5 mol%), 7**g** (5 mol%), D_2O (20 equiv with respect to **1a**), linear regression $[\mathbf{1a}]^{-1} = 10000 + 24.132*t$ (R^2=0.9714).

5. Extended optimization experiments and mechanistic studies

Table S2. Solvent screening in Pd catalyzed enantioselective alkylation of 1,2-dimethylindole with benzyl 2-diazo-2-phenylacetate.[a]

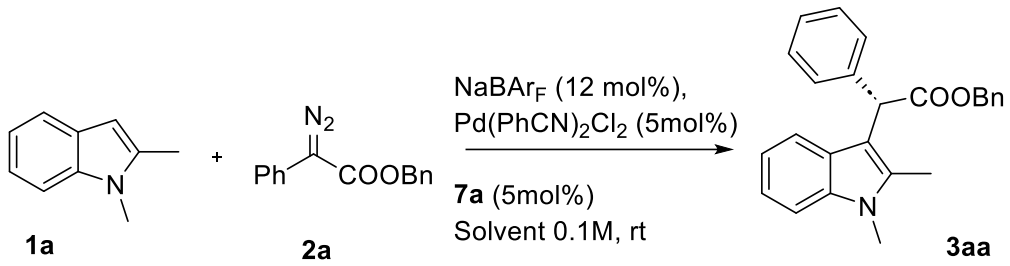

Entry	Solvent	Yield (%)	ee (%)
1	DCM	96	82
2	THF	9	2
3	MeCN	7	0
4	Toluene	90	61
5	1,2-Dichloroethane	95	75
6	$CHCl_3$	92	40
7	PhCl	83	61
8	DMF	40	0

[a] The reaction was carried out using 0.20 mmol of diazoester **2a**, 0.24 mmol of indole **1a**, 5 mol% of Pd source, 5 mol% of **7a**, and 12 mol% of $NaBAr_F$ in 2 mL of the given solvent at room temperature.

Table S3. Effect of $NaBAr_F$ loading on the enantioselectivity of the reaction.

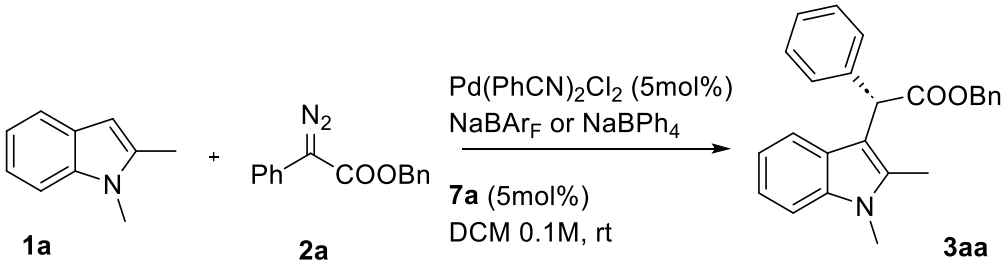

Entry	Loading of salt (mol %)	Yield (%)	ee (%)
1	6	85	61
2	12	96	82
3	18	95	81
4	12[b]	-	-

[a] The reaction was carried out using 0.20 mmol of diazoester **2a**, 0.24 mmol of indole **1a**, 5 mol% of Pd source, 5 mol% of ligand **7a**, and the given amount of NaBArF in 2 mL of DCM at room temperature. [b] 10 mol% of $NaBPh_4$ was used instead of $NaBAr_F$, with no reaction.

Table S4. Optimization of catalyst loading.

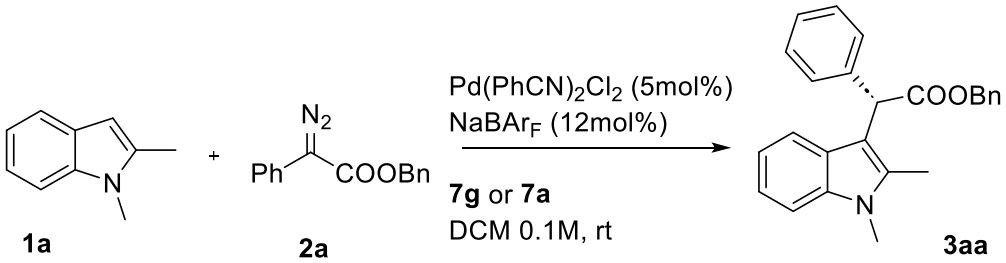

Entry	$Pd(PhCN)_2Cl_2$, (mol%)	Ligand*, (mol%)	Yield, (%)	ee, (%)
1	5	5	96	90
2	1	1	92	89
3	0.5	0.5	90	87
4	0.25	0.25	71	60
5[b]	0.5	0.5	-	-

[a] The reaction was carried out using 0.20 mmol of diazoester **2a**, 0.24 mmol of indole **1a**, the given amount of $Pd(PhCN)_2Cl_2$, the given amount of **7g**, and 12 mol% of $NaBAr_F$ in 2 mL of DCM at room temperature. [b] Ligand **7a** was used instead of **7g**, with no reaction.

Table S5. Effect of reaction temperature on enantioselectivity

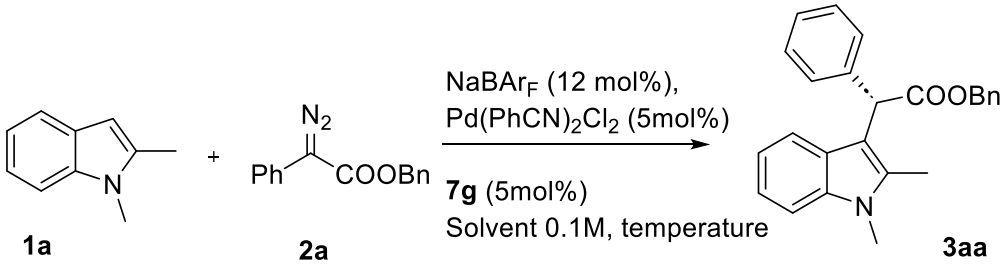

Entry	T, (°C)	Yield, (%)	ee, (%)
1	0	88	83
2	20	96	90
3	40	94	88
4[b]	60	92	85

[a] The reaction was carried out using 0.20 mmol of diazoester **2a**, 0.24 mmol of indole **1a**, 5 mol% of Pd source, 5 mol% of **7g**, and 12 mol% of $NaBAr_F$ in 3 mL of DCM at the given temperature. [b] DCE was used as a solvent instead of DCM.

Insertion of diazoesters into Borylated 1,2-dimethylindole

Trifluoro(2-(piperidin-1-ium-1-yl)phenyl)borate and a BPin-1,2-dimethylindole were synthesized according to the literature protocol.[S10]

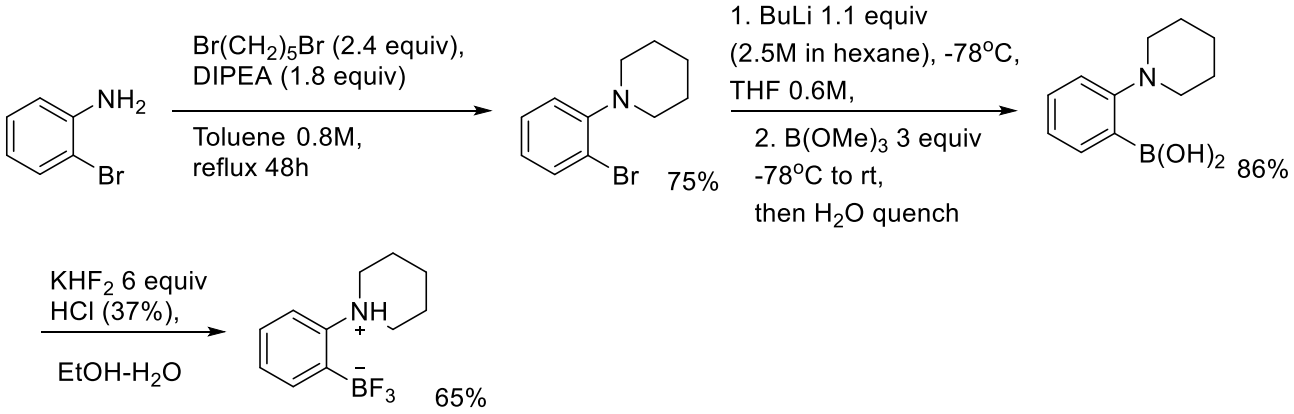

*1,2-dimethyl-3-(4,4,5,5-tetramethyl-1,3,2-dioxaborolan-2-yl)-1H-indole (**10a**)*

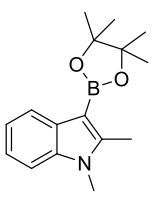

HBPin (450 µL, 2 equiv) was added dropwise via syringe to the stirred under argon mixture of trifluoro(2-(piperidin-1-ium-1-yl)phenyl)borate (36 mg, 10 mol%) and 1,2-dimethylindole (225 mg, 1 equiv) in an oven-dried 50 mL test tube. The reaction mixture was first stirred at room temperature for 10 min and then at 80 °C for 5-10 minutes which led the reaction mixture to liquefy initially and solidify later within 5-10 min. Therefore, 1 mL of THF

was added to bring the reaction mixture to a solution phase. Next, the reaction flask was heated at 80 °C for 16 hours. The resulting crude reaction mixture was subsequently kept under a high vacuum for 30 min at 50 °C to remove volatiles, followed by filtration of the residue through a short column of Al_2O_3 using diethyl ether as an eluent (40 mL). After evaporation of the solvent under reduced pressure, the desired BPin-indole was obtained as a white solid (364 mg, 87%).**^{1}H NMR** (400 MHz, C_6D_6): δ_H 1.23 (s, 12H), 2.46 (s, 3H), 2.81 (s, 3H), 7.03 (m, 1H), 7.27 (m, 1H), 7.35 (m, 1H), 8.63 (m, 1H) (Figure S19). **^{11}B NMR** (128 MHz, C_6D_6): δ_B 31.0 (Figure S21). **^{13}C NMR** (101 MHz, C_6D_6): δ_C 11.7, 24.2, 27.7, 81.4, 107.8, 119.7, 120.3, 121.9, 132.7, 137.6, 146.5(Figure S20). In agreement with literature.[S11]

*Procedure for the reaction of diazoester **1c** with boronic ester **10a**.*

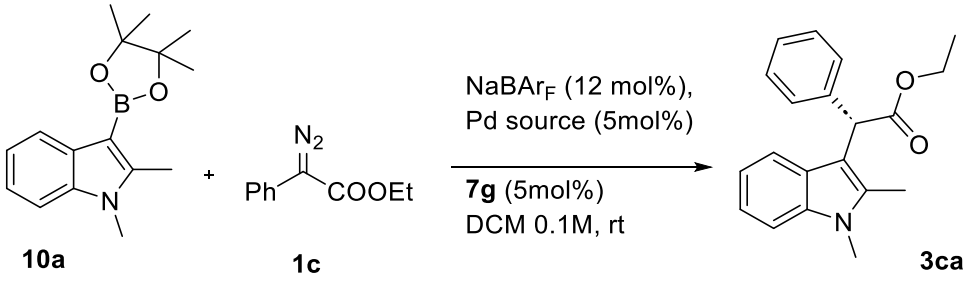

A solution of **7g** (0.01 mmol, 5 mol%), $Pd(PhCN)_2Cl_2$ (0.01 mmol, 5 mol%), and $NaBAr_F$ (0.024 mmol, 12 mol%) in DCM (2.0 mL) was stirred at room temperature for 1 hour. Then the indole derivative (0.24 mmol, 1.2 eq) and the diazoester (0.2 mmol, 1.0 eq) were dissolved in 0.3 mL of dry toluene and added slowly to that mixture over 1h at room temperate. The reaction mixture was left stirring at rt for 30 minutes. The solution was concentrated in vacuo and the crude product was purified by flash column chromatography using a mixture of petroleum ester/ethyl acetate (9:1) to give the desired product **(3ca)** as a light-yellow oil (25 mg, 41%), 76% ee. Enantiomeric excess was determined by chiral HPLC (Lux (5µm) Cellulose-1 column, water/MeCN = 50:50; flow rate 0.3 mL/min at 35 °C, UV detection at 225 nm; t_{major} = 105.9 min, t_{minor} = 109.0 min.

Attempt on proving the "cocktail of catalysts"

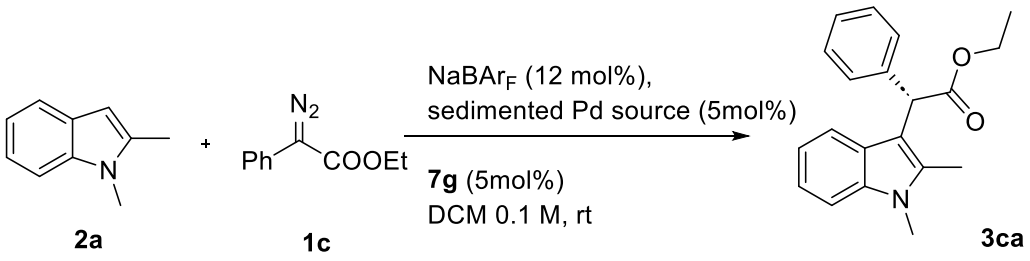

Preparation of Pd-source: 200 mg of $Pd(PhCN)_2Cl_2$ was introduced to an oven-dried, nitrogen-flushed test tube, and stirred overnight in dry DCM. Therefore, the precipitate was centrifuged off, decanted and washed with 5 mL of DCM 5 times. Obtained brown solid was dried under vacuum at 60ºC for 2 hours and used for further reaction. A solution of **7g** (5.4 mg, 0.01 mmol,), Pd-source (1.77 mg, corresponds to

0.01 mmol of $PdCl_2$), and $NaBAr_F$ (21 mg 0.024 mmol) in DCM 3.00 mL was stirred at room temperature for 1 hour. Then 1,2-dimethylindole (34.8 mg, 0.24 mmol) and diazo compound (38 mg, 0.2 mmol) were added in one portion at room temperate and the reaction mixture was left for 30 mins. The solution was concentrated in vacuo. The crude product was purified by flash column chromatography using a mixture of petroleum ester/ethyl acetate (9:1) to give the desired product (**3ca)** as a light-yellow oil (59 mg, 80%), 53% ee. Enantiomeric excess was determined by chiral HPLC (IC-3 column, *n*-hexane/*i*-PrOH = 95:5, flow rate 1.0mL/min, UV detection at 254nm), t_{major} = 12.8, t_{minor} = 20.2.

Experiment with the order of addition

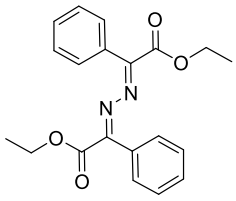

A solution of **7g** (0.01 mmol and MS 4Aº, 100 mg), $Pd(PhCN)_2Cl_2$ (0.01 mmol, 5 mol%), $NaBAr_F$ (0.024 mmol, 12 mol%) in DCM 2.00 mL was stirred at room temperature for 1 hour. Then diazo compound (0.4 mmol) was added in one portion and the reaction mixture was stirred for 30 minutes. After that, the solution of 1,2-dimethylindole (58 mg, 0.4 mmol) in 0.2 mL of DCM was added, and the mixture was stirred additionally for 15 minutes. The solution was concentrated in vacuo. The crude product was purified by flash column chromatography using a mixture of petroleum ester/ethyl acetate (9:1) to give (**9a)** as a yellow solid (51 mg, 74%). **^{1}H NMR** (400 MHz, $CDCl_3$): δ_H 1.43 (t, *J* = 7.1 Hz, 6H), 4.51 (q, *J* = 7.1 Hz, 4H), 7.46 (m, 1H), 7.80 (m, 1H) (Figure S22). **^{13}C NMR** (101 MHz, $CDCl_3$): δ_C 14.6, 61.8, 128.1, 128.9, 131.5, 132.1, 162.3, 165.4(Figure S23). In agreement with literature.[S12]

(7R,7'R,9R,9'R)-8,8,8',8'-tetramethyl-3,3'-di(thiophen-2-yl)-7,7',8,8',9,9',11,11'-octahydro-6H,6'H-1,1'-bi(6,8-methanoisoquinoline) (**8g**)

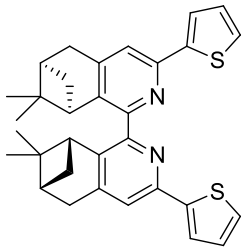

Bipyridine **8g** was obtained by our previously published method [S9]. Bipyridine N,N'-oxide **7g** (0.1 g, 0.185 mmol) was dissolved in THF (3.00 mL) and saturated aqueous solution of NH_4Cl (3.00 mL). An excess of zinc dust (243 mg, 3.71 mmol) was added to the solution and the mixture was heated under reflux for 24 hours. The reaction mixture was cooled to room temperature, the solids were removed by filtration. The filtrate was diluted with DCM (10.0 mL) and the aqueous layer was extracted with DCM (2×30 mL). The organic layers were combined, dried over Na_2SO_4 and concentrated in vacuo, to give pure **8g** as white solid (0.079g, 84 %), m.p. 238-240 ºC (decomp.). **^{1}H NMR** (400 MHz, $CDCl_3$): δ_H 0.94 (s, 3H), 1.23 (d, *J* = 9.6 Hz, 1H), 1.41 (s, 3H), 2.30 (m, 1H), 2.56 (dt, *J* = 9.9, 5.8 Hz, 1H), 3.08 (m, 2H), 3.18 (t, *J* = 5.5 Hz, 1H), 7.07 (dd, *J* = 5.0, 3.7 Hz, 1H), 7.30 (dd, *J* = 5.0, 1.0 Hz, 1H), 7.55 (dd, *J* = 3.6, 1.0 Hz, 1H) (Figure S24. 1H **NMR**, 8g. **^{13}C NMR** (101 MHz, $CDCl_3$): δ_C 21.6, 26.3, 31.7, 33.9, 39.4, 40.2, 43.3, 117.5, 123.4, 126.7, 127.7, 141.1, 146.4, 146.4, 148.6, 153.3 (Figure S25. ^{13}C NMR, 8g.

Reactions with bipyridine ligand ***8g***

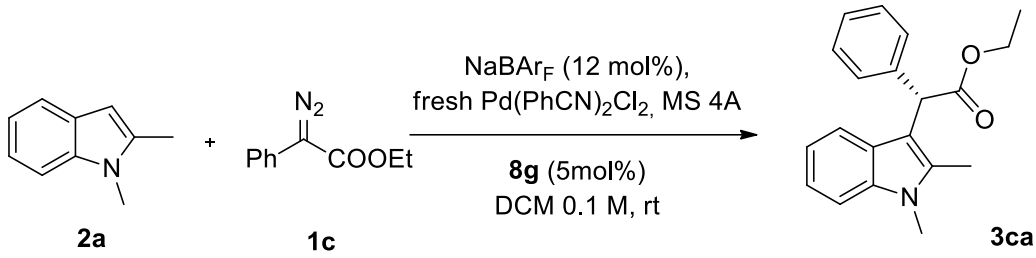

The mixture of $Pd(PhCN)_2Cl_2$ (3.8 mg, 0.01 mmol, 5 mol%), $NaBAr_F$ (21 mg, 0.024 mmol, 12 mol%), bipyridine **8g** (5.1 mg, 0.01 mmol, 5 mol%), 200 mg MS 4A and 2mL of DCM was stirred in 10ml Shlenk tube at room temperature for 1 hour. Then the solution of 1,2-dimethylindole **2a** (35 mg, 0.24 mmol, 1.2 eq) and diazoester **1c** (38 mg, 0.2 mmol, 1.0 eq) in 0.5 mL of DCM was added in one portion at room temperate. The reaction mixture was left stirring for 15 minutes, filtered through Celite and the solution was concentrated in vacuo. The crude product was purified by flash column chromatography using a mixture of petroleum ester/ethyl acetate (9:1) to give the desired product (**3ca)** as a light-yellow oil (54 mg, 88%), 5% ee. Enantiomeric excess was determined by chiral HPLC (IA-U column, 1.6 µm, *n*-hexane/ *i*-PrOH = 98:2, flow rate 0.4 mL/min, at 35 °C, UV detection at 254nm), t_{minor} = 3.6, t_{major} = 4.0.

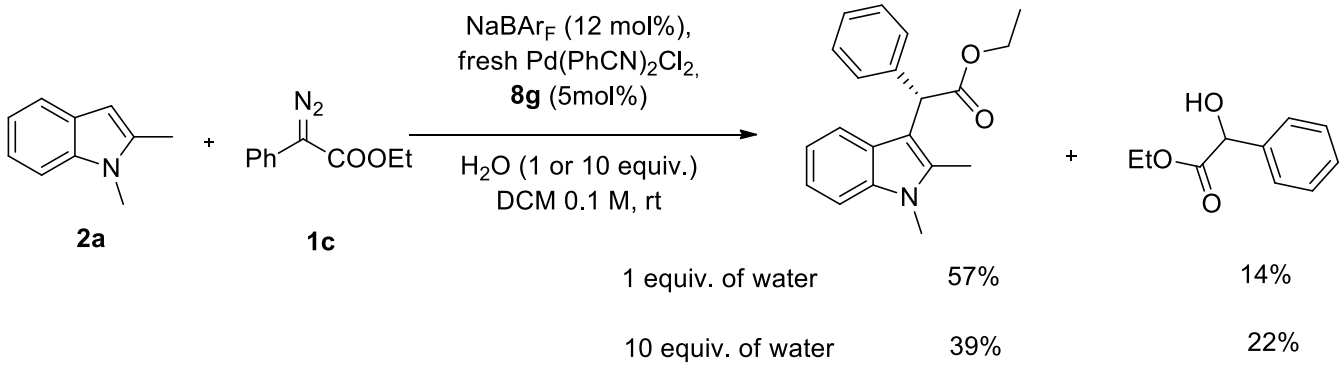

The mixture of $Pd(PhCN)_2Cl_2$ (3.8 mg, 0.01 mmol, 5 mol%), $NaBAr_F$ (21 mg, 0.024 mmol, 12 mol%), bipyridine **8g** (5.1 mg, 0.01 mmol, 5 mol%) and 2mL of DCM was stirred in 10ml Shlenk tube at room temperature for 1 hour. Then water (3.6µL, 0.2 mmol, 1 equiv.) was added using a microsyringe and the mixture was stirred for another 10 minutes. After the solution of 1,2-dimethylindole **2a** (35 mg, 0.24 mmol, 1.2 eq) and diazoester **1c** (38 mg, 0.2 mmol, 1.0 eq) in 0.5 mL of DCM was added in one portion at room temperate. The reaction mixture was left stirring for 15 minutes. The solution was concentrated in vacuo. The crude product was purified by flash column chromatography using a mixture of petroleum ester/ethyl acetate (gradient elution 20:1 to 4:1) to give in the order of elution the desired product (**3ca)** (35 mg, 57%, racemate) and ethyl mandelate (5 mg, 14%), 10% ee. Enantiomeric excess was determined by chiral HPLC (IB-U column, 1.6 µm, *n*-hexane/ *i*-PrOH = 90:10, flow rate 0.2 mL/min, at 35 °C, UV detection at 254nm), t_{major} = 4.7 t_{minor} = 5.8.

The mixture of $Pd(PhCN)_2Cl_2$ (3.8 mg, 0.01 mmol, 5 mol%), $NaBAr_F$ (21 mg, 0.024 mmol, 12 mol%), bipyridine **8g** (5.1 mg, 0.01 mmol, 5 mol%) and 2mL of DCM was stirred in 10ml Shlenk tube at room temperature for 1 hour. Then water (36μL, 2 mmol, 10 equiv.) was added using microsyringe and the mixture was stirred for another 10 minutes. After the solution of 1,2-dimethylindole **2a** (35 mg, 0.24 mmol, 1.2 eq) and diazoester **1c** (38 mg, 0.2 mmol, 1.0 eq) in 0.5 mL of DCM was added in one portion at room temperate. The reaction mixture was left stirring for 15 minutes. The solution was concentrated in vacuo. The crude product was purified by flash column chromatography using a mixture of petroleum ester/ethyl acetate (gradient elution 20:1 to 4:1) to give in the order of elution the desired product (**3ca)** (24 mg, 39%, racemate) and ethyl mandelate (8 mg, 22%), 10% ee.

6. Preparation of palladium source and general procedure for the alkylation of indoles

$Pd(PhCN)_2Cl_2$ was prepared using a slightly modified protocol [S13]. Benzonitrile 20 mL was added to 0.5 g (2.82 mmol) of palladium chloride. The reaction mixture was heated to 100 °C, stirred for 2 hours and filtered. 100 mL *n*-hexane was added to the filtrate followed by the formation of a yellow precipitate. The precipitate was separated by filtration, washed twice with 50 mL of hexane and dried in vacuo.

General method for the catalytic enantioselective alkylation of indoles with diazoacetates.

A solution of **7g** (0.01 mmol, 5 mol%), $Pd(PhCN)_2Cl_2$ (0.01 mmol, 5 mol%), and $NaBAr_F$ (0.024 mmol, 12 mol%) in DCM 2.00 mL was stirred at room temperature for 1 hour. Then indole derivative (0.240 mmol, 1.2 eq) and diazo compound (0.200 mmol, 1.0 eq) were added in one portion at room temperate and the reaction mixture was left for 10 minutes. The solution was concentrated in vacuo. The crude product was purified by flash column chromatography using a mixture of hexane/ethyl acetate (gradient elution 15:1 to 8:1) to give the desired product.

7. Characterization of functionalized indoles.

*(S)-Benzyl 2-(1,2-dimethyl-1H-indol-3-yl)-2-phenylacetate (**3aa**)*

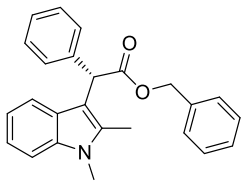

Obtained from 1,2-dimethylindole (34.8 mg, 0.240 mmol), benzyl 2-diazo-2-phenylacetate 50.4 mg, 0.200 mmol). Yellow oil (71.0 mg, 96%), 90% ee. Enantiomeric excess was determined by chiral HPLC (IC-3 column, *n*-hexane/ *i*-PrOH = 95:5, flow rate 1.0mL/min, UV detection at 254nm), t_{major}= 13.5 t_{minor}=18.5(Figure S60, Figure S61). $[\alpha]_D^{25}$= 74.25 (c = 0.37, $CHCl_3$). **^{1}H NMR** (400 MHz, $CDCl_3$): δ_H 2.37 (s, 3H), 3.69 (s, 3H), 5.13 (d, *J* = 12.4 Hz, 1H), 5.22 (d, *J* = 12.4 Hz, 1H), 5.45 (s, 1H), 7.08 (m, 1H), 7.22 (m, 1H), 7.34 (m, 11H), 7.54 (m, 1H) (Figure S26). **^{13}C NMR** (101 MHz, $CDCl_3$): δ_c 10.9, 29.8, 48.5, 66.8, 107.9, 108.8, 119.4, 119.6, 120.9, 126.8, 127.0, 128.2, 128.3, 128.4, 128.4, 128.5, 135.0, 136.1, 136.8, 138.9, 173.2 (Figure S27). In agreement with literature.[S7]

*(S)-Benzyl 2-(2-ethyl-1-methyl-1H-indol-3-yl)-2-phenylacetate (**3ab**)*

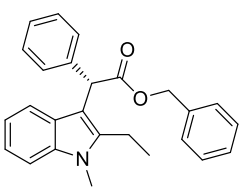

Obtained from 2-Ethyl-1-metylmethylindole (38.2 mg, 0.240 mmol) and benzyl 2-diazo-2-phenylacetate (50.4 mg, 0.200 mmol). Yellow oil (72.9 mg, 94%), 90% ee. Enantiomeric excess was determined by chiral HPLC (IC-3 column, *n*-hexane/ *i*-PrOH = 95:5, flow rate 1.0mL/min, UV detection at 254nm), t_{major}= 12.4 t_{minor}=18.1 (Figure S62, Figure S63). $[\alpha]_D^{25}$= 68.39 (*c* = 0.30, $CHCl_3$).**^{1}H NMR** (400 MHz, $CDCl_3$): δ_H 1.09 (t, *J*=7.2 Hz, 3H), 2.80 (q, *J*=7.2 Hz, 2H), 3.70 (s, 3H), 5.12 (d, *J* = 12.4 Hz, 1H), 5.24 (d, *J* = 12.4 Hz, 1H), 5.35 (s, 1H), 6.99 (m, 1H), 7.16

(m, 1H), 7.25 (m, 11H), 7.46 (m, 1H)(Figure S28). **^{13}C NMR** (101 MHz, $CDCl_3$): δc 14.3, 18.1, 29.7, 48.5, 66.8, 107.2, 108.8, 119.4, 120.3, 121.0, 126.8, 126.9, 128.2, 128.3, 128.3, 128.4, 128.5, 136.1, 137.0, 139.1, 140.7, 173.1(Figure S29). **HRMS (ESI)** 384.1964 ($C_{26}H_{26}NO_2$ $[M+H]^+$ requires 384.1964).

*(S)-Benzyl 2-(2-phenyl-1-methyl-1H-indol-3-yl)-2-phenylacetate (**3ac**)*

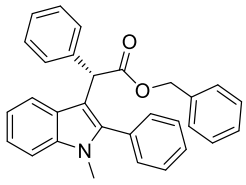

Obtained from 1-Methyl-2-phenyl-indole (49.7 mg,) and Benzyl 2-diazo-2-phenylacetate (50.4 mg, 0.200 mmol). Yellow oil (81.9 mg, 95%), 77% ee. Enantiomeric excess was determined by chiral HPLC (IC-3 column, *n*-hexane/*i*-PrOH = 95:5, flow rate 1.0mL/min, UV detection at 254nm), t_{major} = 12.5 t_{minor} = 21.3(Figure S64, Figure S65). $[\alpha]_D^{25}$= 51.44 (c= 0.20, $CHCl_3$). **^{1}H NMR** (500 MHz, $CDCl_3$): δ_H 3,62 (s, 3H), 5.14 (d, *J* = 12.5 Hz, 1H), 5.18 (d, *J* = 12.5 Hz, 1H), 5.23(s, 1H), 7.07(m, 1H), 7.25(m, 8H), 7.30(m, 3H), 7.46(m, 3H), 7.59 (m, 1H)(Figure S30). **^{13}C NMR** (126 MHz, $CDCl_3$): δ_c 32.9. 49.0, 66.9, 109.4, 112.1, 119.2, 119.3, 121.9, 127.2, 127.3, 128.0, 128.3, 128.3, 128.6, 128.6, 128.6, 136.0, 137.1, 138.8, 173.0(Figure S31). In agreement with literature.[S7]

*(S)-Benzyl 2-(1-methyl-1H-indol-3-yl)-2-phenylacetate (**3ad**)*

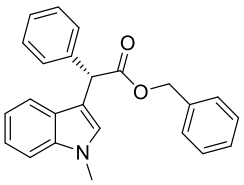

Obtained from 1-Methyl-indole (31.4 mg, 0.240 mmol) and benzyl 2-diazo-2-phenylacetate (50.4 mg, 0.200 mmol). Colorless oil (67.5 mg, 95%), 34 % ee. Enantiomeric excess was determined by chiral HPLC (IC-3 column, *n*-hexane/*i*-PrOH = 95:5, flow rate 1.0mL/min, UV .detection at 254nm), t_{major} = 9.7 t_{minor} = 14.3(Figure S66, Figure S67). $[\alpha]_D^{25}$= 14.88 (*c*= 0.35, $CHCl_3$). **^{1}H NMR** (400 MHz, $CDCl_3$): δ_H 3.73 (s, 3H), 5.19 (d, *J* = 12.4 Hz, 1H), 5.24 (d, *J* = 12.4 Hz, 1H), 5.33 (s, 1H), 7.03 (s, 1H), 7.05 (m, 1H), 7.29 (m, 10H), 7.44 (m, 3H)(Figure S32). **^{13}C NMR** (101 MHz, $CDCl_3$): δ_c 32.9, 49.0, 66.9, 109.4, 112.1, 119.2, 119.3, 121.9, 127.2, 127.3, 127.3, 128.0, 128.3, 128.3, 128.6, 128.6, 128.6, 136.0, 137.1, 138.8, 173.0(Figure S33). In agreement with literature.[S14]

*(S)-Benzyl 2-(1-ethyl-2-methyl-1H-indol-3-yl)-2-phenylacetate (**3ae**)*

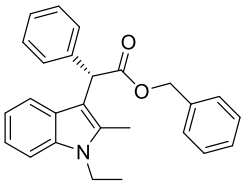

Obtained from 1-Ethyl-2-methyl-indole (38.2 mg, 0.240 mmol) and benzyl 2-diazo-2-phenylacetate (50.4 mg, 0.200 mmol). Pale-yellow oil (71.2 mg, 93%), 89% ee. Enantiomeric excess was determined by chiral HPLC (IC-3 column, *n*-hexane/*i*-PrOH = 95:5, flow rate 1.0mL/min, UV .detection at 254nm), t_{major} = 11.3, t_{minor} = 13.8(Figure S68, Figure S69). $[\alpha]_D^{25}$ = 64.38 (*c* = 0.25, $CHCl_3$). **^{1}H NMR** (500 MHz, $CDCl_3$): δ_H 1.37 (t, *J* = 7.0 Hz, 3H), 2.35 (s, 3H), 4.16 (q, *J* = 7.0 Hz, 2H), 5.19 (d, *J* = 12.4 Hz, 1H), 5.26 (d, *J* = 12.4 Hz, 1H), 5.42(s, 1H), 7.05 (m, 1H), 7.19 (m, 1H), 7.28 (m, 11H), 7.52 (m, 1H)(Figure S34). **^{13}C NMR** (126 MHz, $CDCl_3$): δ_c 10.6,

15.4, 38.0, 48.4, 66.70, 107.9, 108.8, 119.3, 119.7, 120.8, 126.8, 127.2, 128.1, 128.2, 128.3, 128.4, 128.5, 134.1, 135.7, 136.1, 138.9, 173.1(Figure S35). In agreement with literature.[S15]

*(S)-Benzyl 2-(1-benzyl-2-methyl-1H-indol-3-yl)-2-phenylacetate (**3af**)*

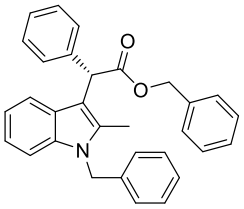

Obtained from 1-Benzyl-2-methyl-indole (53.0 mg, 0.240 mmol) and benzyl 2-diazo-2-phenylacetate (50.4 mg, 0.200 mmol). Colorless oil (81.9 mg, 92 %), 86% ee. Enantiomeric excess was determined by chiral HPLC (IC-3 column, *n*-hexane/*i*-PrOH = 95:5, flow rate 1.0mL/min, UV .detection at 254nm), t_{major} = 12.2, t_{minor} = 18.9(Figure S70, Figure S71). $[\alpha]_D^{25}$ = 48.57 (*c* = 0.20, $CHCl_3$) **^{1}H NMR** (400 MHz, $CDCl_3$): δ_H 2.25 (s, 3H), 5.17 (d, *J* = 12.5 Hz, 1H), 5.21 (d, *J* = 12.5 Hz, 1H), 5.32(s, 2H), 5.40(s, 1H), 6.95 (m, 2H), 7.01 (m, 1H), 7.11 (m, 1H), 7.25 (m, 14H), 7.49 (m, 1H)(Figure S36). **^{13}C NMR** (101 MHz, $CDCl_3$): δc 10.9, 46.7, 48.4, 66.8, 108.6, 109.2, 119.7, 121.3, 126.0, 126.9, 127.3, 127.4, 128.2, 128.2, 128.4, 128.4, 128.5, 129.0, 134.9, 136.1, 136.7, 137.8, 138.7, 173.1(Figure S37). In agreement with literature.[S7]

*(S)-Benzyl 2-(5-chloro-1,2-dimethyl-1H-indol-3-yl)-2-phenylacetate (**3ag**)*

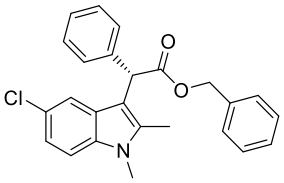

Obtained from 5-Chloro-1,2-dimethyl-indole (43.0 mg, 0.240 mmol) and benzyl 2-diazo-2-phenylacetate (50.4 mg, 0.200 mmol). Colorless oil (72.5 mg, 90%), 84% ee. Enantiomeric excess was determined by chiral HPLC (IC-3 column, *n*-hexane/*i*-PrOH = 95:5, flow rate 1.0mL/min, UV .detection at 254nm), t_{major} = 15.3, t_{minor} = 17.1(Figure S72, Figure S73). $[\alpha]_D^{25}$= 57.95 (*c*=0.25, $CHCl_3$). **^{1}H NMR** (400 MHz, $CDCl_3$): δ_H 2.29 (s, 3H), 3.63 (s, 3H), 5.15 (d, *J* = 12.4 Hz, 2H), 5.21 (d, *J* = 12.4 Hz, 2H), 5.30 (s, 1H), 7.08 (m, 1H), 7.15 (m 1H, **Ar**), 7.25 (m, 10H), 7.41 (m, 1H)(Figure S38). **^{13}C NMR** (101 MHz, $CDCl_3$) δc 11.0, 29.9, 48.4, 67.0, 107.7, 109.8, 119.0, 121.2, 125.2, 127.0, 128.0, 128.3, 128.3, 128.4, 128.5, 128.6, 135.3, 135.9, 136.8, 138.5, 172.9(Figure S39). **HRMS (ESI)** 404.1412 ($C_{25}H_{23}{}^{35}ClNO_2$ $[M+H]^+$ requires 404.1417).

*(S)-Benzyl 2-(1,2-Dimethyl-1H-indol-5-methoxy-3-yl)-2-phenylacetate (**3ah**)*

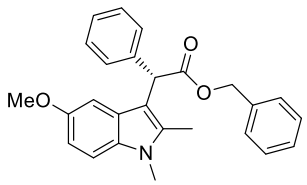

Obtained from 1,2-Dimethyl-5-methoxy-indole (42.0 mg, 0.240 mmol) and benzyl 2-diazo-2-phenylacetate (50.4 mg, 0.200 mmol). Pale-yellow oil (75.8 mg, 95%), 92% ee. Enantiomeric excess was determined by chiral HPLC (IC-3 column, *n*-hexane/*i*-PrOH = 95:5, flow rate 1.0mL/min, UV .detection at 254nm), t_{major} = 23.0, t_{minor} = 28.2 (Figure S74, Figure S75). $[\alpha]_D^{25}$= 63.76 (*c*=0.24, $CHCl_3$). **^{1}H NMR** (400 MHz, $CDCl_3$): δ_H 2.28 (s, 3H), 3.62 (s, 3H), 3.63 (s, 3H), 5.14 (d, *J* =12.6 Hz, 1H), 5.20 (d, *J* =12.6 Hz, 1H), 5.32 (s, 1H), 6.78 (m, 1H), 6.87 (m, 1H), 7.14 (m, 1H), 7.24 (m, 10H)(Figure S40). **^{13}C NMR** (101 MHz, $CDCl_3$): δ_c

11.0, 29.9, 48.5, 55.9, 66.8, 101.8, 107.4, 109.4, 110.8, 126.9, 127.3, 128.2, 128.3, 128.4, 128.5, 132.1, 135.6, 136.1, 138.8, 154.0, 173.2(Figure S41) In agreement with literature.[S7]

*(S)-Methyl 2-(1,2-Dimethyl-1H-indol-3-yl)-2-phenylacetate (**3ba**)*

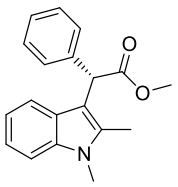

Obtained from 1,2-Dimethyl-indole (34.8 mg, 0.240 mmol) and methyl 2-diazo-2-phenylacetate (35.2 mg, 0.200 mmol). Colorless oil (55.1 mg, 94%), 89% ee. Enantiomeric excess was determined by chiral HPLC (IC-3 column, *n*-hexane/*i*-PrOH = 95:5, flow rate 1.0mL/min, UV .detection at 254nm), t_{major} = 13.2, t_{minor} = 19.9(Figure S76, Figure S77). $[\alpha]_D^{25}$= 60.51 (*c*=0.20, $CHCl_3$). **^{1}H NMR** (400 MHz, $CDCl_3$): δ_H 2.35 (s, 3H), 3.67 (s, 3H), 3.72 (s, 3H), 5.31 (s, 1H), 7.03 (m, 1H), 7.15 (m, 1H), 7.26 (m, 6H), 7.47 (m, 1H)(Figure S42). **^{13}C NMR** (101 MHz, $CDCl_3$): δ_c 10.9, 29.8, 48.3, 52.3, 108.0, 108.9, 119.4, 119.5, 120.9, 126.9, 127.0, 128.4, 128.4, 134.9, 136.8, 139.0, 173.9(Figure S43). In agreement with literature.[S16]

*(S)-Ethyl 2-(1,2-Dimethyl-1H-indol-3-yl)-2-phenylacetate (**3ca**)*

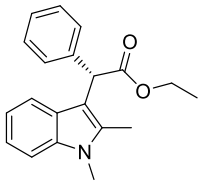

Obtained from 1,2-Dimethyl-indole (34.8 mg, 0.240 mmol) and ethyl 2-diazo-2-phenylacetate (38.0 mg, 0.200 mmol). Pale-yellow oil (59.6 mg, 97%), 93% ee. Enantiomeric excess was determined by chiral HPLC (IC-3 column, *n*-hexane/*i*-PrOH = 95:5, flow rate 1.0mL/min, UV .detection at 254nm), t_{major} = 12.8, t_{minor} = 20.2(Figure S78, Figure S79). $[\alpha]_D^{25}$ = 62.48 (*c* = 0.25, $CHCl_3$). **^{1}H NMR** (500 MHz, $CDCl_3$): δ_H 2.38 (s, 3H), 3.69 (s, 3H), 4.22 (m, 2H), 5.32 (s, 1H), 7.05 (m, 1H), 7.17 (m, 1H), 7.24 (m, 1H), 7.29 (m, 5H), 7.52 (m, 1H)(Figure S44). **^{13}C NMR** (126 MHz, $CDCl_3$): δ_c 10.9, 14.4, 29.7, 48.5, 61.2, 108.0, 108.8, 119.3, 119.6, 120.8, 126.8, 127.0, 128.4, 134.9, 136.8, 139.2, 173.4(Figure S45). In agreement with literature.[S17]

*(S)-Isopropyl 2-(1,2-Dimethyl-1H-indol-5-3-yl)-2-phenylacetate (**3da**)*

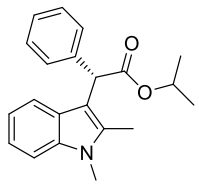

Obtained from 1,2-Dimethyl-indole (34.8 mg, 0.240 mmol) and isopropyl 2-diazo-2-phenylacetate (40.8 mg, 0.200 mmol). Yellow oil (59.7 mg, 93 %), 90 %ee. Enantiomeric excess was determined by chiral HPLC (IC-3 column, *n*-hexane/*i*-PrOH = 95:5, flow rate 1.0mL/min, UV .detection at 254nm), t_{major} = 7.3, t_{minor} = 9.5(Figure S80, Figure S81). $[\alpha]_D^{25}$= 64.88 (*c*=0.20, $CHCl_3$). **^{1}H NMR** (400 MHz, $CDCl_3$): δ_H 1.17 (d, *J* = 6.3 Hz, 3H), 1.25 (d, *J* = 6.3 Hz, 3H),), 2.36 (s, 3H), 3.67 (s, 3H), 5.09 (hept, *J* = 6.3 Hz, 1H), 5.27 (s, 1H), 7.02 (m, 1H), 7.15 (m, 1H), 7.21 (m, 1H), 7.27 (m, 5H), 7.51 (m, 1H)(Figure S46). **^{13}C NMR** (101 MHz, $CDCl_3$): δ_c 10.9, 21.9, 22.0, 29.7, 48.8, 68.6, 108.2, 108.7, 119.2, 119.8, 120.8, 126.7, 127.1, 128.3, 134.9, 136.8, 139.4, 172.9(Figure S47). **HRMS (ESI)** 322.1804 ($C_{21}H_{24}NO_2$ $[M+H]^+$ requires 322.1807).

*(S)-Benzyl 2-(1,2-Dimethyl-1H-indol-5-methoxy-3-yl)-2-(4-chloro phenyl) acetate (**3ea**)*

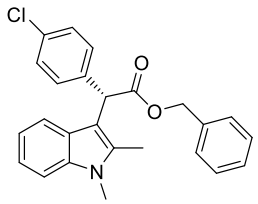

Obtained from 1,2-Dimethyl-indole (34.8 mg, 0.240 mmol) and benzyl 2-diazo-2-(4-chlorophenyl) acetate (57.2 mg, 0.200 mmol). Colorless oil (77.4 mg, 96%), 93% ee. Enantiomeric excess was determined by chiral HPLC (IA-3 column, *n*-hexane/*i*-PrOH = 99.5:0.5, flow rate 0.6 mL/min, UV .detection at 254nm), t_{major} = 57.8, t_{minor} = 67.6(Figure S82, Figure S83). $[\alpha]_D^{25}$= 71.33 (*c*=0.25, $CHCl_3$). **^{1}H NMR** (400 MHz, $CDCl_3$): δ_H 2.32 (s, 3H), 3.67 (s, 3H), 5.14 (d, *J* = 12.4 Hz, 1H), 5.23 (d, *J* = 12.4 Hz, 1H), 5.32 (s, 1H), 7.02 (m, 1H), 7.25 (m, 10H), 7.43 (m, 1H)(Figure S48). **^{13}C NMR** (101 MHz, $CDCl_3$): δ_c 10.8, 29.7, 47.8, 67.0, 107.4, 108.9, 119.4, 119.5, 121.0, 126.8, 128.3, 128.4, 128.5, 128.5, 129.8, 132.7, 135.0, 135.9, 136.8, 137.4, 172.8(Figure S49). In agreement with literature.[S7]

*(S)-Benzyl 2-(1,2-Dimethyl-1H-indol-5-methoxy-3-yl)-2-(4-methoxy phenyl) acetate (**3fa**)*

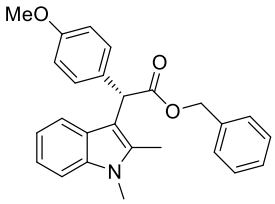

Obtained from 1,2-Dimethyl-indole (34.8 mg, 0.240 mmol) and benzyl 2-diazo-2-(4-methoxyphenyl) acetate (56.4 mg, 0.200 mmol). Colorless oil (73.4 mg, 92%), 84% ee. Enantiomeric excess was determined by chiral HPLC (IA-3 column, *n*-hexane/*i*-PrOH = 98:2, flow rate 1.0 mL/min, UV .detection at 254nm), t_{major} = 19.5, t_{minor} = 22.0(Figure S84, Figure S85). $[\alpha]_D^{25}$= 67.50 (*c*=0.20, $CHCl_3$). **^{1}H NMR** (400 MHz, $CDCl_3$): δ_H 2.33 (s, 3H), 3.66 (s, 3H), 3.77 (s, 3H), 5.15 (d, J = 12.4 Hz, 1H), 5.24 (d, J = 12.4 Hz, 1H), 5.33 (s, 1H), 6.82 (m, 2H), 7.03 (m, 1H), 7.25 (m, 9H), 7.49 (m, 1H)(Figure S54). **^{13}C NMR** (101 MHz, $CDCl_3$) δ_c 10.8, 29.7, 47.6, 55.3, 66.8, 108.1, 108.7, 113.7, 119.3, 119.5, 120.8, 127.0, 128.1, 128.3, 128.5, 129.4, 131.0, 134.8, 136.1, 136.8, 158.4, 173.4(Figure S55) In agreement with literature.[S7]

*(S)-Benzyl 2-(1,2-Dimethyl-1H-indol-5-methoxy-3-yl)-2-(2-naphtalene-2-yl) acetate (**3ga**)*

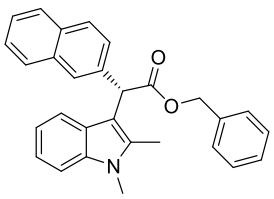

Obtained from 1,2-Dimethyl-indole (34.8 mg, 0.240 mmol) and benzyl 2-diazo-2-naphthylacetate (60.4 mg, 0.200 mmol). Colorless foam (77.1 mg, 92%), 87% ee. Enantiomeric excess was determined by chiral HPLC (IC-3 column, *n*-hexane/*i*-PrOH = 90:10, flow rate 1.0 mL/min, UV .detection at 254nm), t_{major} = 11.9, t_{minor} = 13.3(**Figure S86**, **Figure S87**). $[\alpha]_D^{25}$= 59.67 (*c*=0.15, $CHCl_3$). **^{1}H NMR** (400 MHz, $CDCl_3$): δ_H 2.33 (s, 3H), 3.67 (s, 3H), 5.19 (d, J = 12.4 Hz, 1H), 5.28 (d, J = 12.4 Hz, 1H), 5.54 (s, 1H), 7.01 (m, 1H), 7.17 (m, 1H), 7.29(m, 6H), 7.41 (m, 3H), 7.50 (m, 1H), 7.74 (m, 4H)(**Figure S52**). **^{13}C NMR** (101 MHz, $CDCl_3$): δ_c 10.9, 29.7, 48.6, 66.9, 107.8, 108.8, 119.5, 120.9, 125.8, 126.0, 126.6, 127.0, 127.1, 127.6, 128.0, 128.1, 128.2, 128.5, 128.6, 132.5, 133.4, 135.1, 136.1, 136.5, 136.8, 173.1(**Figure S53**). In agreement with literature [S7].

*(S)-Methyl 2-(1,2-Dimethyl-1H-indol-5-methoxy-3-yl)-2-(2-naphtalene-2-yl) acetate (**3ha**)*

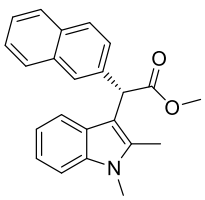

Obtained from 1,2-Dimethyl-indole (34.8 mg, 0.240 mmol) and methyl 2-diazo-2-naphthylacetate (45.2 mg, 0.200 mmol). Colorless foam (64.5 mg, 94%), 87% ee. Enantiomeric excess was determined by chiral HPLC (IC-3 column, *n*-hexane/*i*-PrOH = 90:10, flow rate 1.0 mL/min, UV .detection at 254nm), t_{major} = 12.4, t_{minor} = 16.2. $[\alpha]_D^{25}$= 62.31(**Figure S88**, **Figure S89**) (*c*=0.20, $CHCl_3$). **^{1}H NMR** (400 MHz, $CDCl_3$): δ_H 2.39 (s, 3H), 3.70 (s, 3H), 3.78 (s, 3H), 5.50 (s, 1H), 7.07(m, 1H), 7.19 (m, 1H), 7.31 (m, 1H), 7.44 (m, 3H), 7.55 (m, 1H), 7.78 (m, 4H)(**Figure S54**). **^{13}C NMR** (101 MHz, $CDCl_3$) δ_c 10.9, 29.8, 48.5, 52.4, 107.8, 108.9, 119.3, 119.6, 121.0, 125.8, 126.1, 126.6, 127.0, 127.1, 127.7, 128.1, 128.1, 132.5, 133.4, 135.1, 136.5, 136.8, 173.9(**Figure S55**). **HRMS (ESI)** 344.1650 ($C_{23}H_{22}NO_2$ $[M+H]^+$ requires 344.1651.

*(S)-Methyl 2-(4-chlorophenyl)-2(1,2-dimethyl-1H-indol-3-yl)-acetate (**3ia**)*

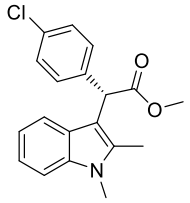

Obtained from 1,2-Dimethyl-indole (34.8 mg, 0.240 mmol) and methyl 2-(4-chlorophenyl)-2-diazoacetate (42.1 mg, 0.200 mmol). White solid (60 mg, 91%), m.p. 128-130ºC. 86% ee. Enantiomeric excess was determined by chiral HPLC (IA-3 column, *n*-hexane/*i*-PrOH = 98:2, flow rate 0.4 mL/min, UV .detection at 254nm), t_{major} = 39.1, t_{minor} = 33.6. $[\alpha]_D^{25}$ = 63.71(Figure S90, Figure S91) (*c*=0.45, $CHCl_3$). **^{1}H NMR** (400 MHz, $CDCl_3$): δ_H), 2.35 (s, 3H), 3.68 (s, 3H), 3.72 (s, 3H), 5.26 (s, 1H), 7.04 (m, 1H), 7.21 (m, 5H), 7.28 (m, 1H),) 7.45 (m, 1H)(Figure S56). **^{13}C NMR** (101 MHz, $CDCl_3$) δ_c 10.74, 29.8, 47.60, 52.4, 107.5, 108.9, 119.1, 119.6, 121.1, 126.7, 128.5, 129.8, 132.7, 134.9, 136.8, 137.5, 173.5(Figure S57). In agreement with literature.[S18]

*(S)-Methyl 2-(1,2-dimethyl-1H-indol-3-yl)-2-(4-iodophenyl)acetate (**3ka**)*

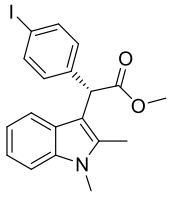

Obtained from 1,2-Dimethyl-indole (100 mg, 0.689 mmol) and methyl 2-(4-iodophenyl)-2-diazoacetate (173 mg, 0.574 mmol). White solid (225 mg, 94%), m.p. 139 ºC. 84% ee. Enantiomeric excess was determined by chiral HPLC (i-Amylose-1, MeCN/H_2O= 40:60, flow rate 0.6 mL/min, UV .detection at 254 nm), t_{major} =181.1.1, t_{minor} = 187.3(Figure S92, Figure S93). $[\alpha]_D^{23}$ = 59.67 (*c*=1.365, $CHCl_3$). **^{1}H NMR** (400 MHz, $CDCl_3$): δ_H 2.35 (s, 3H), 3.68 (s, 3H), 3.73 (s, 3H), 5.24 (s, 1H), 7.04 (m, 3H), 7.17 (m, 1H), 7.28 (m, 1H), 7.45 (m, 1H), 7.59 (m, 2H)(Figure S58). **^{13}C NMR** (101 MHz, $CDCl_3$) δ_c 10.8, 29.8, 47.9, 52.3, 92.4, 107.5, 109.0, 119.2, 121.1, 126.9, 130.6, 134.9, 136.9, 137.5, 138.8, 173.3(Figure S59).

.

8. X-Ray characterization data 3ka

Crystals for XRD measurements were grown from ethyl acetate-petroleum ether. In the experiment, a fraction of colorless prismatic crystals was studied on an automatic four-circle diffractometer Xcalibur R with χ-geometry, monochromated Mo*K*α radiation, and ω-scanning. In the study, the software CrysAlisPro was used.[S19] The extinction was accounted for empirically using the algorithm SCALE3 ABSPACK.[S19] The structure was solved and refined by applying the program package SHELX2016.[S20] All nonhydrogen atoms were solved and refined independently in the anisotropic approximation, the hydrogen atoms were placed in the geometrically calculated positions and included in the refinement in the *rider* model with dependent thermal parameters. The structure of molecule **3ka** is shown in Figure S15. All bond lengths and bond angles are within the common value range for the corresponding atoms. The data on the crystal are deposited in the Cambridge Crystallographic Data Center under the number CCDC 2168620.

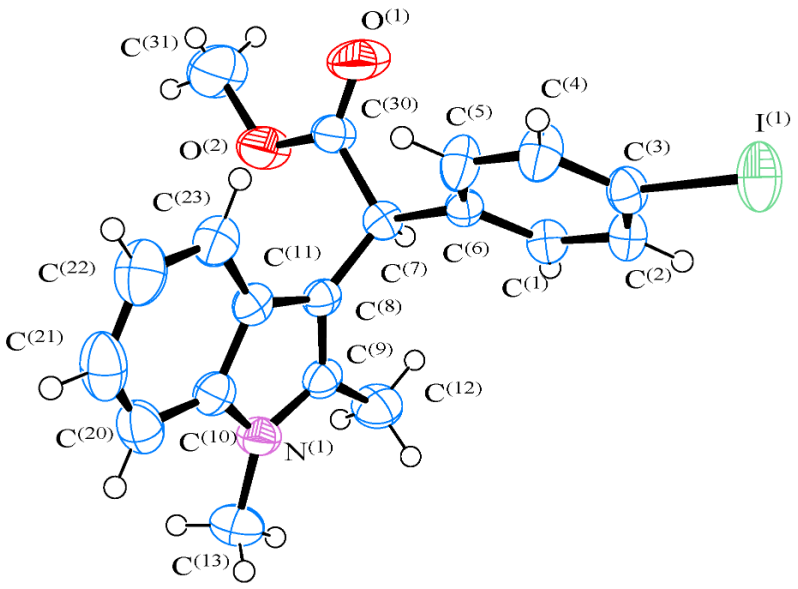

Figure S18. The molecular structure of compound **3ka** presented using thermal ellipsoids of the 50% probability

Table S6. Crystal data and structure refinement for **3ka**

Empirical formula	$C_{19}H_{18}INO_2$	μ/mm^{-1}	1.796
Formula weight	419.265	F(000)	830.9
Temperature/K	290	Crystal size/mm^3	0.6 × 0.4 × 0.2
Crystal system	orthorhombic	Radiation	MoKα (λ = 0.71073)
Space group	$P2_12_12_1$	2Θ range for data collection/°	5.88 to 58.48
a/Å	8.6720(15)	Index ranges	$-7 \le h \le 11$, $-10 \le k \le 15$, $-24 \le l \le 20$
b/Å	11.5386(14)	Reflections collected	8315
c/Å	17.909(2)	Independent reflections	4208 [R_{int} = 0.0225, R_{sigma} = 0.0355]
α/°	90	Data/restraints/parameters	4208/0/213
β/°	90	Goodness-of-fit on F^2	1.017
γ/°	90	Final R indexes [I>=2σ (I)]	R_1 = 0.0312, wR_2 = 0.0648
Volume/$Å^3$	1792.0(4)	Final R indexes [all data]	R_1 = 0.0386, wR_2 = 0.0688
Z	4	Largest diff. peak/hole / e $Å^{-3}$	0.41/-0.82
$\rho_{calc}g/cm^3$	1.554	Flack parameter	0.020(12)

9. Computational Details

Molecular geometries were optimized using density functional theory with the TPSS density functional and the def2-SV(P) basis set along with the associated effective core potential for Pd [S21-23] and the D3(Becke-Johnson) dispersion.[S24] These structure optimizations and subsequent vibrational analyses were performed in gas phase. At the optimized geometries additional D3-TPSS/def2-TZVP single point computations using the SMD model for dichloromethane (DCM) were performed.[25] The reported values (ΔG_{DCM}) are a combination of electronic and solvation free energies obtained from the D3-TPSS(SMD)/def2-TZVP single-point computations along with enthalpy and entropy corrections derived from the D3-TPSS/def2-SV(P) gas-phase vibrational analyses (using the standard free-particle/rigid-rotor/harmonic-oscillator model). Some additional single-point computations employed the M11-L functional.[S26] Computations were carried out using Q-Chem 5.4.[S27] The underlying research data (molecular structures and input/output files of Q-Chem) are available via a separate repository, DOI:10.17028/rd.lboro.19722937.

Computational Results

Table S7. Detailed analysis of computed reaction energies for the S and R reaction paths, presenting gas-phase electronic energies (ΔE_{gas}; D3-TPSS/def2-SV(P)), electronic energies including DCM solvation (ΔE_{DCM}; D3-TPSS/def2-TZVP), enthalpies (ΔH_{DCM}; D3-TPSS/def2-TZVP), and Gibbs free energies (ΔG_{DCM}; D3-TPSS/def2-TZVP).

	***S* reaction path**				***R* reaction path**			
	ΔE_{gas}	ΔE_{DCM}	ΔH_{DCM}	ΔG_{DCM}	ΔE_{gas}	ΔE_{DCM}	ΔH_{DCM}	ΔG_{DCM}
E	0.00	0.00	0.00	0.00				
[E+1]	-38.28	-27.99	-26.90	-11.37	-36.62	-27.94	-28.32	-10.68
TS-1	-36.03	-27.15	-27.00	-12.23	-36.30	-27.86	-27.51	-10.50
F	-54.61	-49.32	-49.34	-44.77	-56.43	-49.10	-50.66	-43.36
TS-2	-52.82	-46.45	-47.59	-39.57	-51.20	-46.24	-46.84	-40.84
C	-85.99	-80.64	-80.09	-76.23	-85.89	-79.00	-78.22	-72.72
B'+H2O	-86.20	-64.26	-63.22	-46.09	-78.33	-62.74	-62.32	-44.47
TS-3	-79.12	-60.04	-60.72	-42.88	-79.42	-58.93	-59.52	-41.59
3aa (bound)	-97.07	-75.58	-72.22	-55.33	-92.66	-74.25	-73.11	-53.39
E + 3aa (free)		-45.23	-44.61	-43.58				

Table S8. Molecular structures, optimized at the D3-TPSS/def2-SV(P) level, for intermediates and transition states leading to product **3aa**. The reaction paths leading to the S and R products are shown to the left and right, respectively.

	S path	R path
[E+1b]	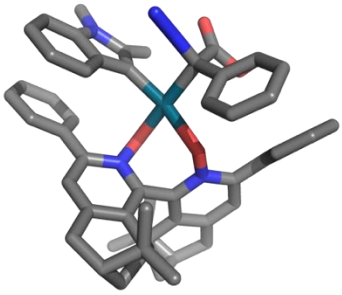	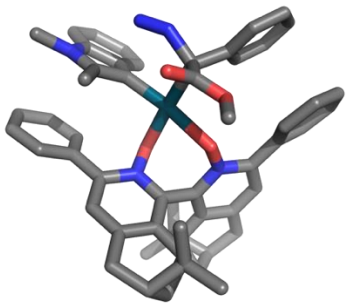
TS-1	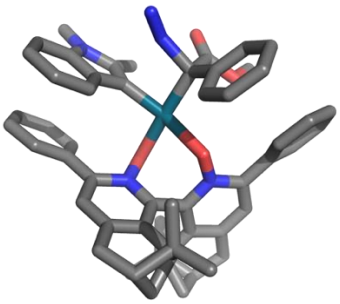	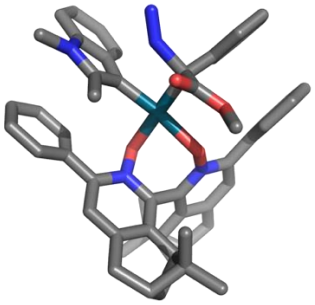
F	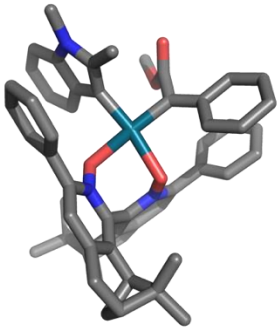	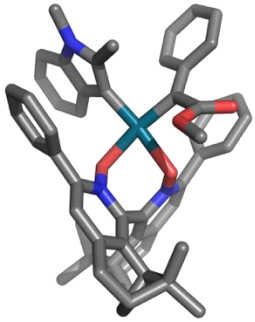
TS-2	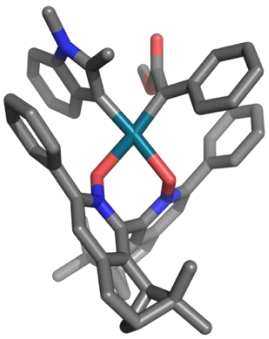	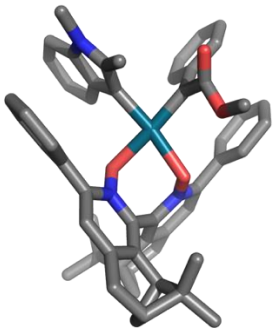

	S path	R path
C	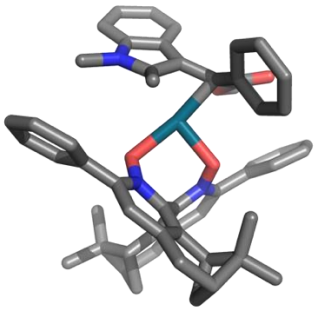	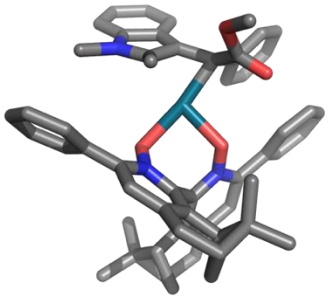
B' + H_2O	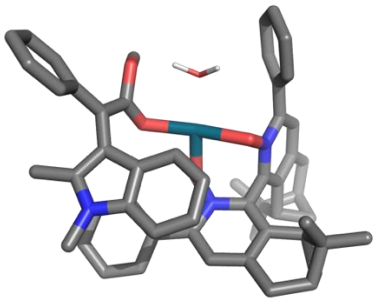	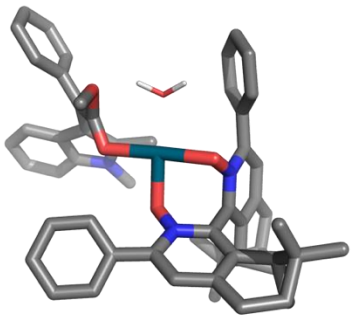
TS-3	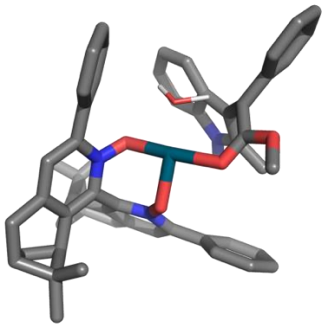	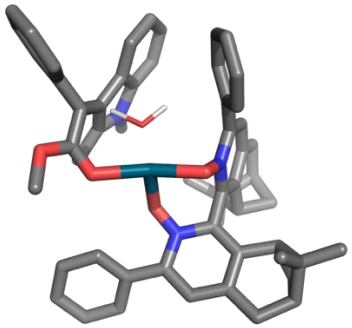
3ba (bound)	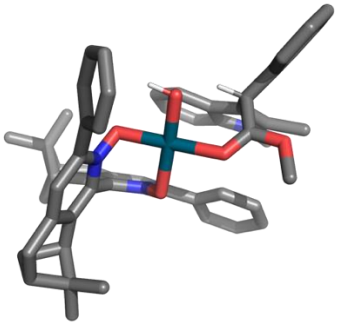	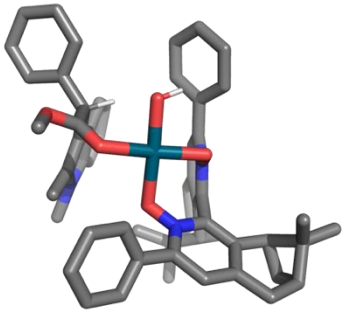
3ba	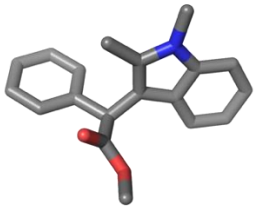	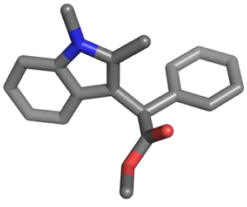

Table S9. Depiction of the molecular dipole moment for the two diastereomers of TS-3 computed at the D3-TPSS(SMD)/def2-TZVP level using D3-TPSS/def2-SV(P) geometries.

	S path	*R* path
TS-3	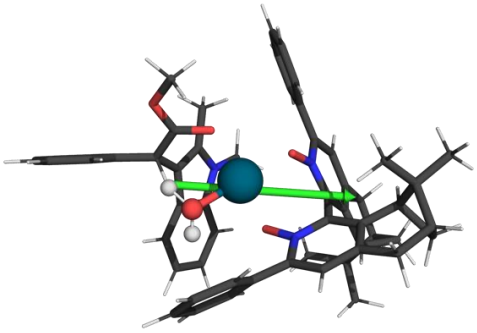	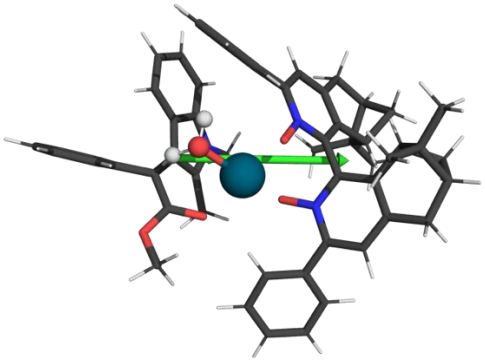

10. NMR spectra

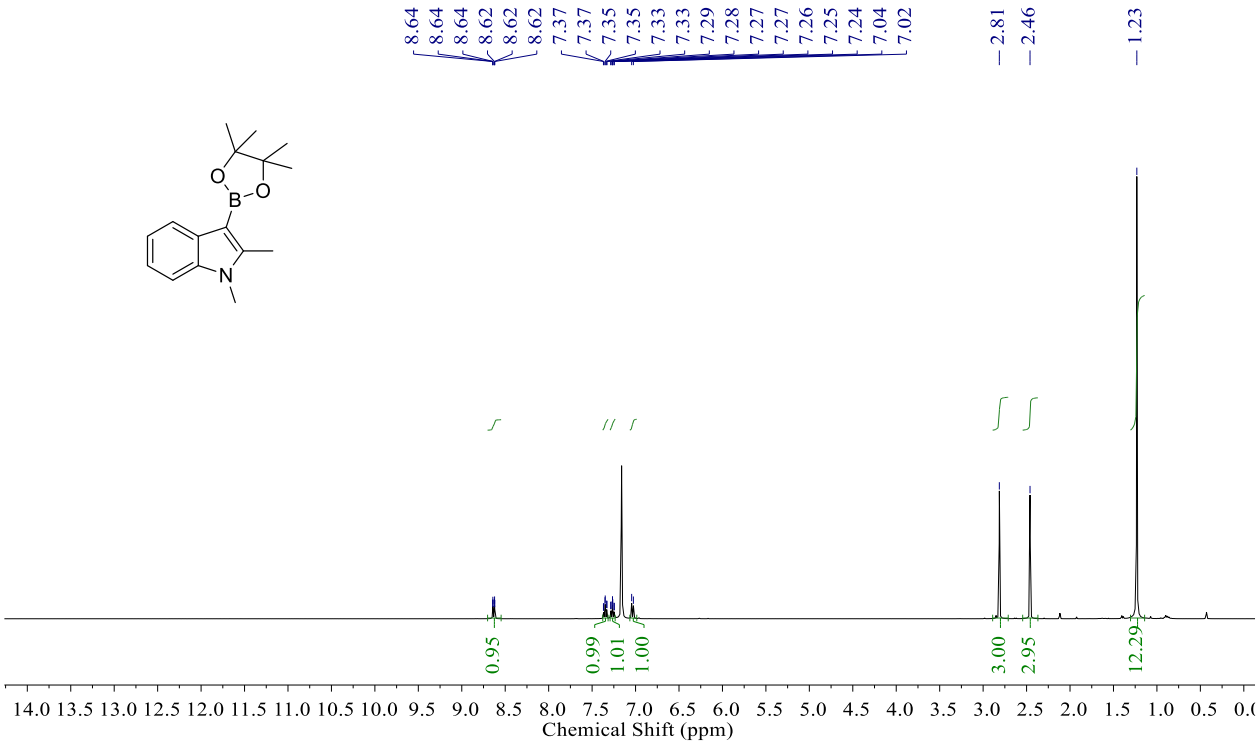

Figure S19. ^{1}H NMR, **10a**

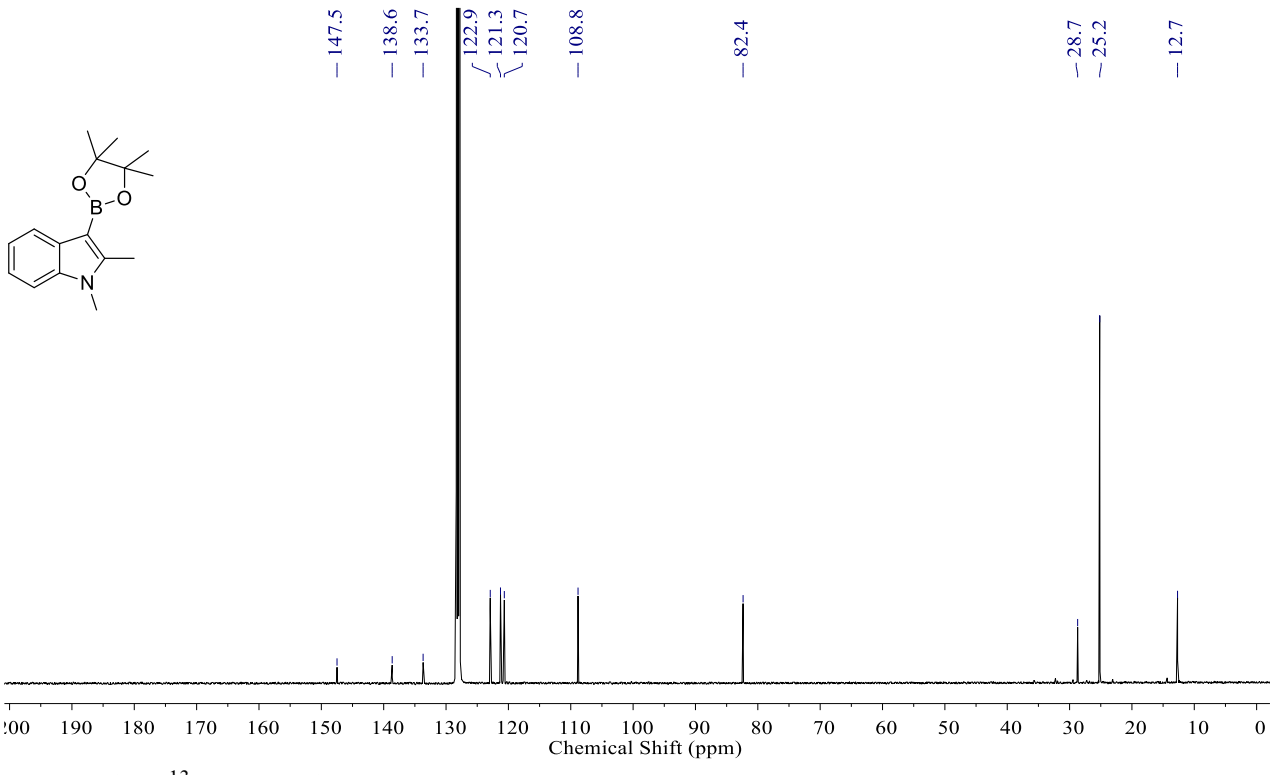

Figure S20. ^{13}C NMR, **10a**

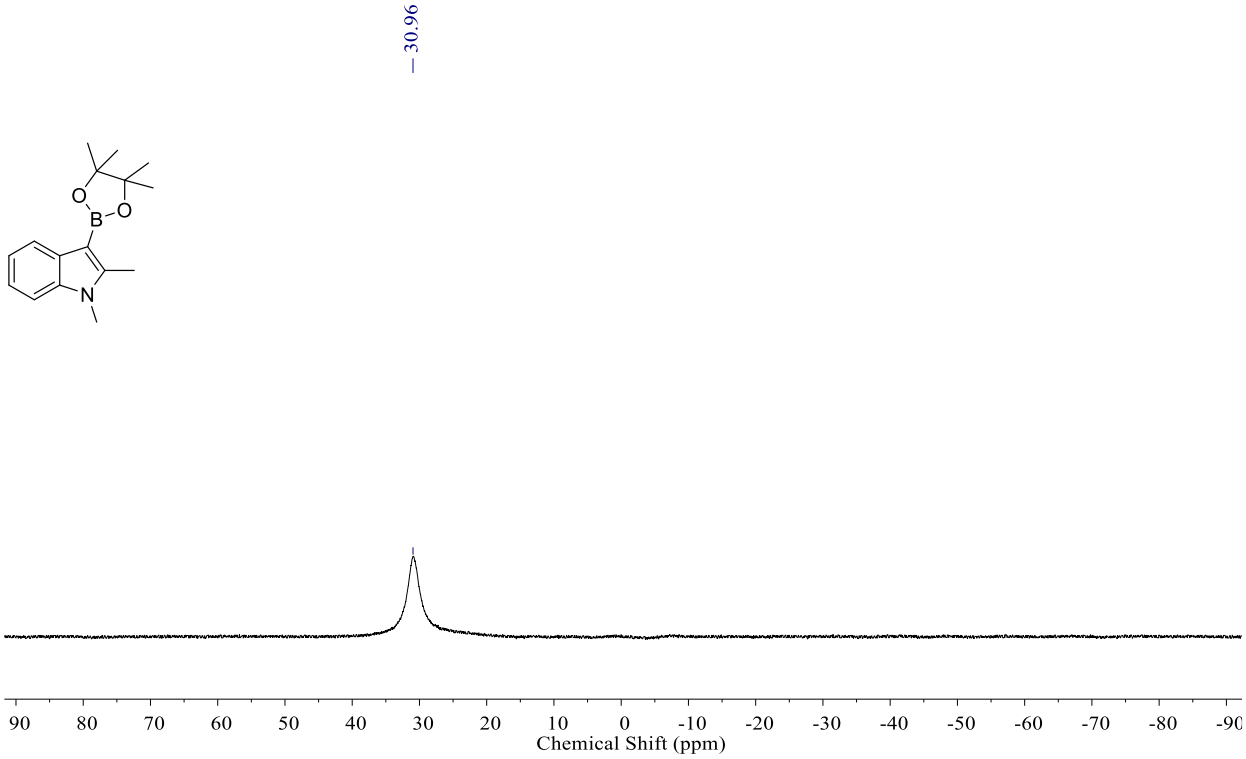

Figure S21. ^{11}B NMR, **10a**

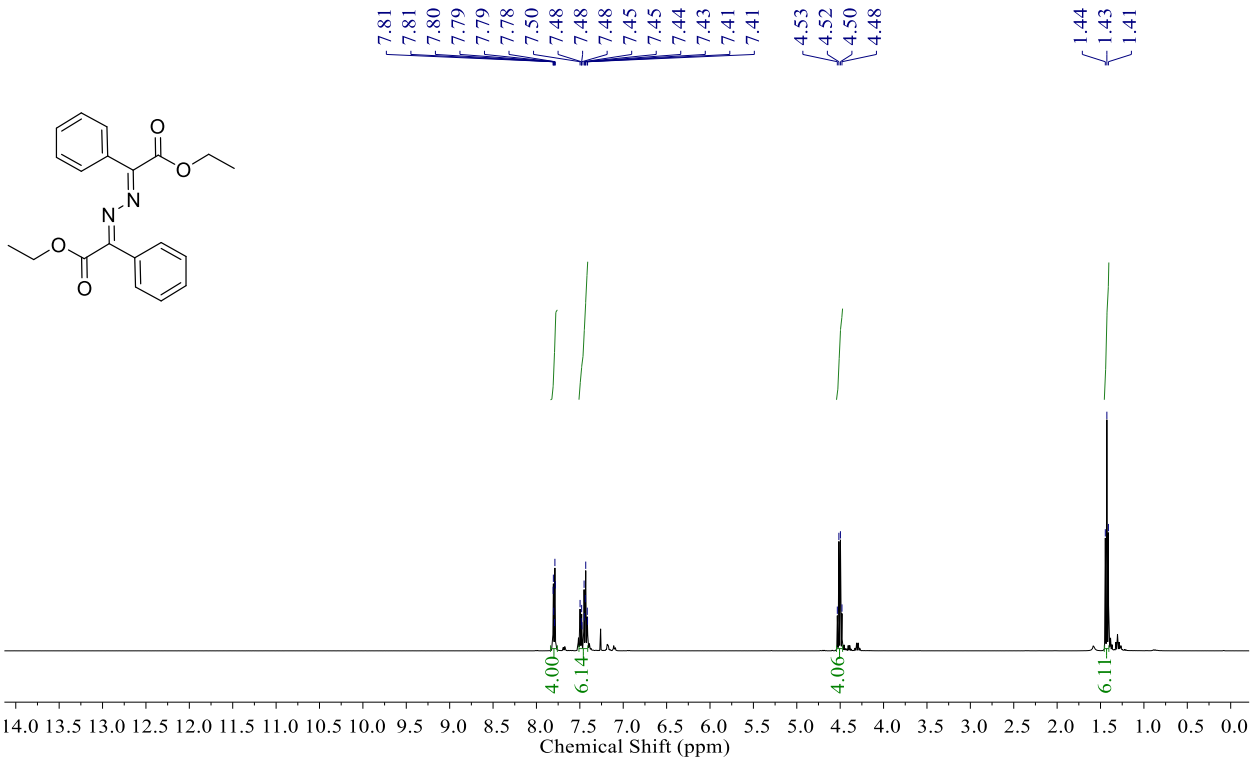

Figure S22. ^{1}H NMR, **9a**

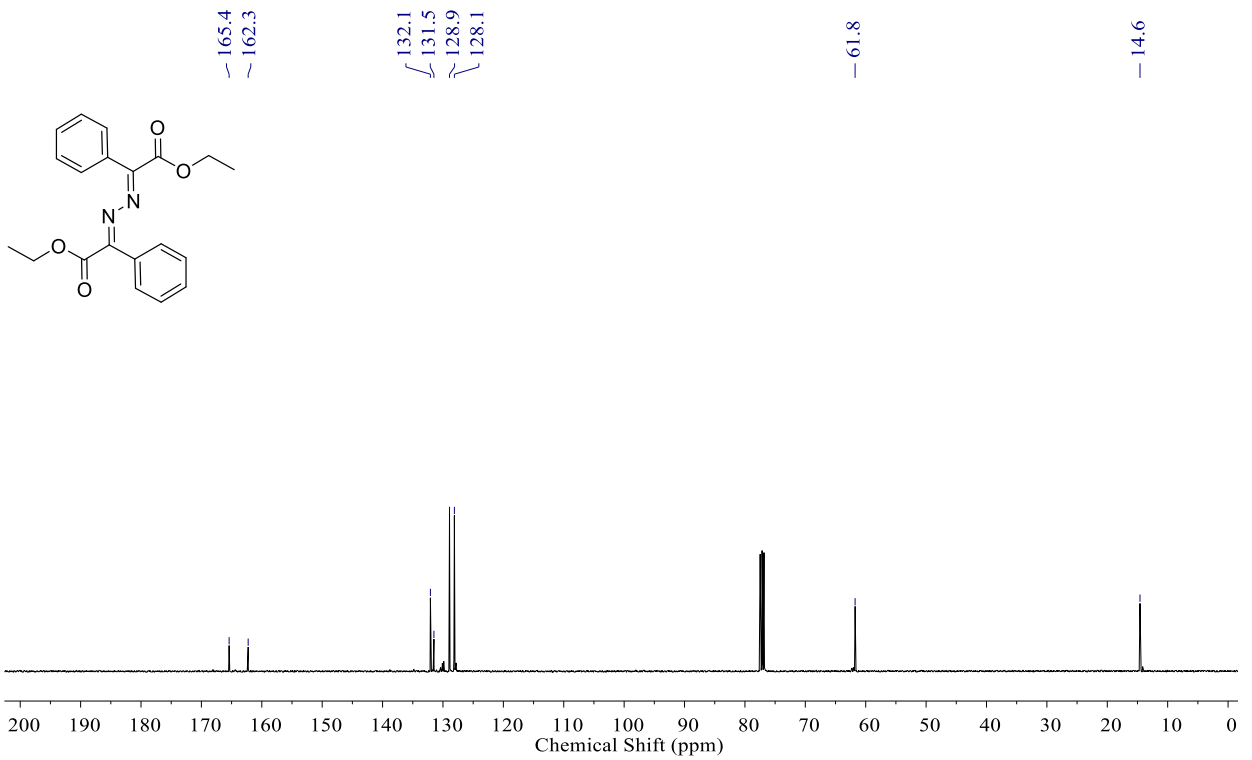

Figure S23. ^{13}C NMR, **9a**

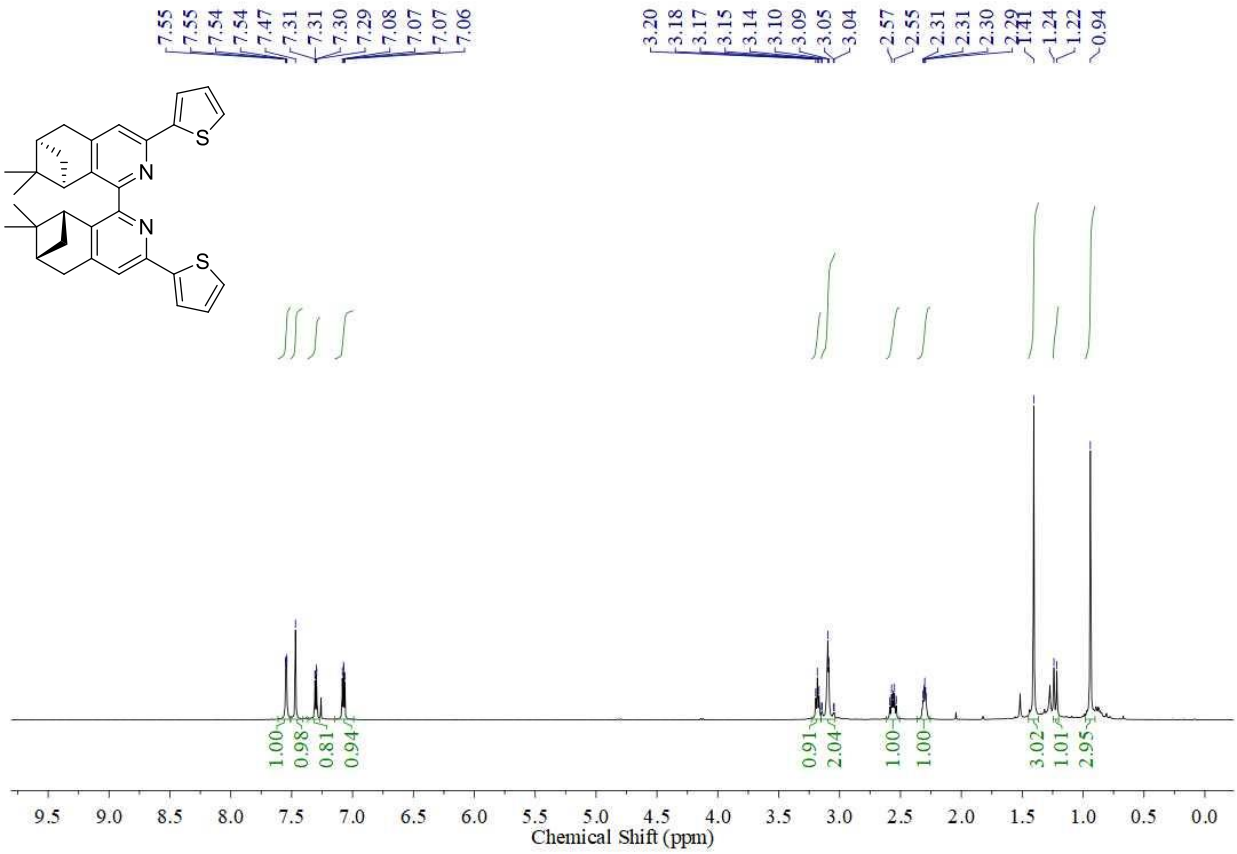

Figure S24. ^{1}H NMR, **8g**

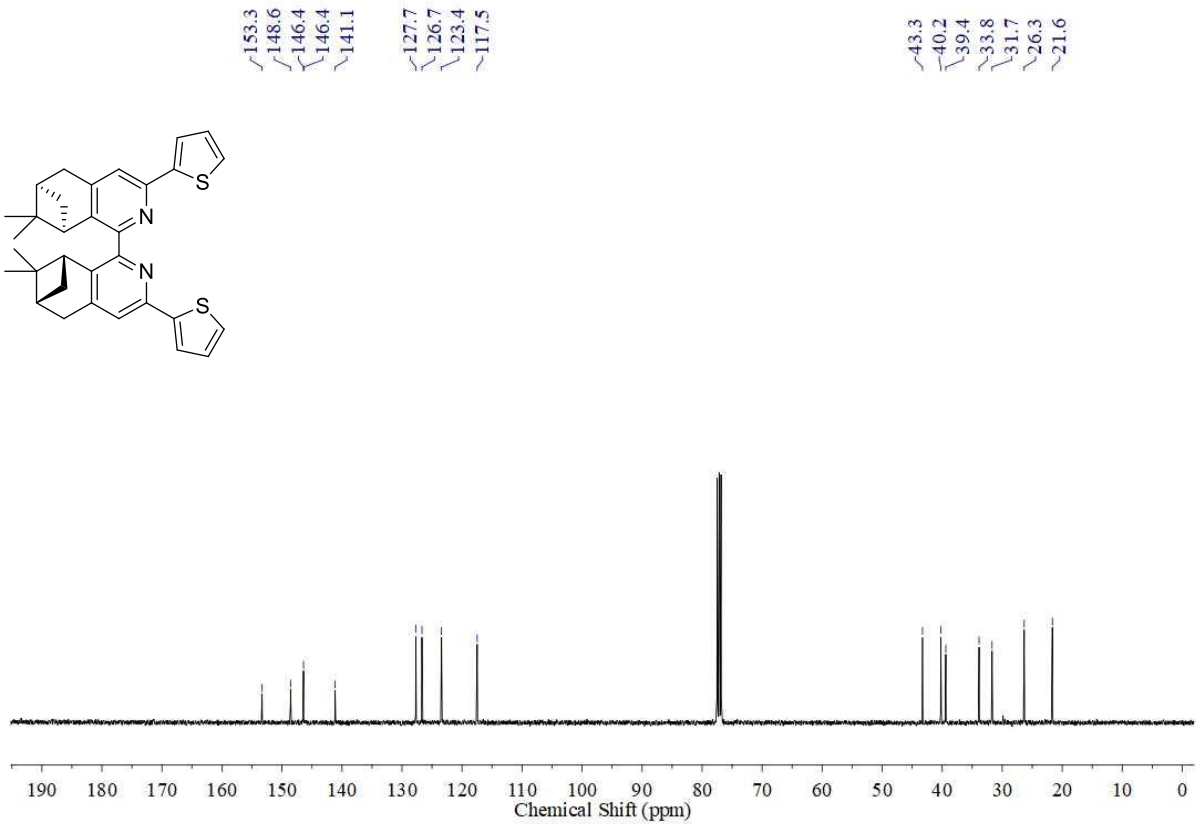

Figure S25. ^{13}C NMR, **8g**

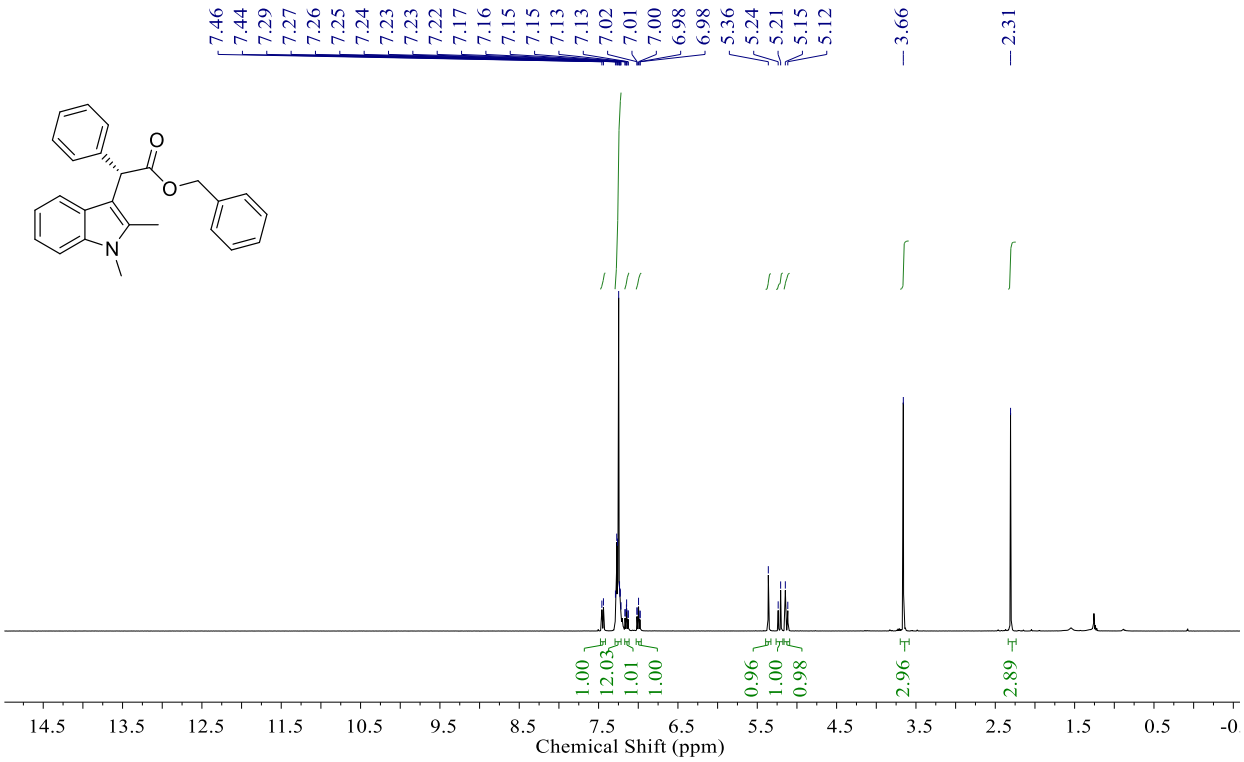

Figure S26. ^{1}H NMR, **3aa**

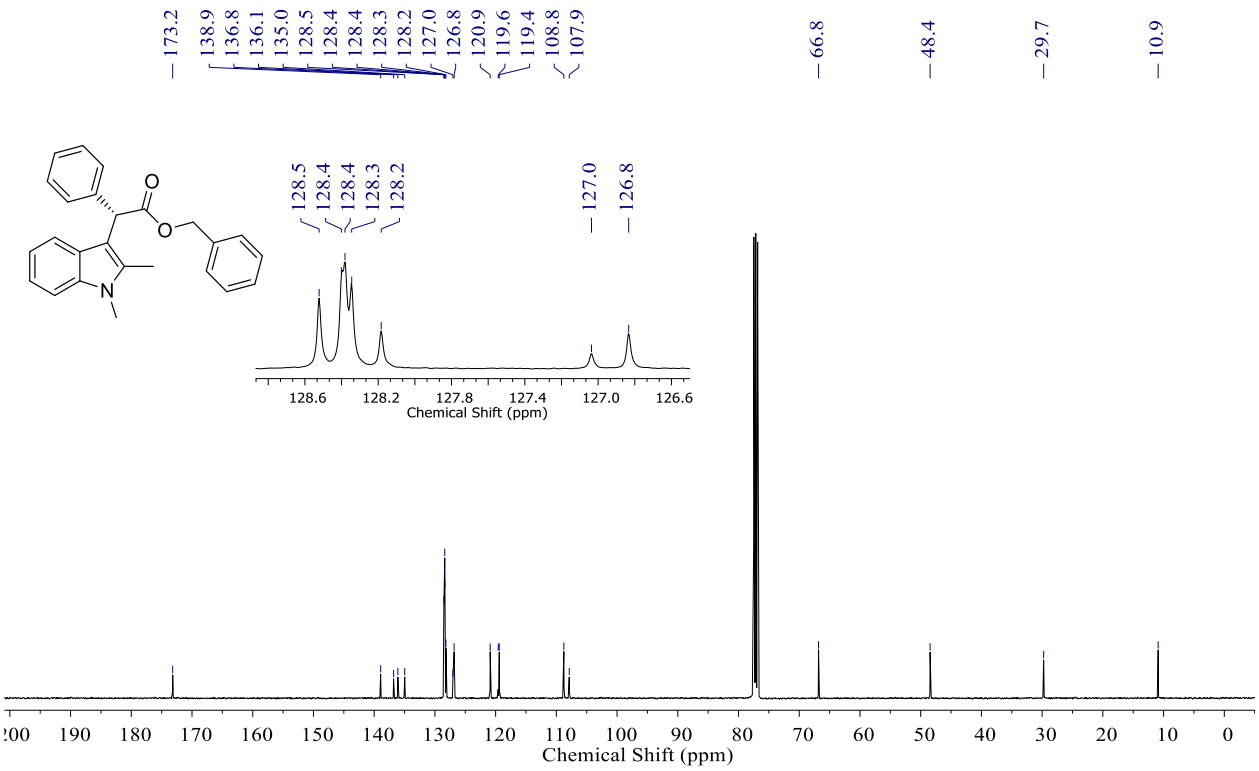

Figure S27. ^{13}C NMR, **3aa**

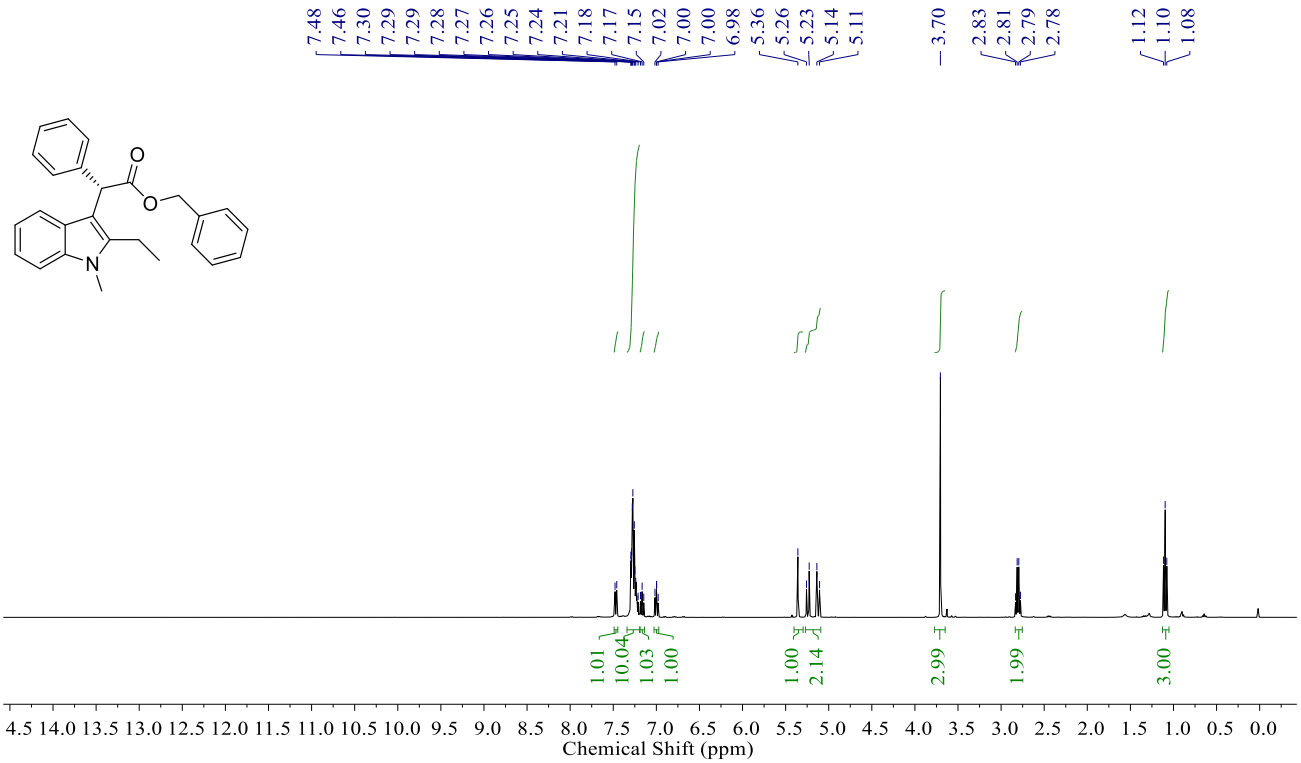

Figure S28. ^{1}H NMR, **3ab**

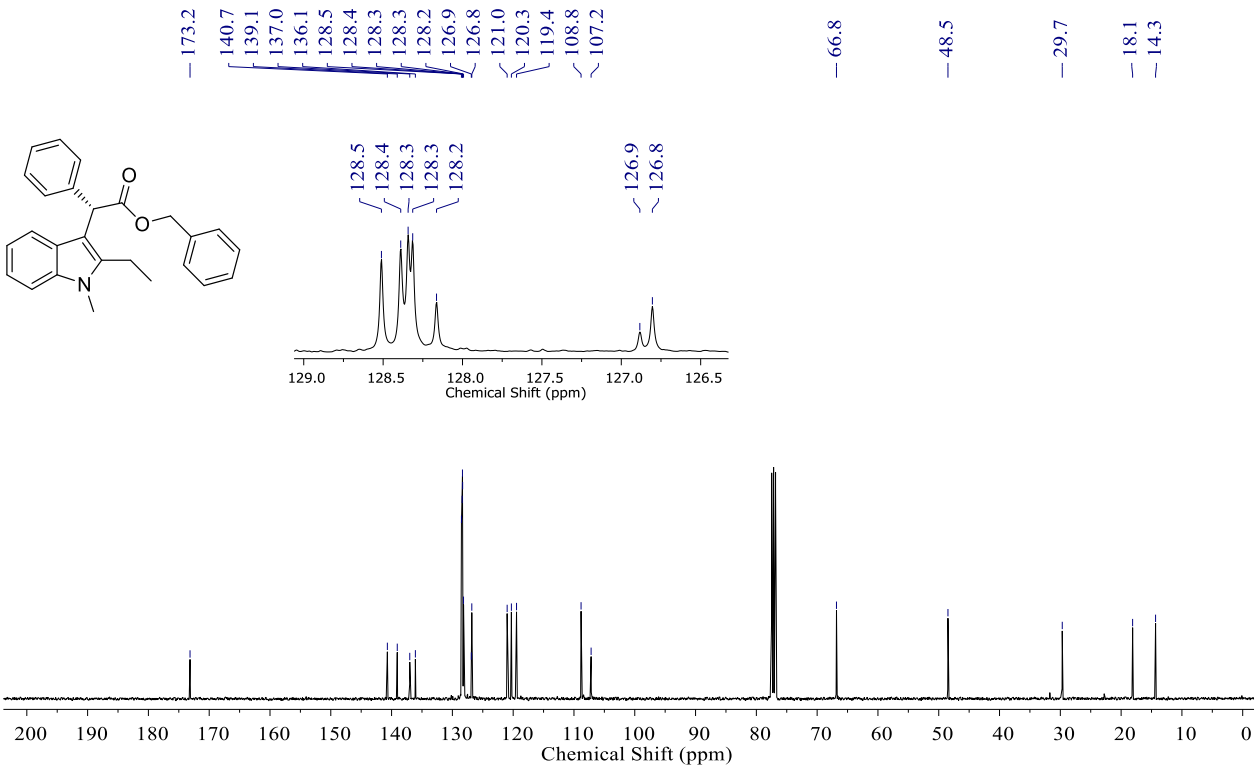

Figure S29. ^{13}C NMR, **3ab**

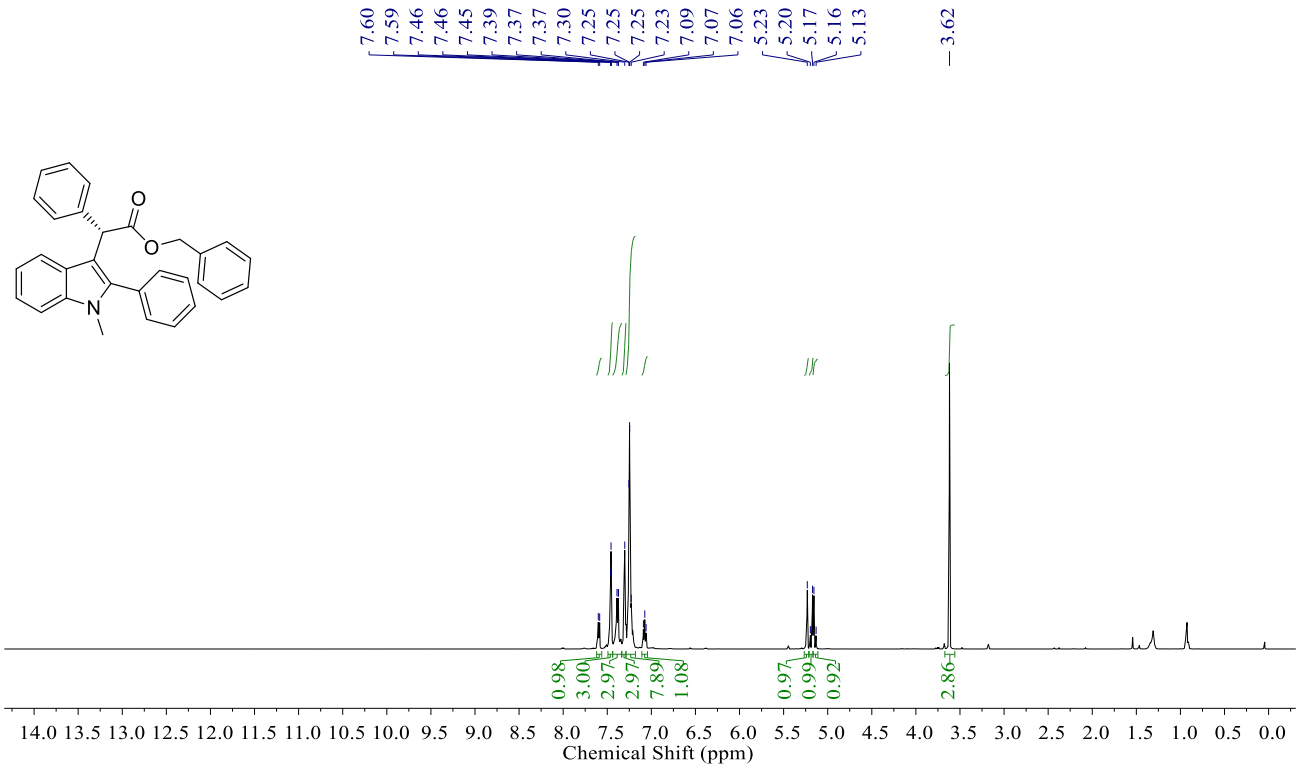

Figure S30. ^{1}H NMR, **3ac**

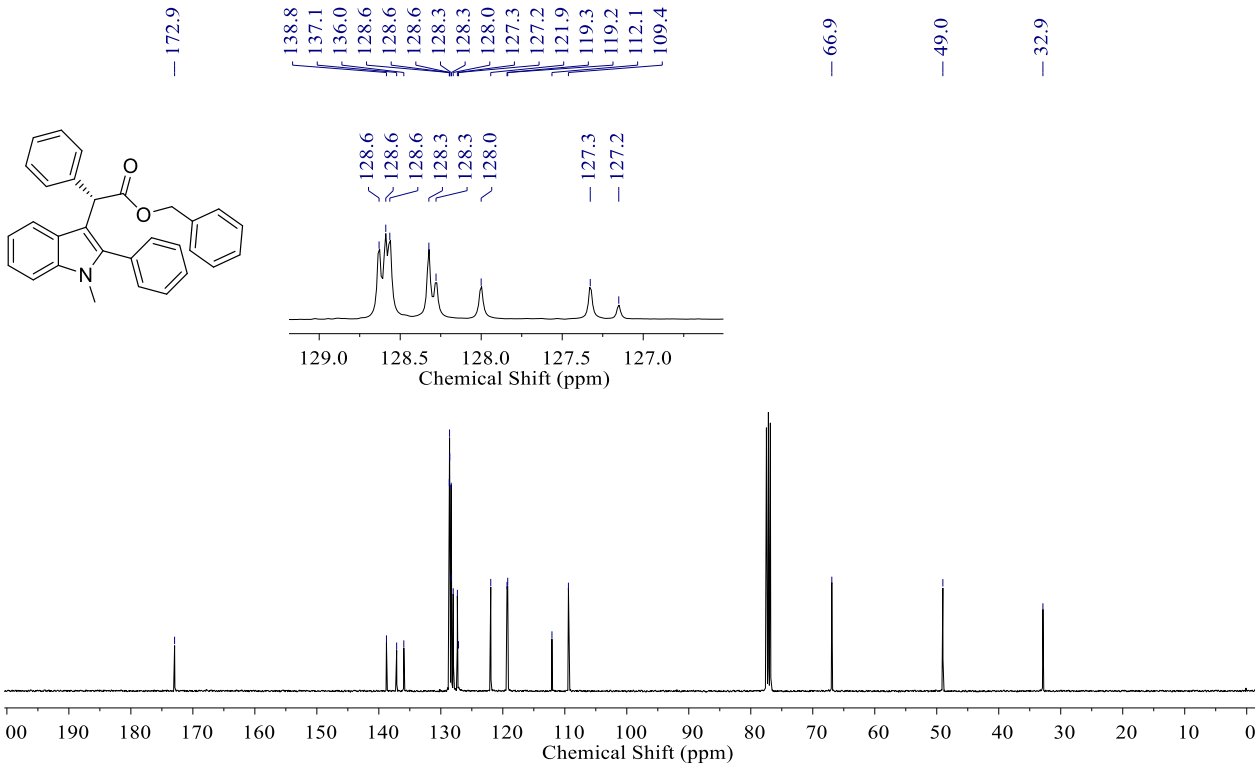

Figure S31. ^{13}C NMR, **3ac**

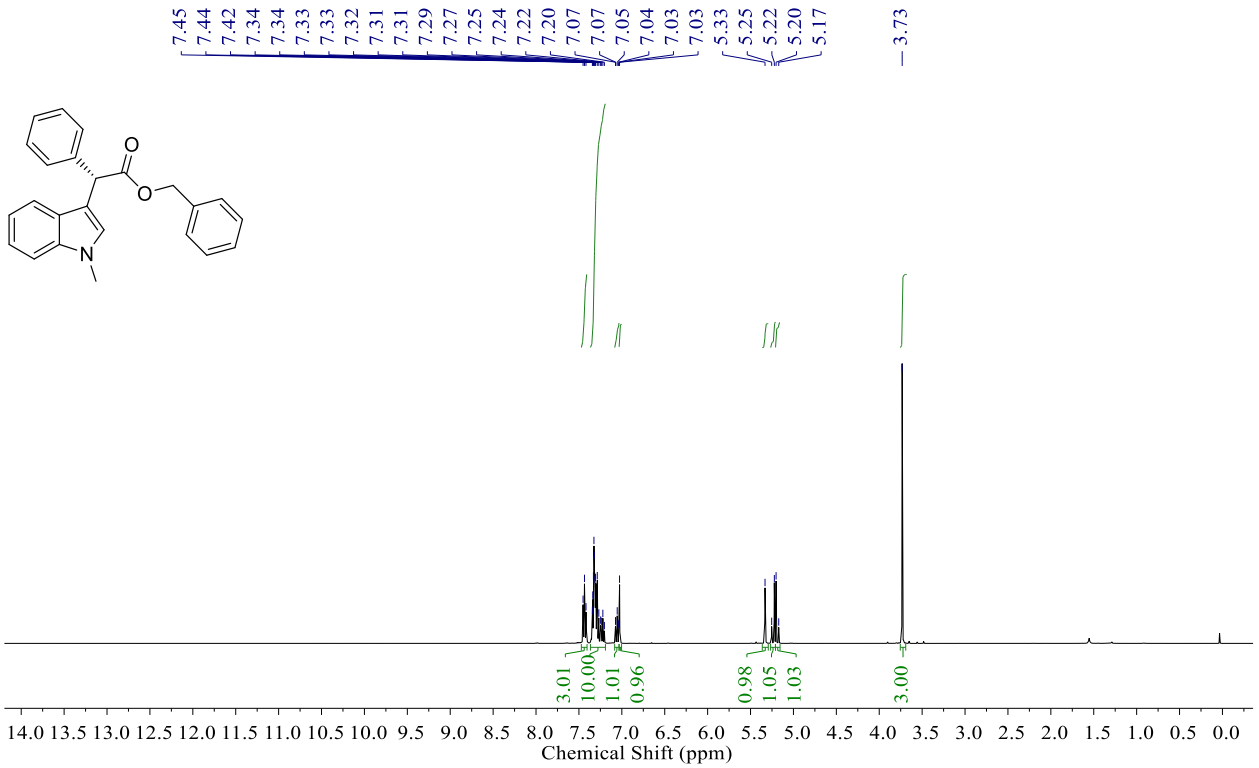

Figure S32. ^{1}H NMR, **3ad**

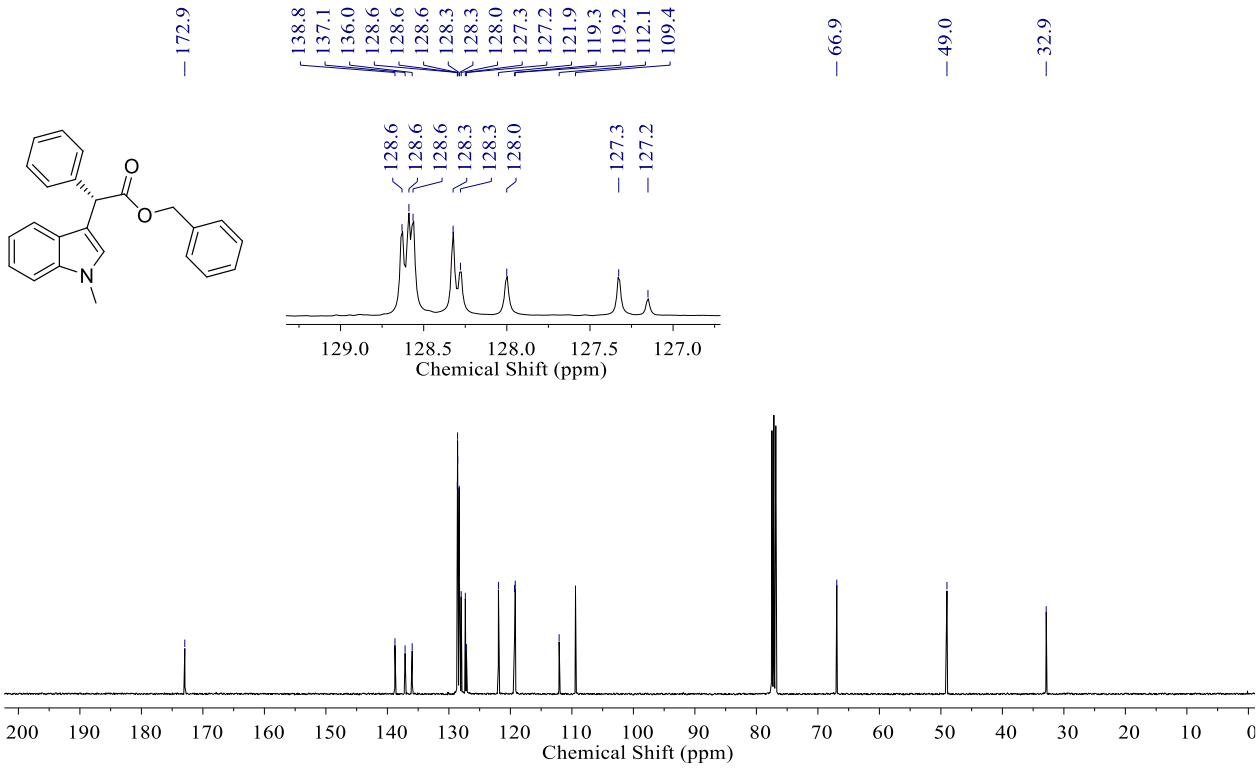

Figure S33. ^{13}C NMR, **3ad**

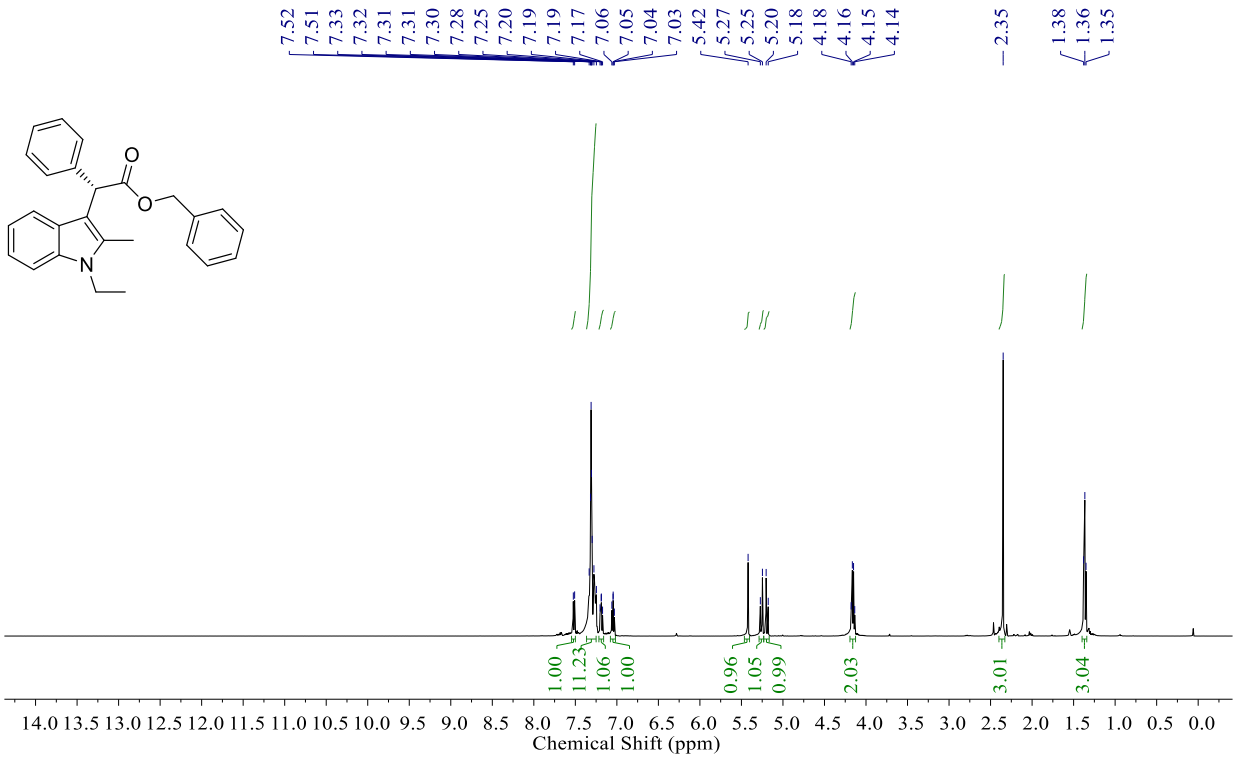

Figure S34. ^{1}H NMR, **3ae**

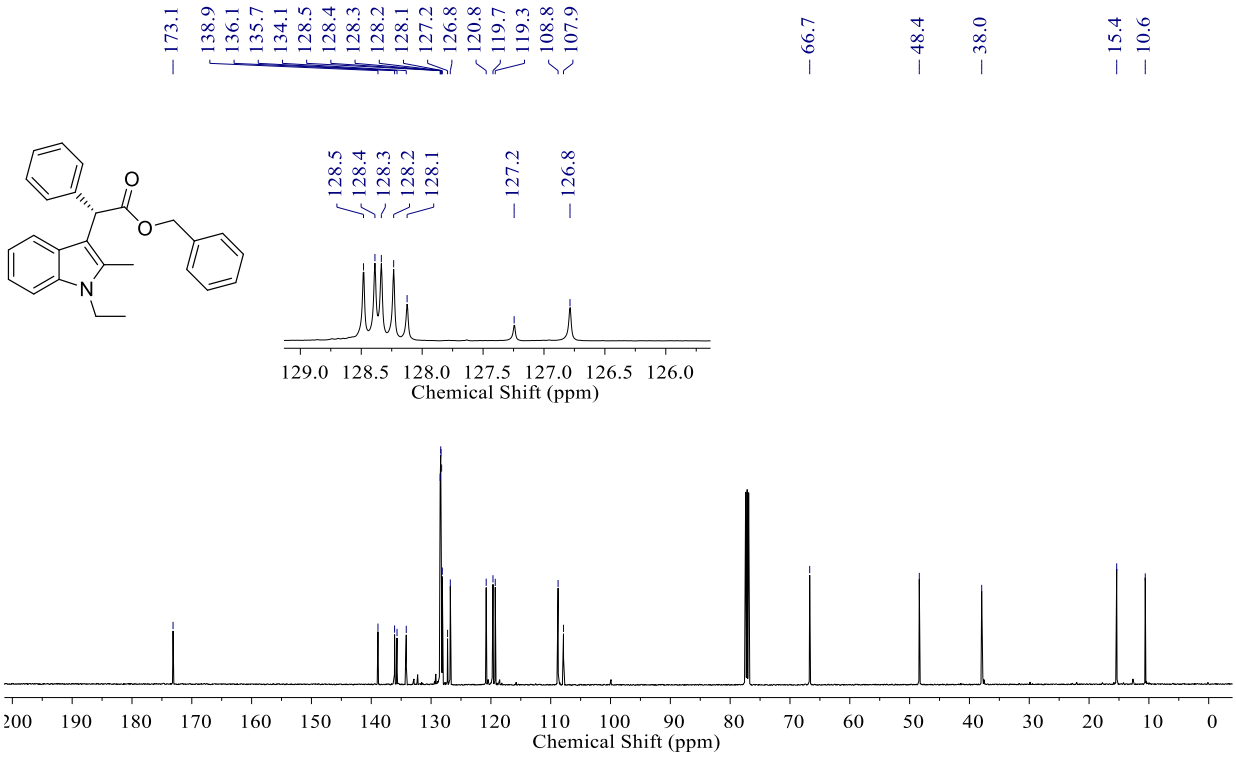

Figure S35. ^{13}C NMR, **3ae**

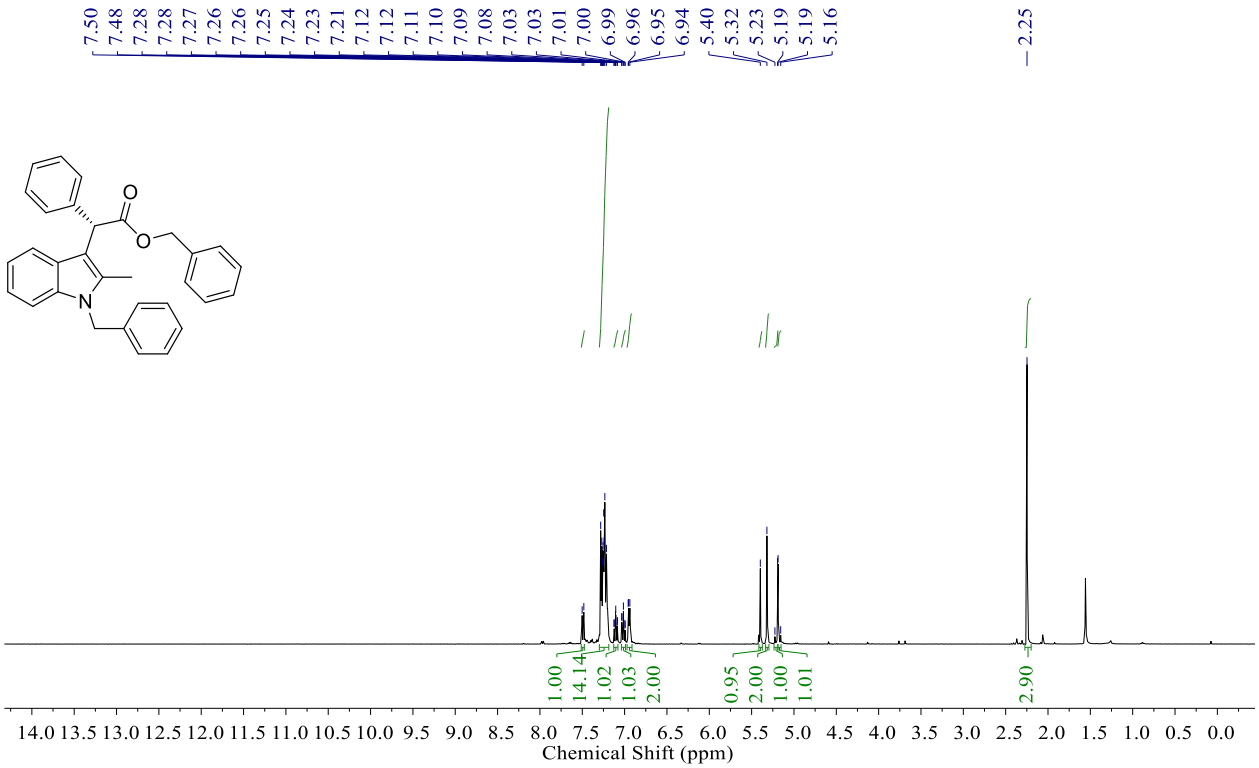

Figure S36. ^{1}H NMR, **3af**

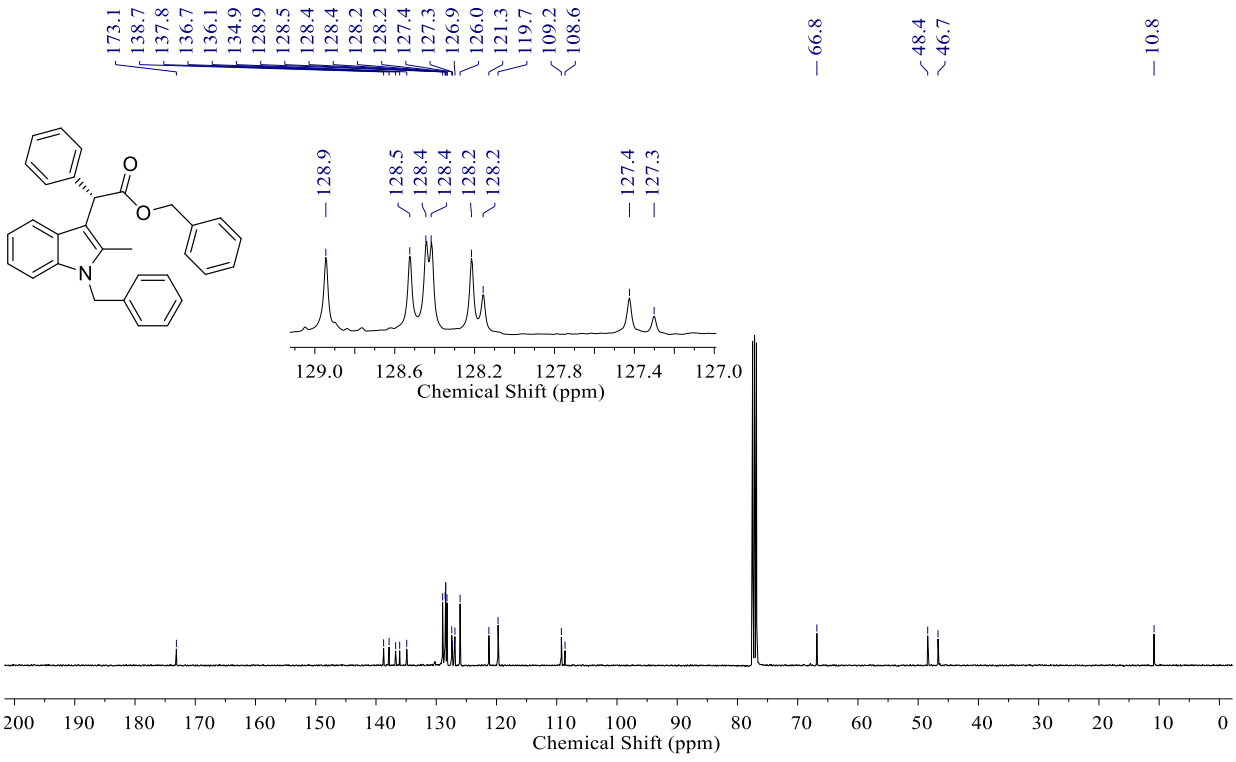

Figure S37. ^{13}C NMR, **3af**

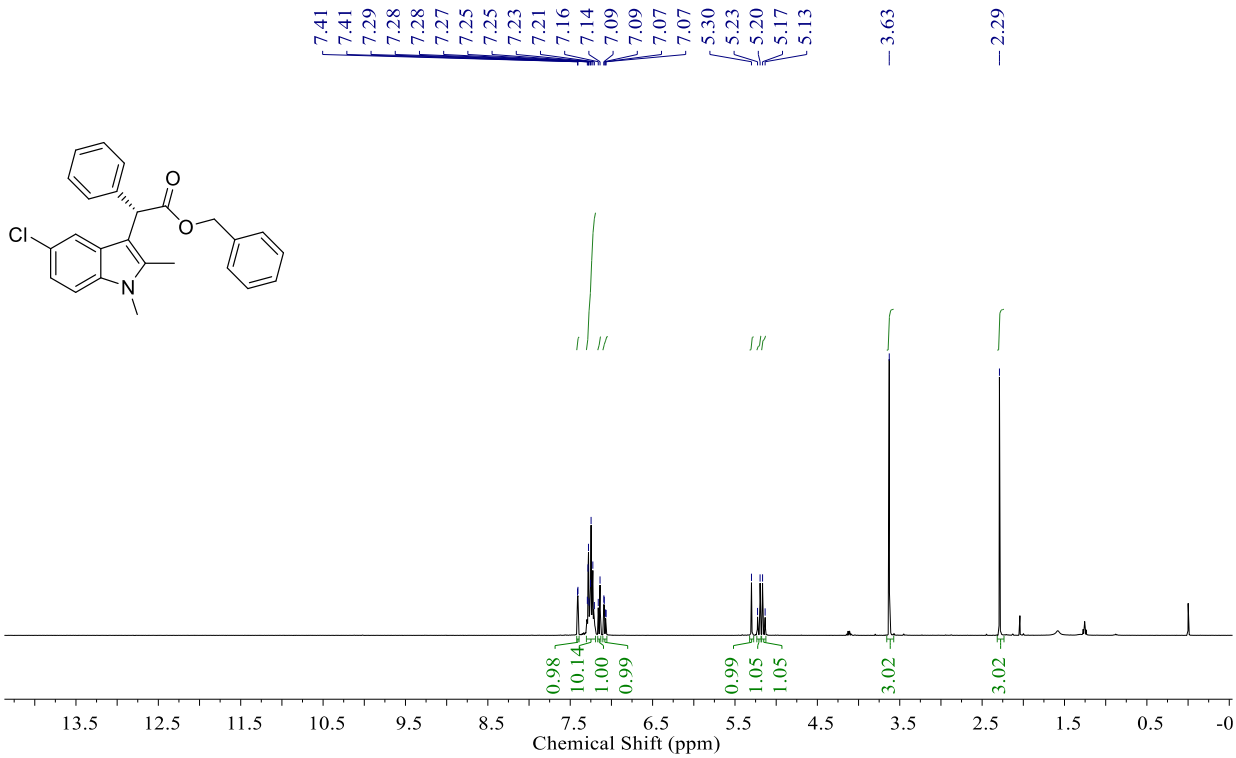

Figure S38. ^{1}H NMR, **3ag**

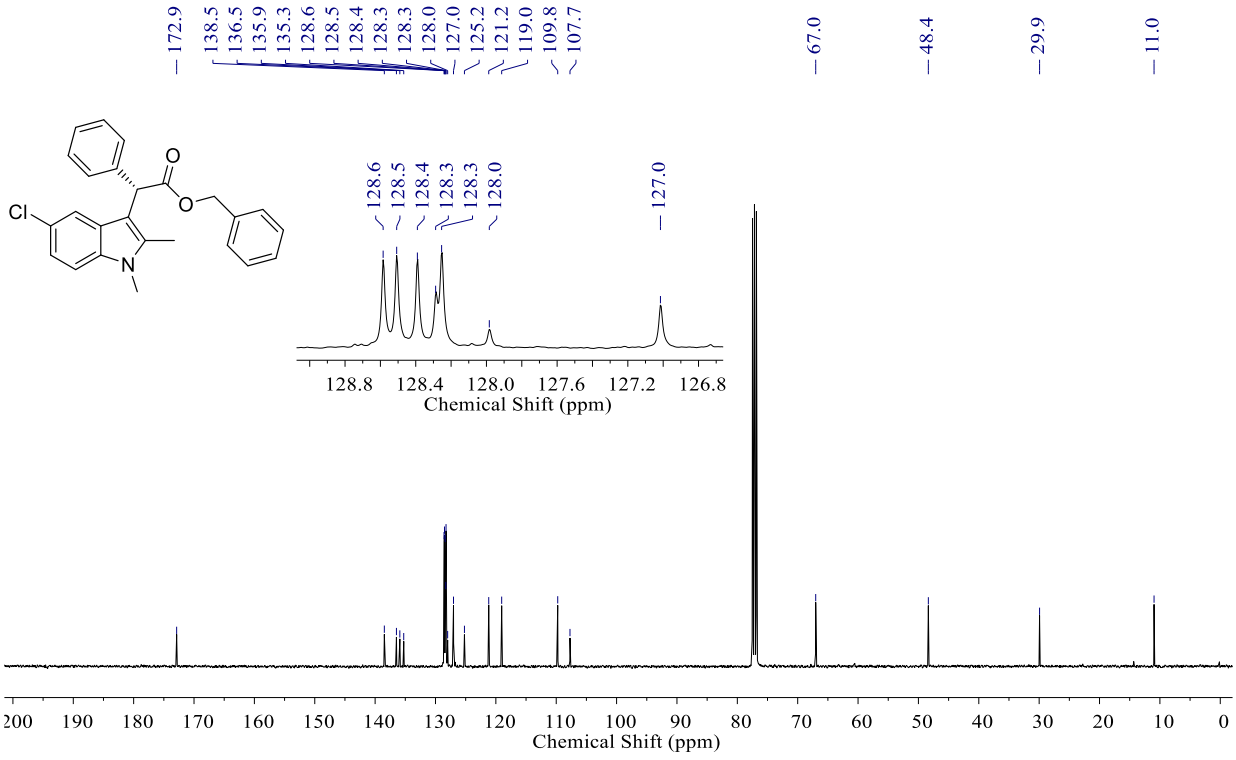

Figure S39. ^{13}C NMR, **3ag**

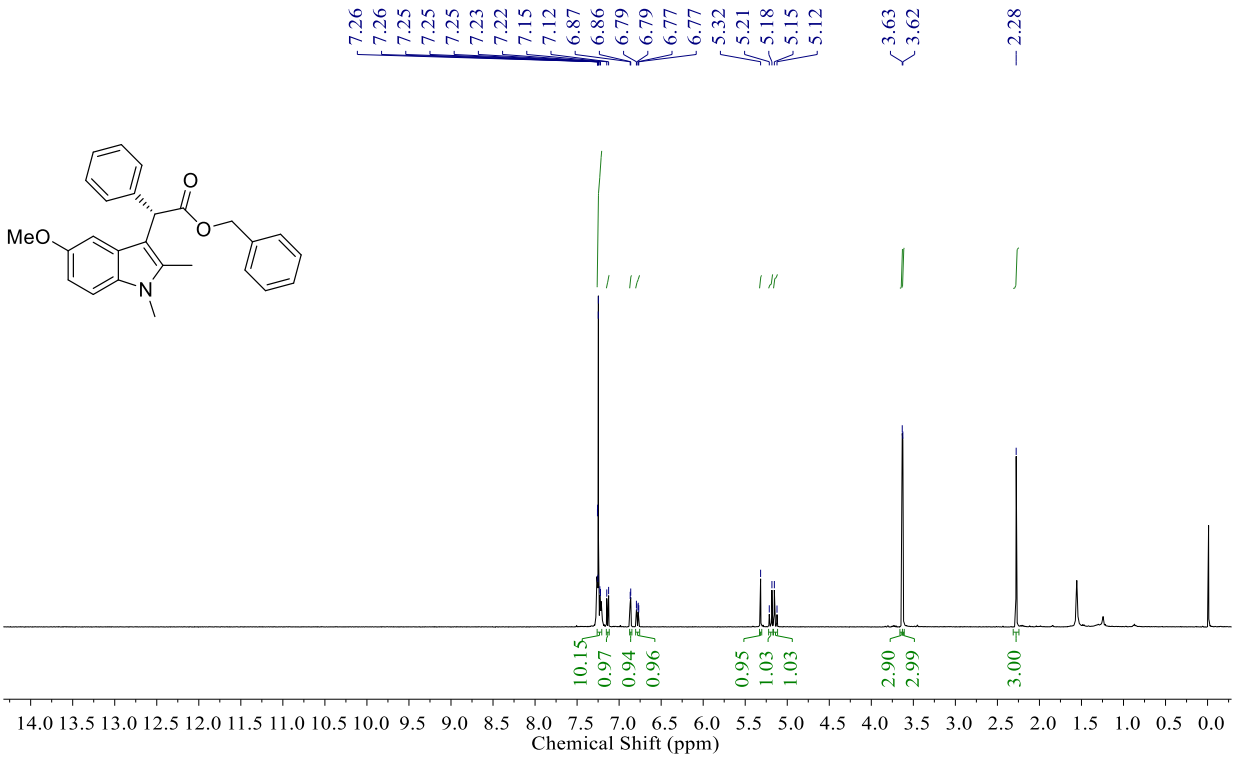

Figure S40. ^{1}H NMR, **3ah**

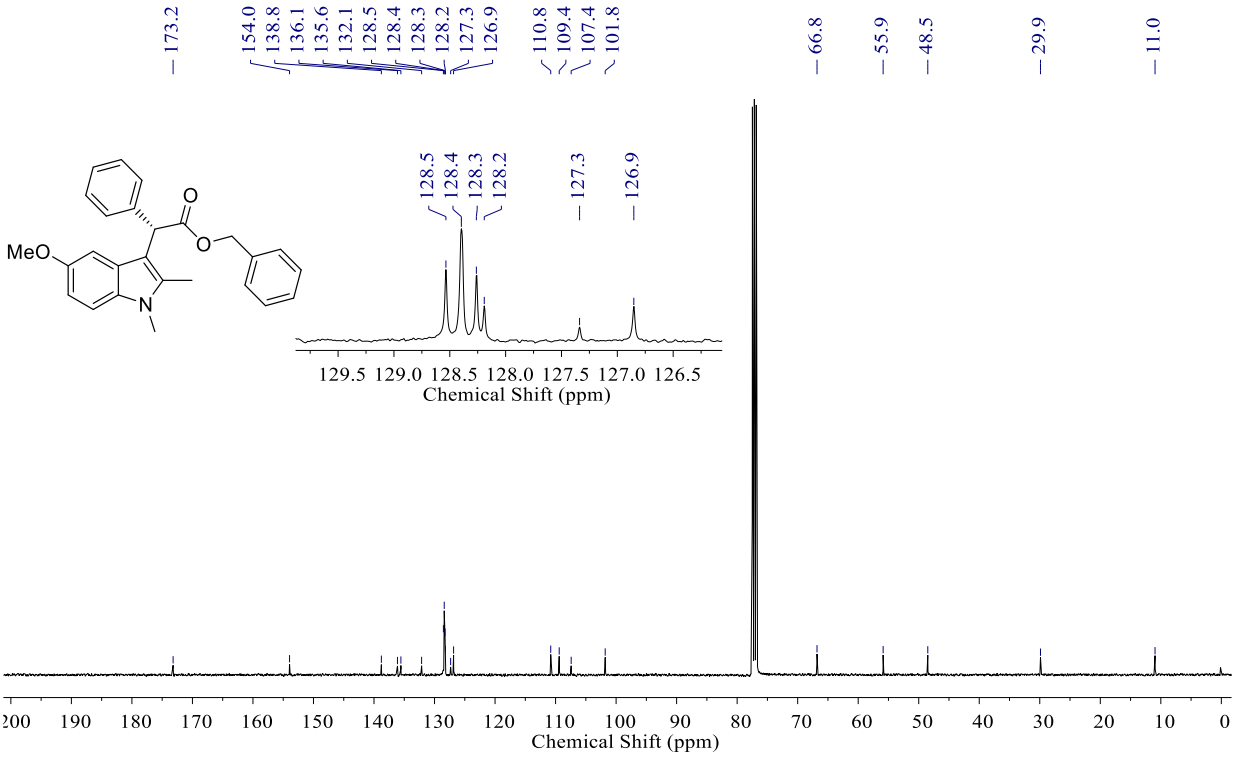

Figure S41. ^{13}C NMR, **3ah**

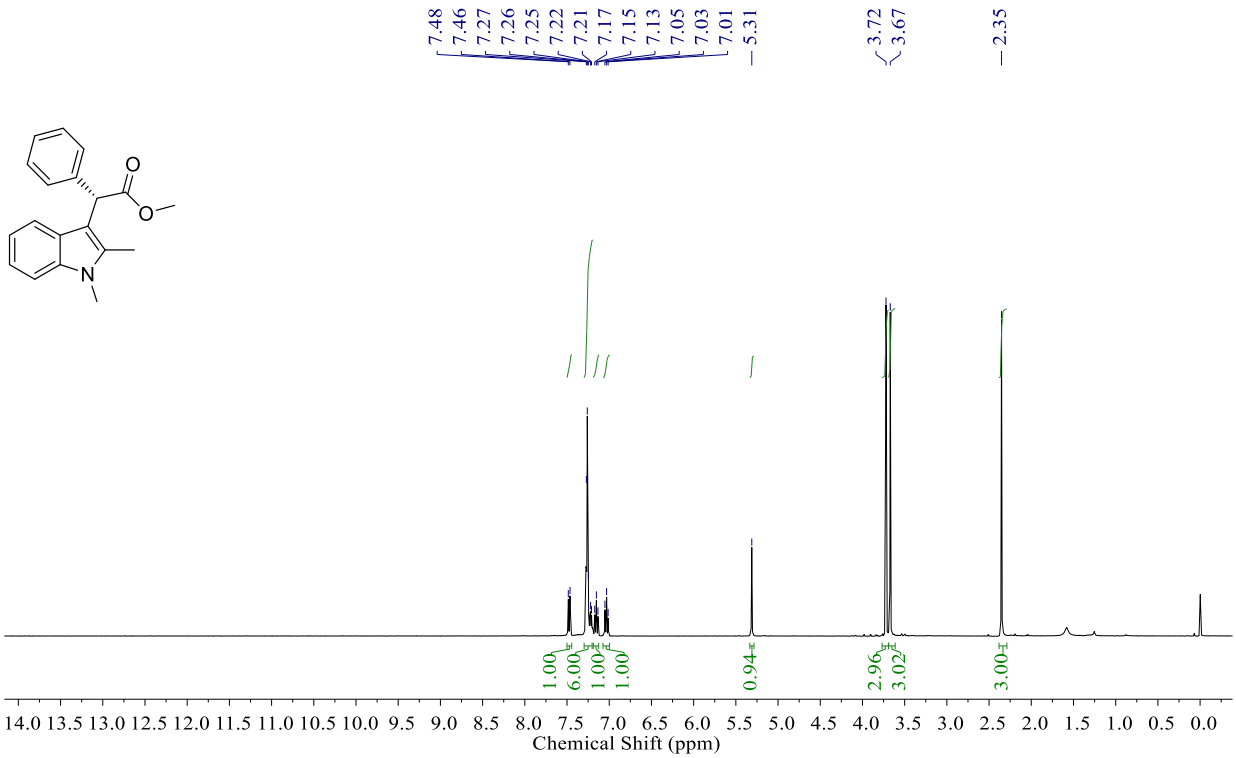

Figure S42. ^{1}H NMR, **3ba**

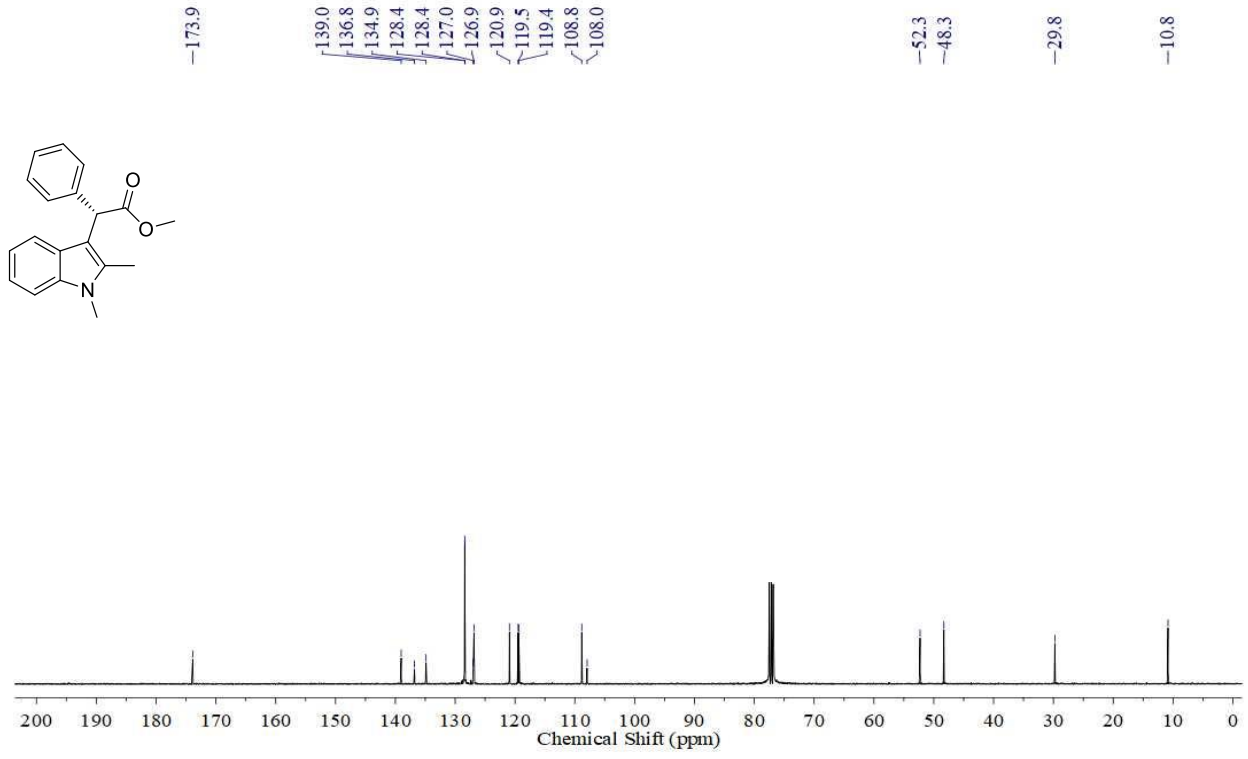

Figure S43. ^{13}C NMR, **3ba**

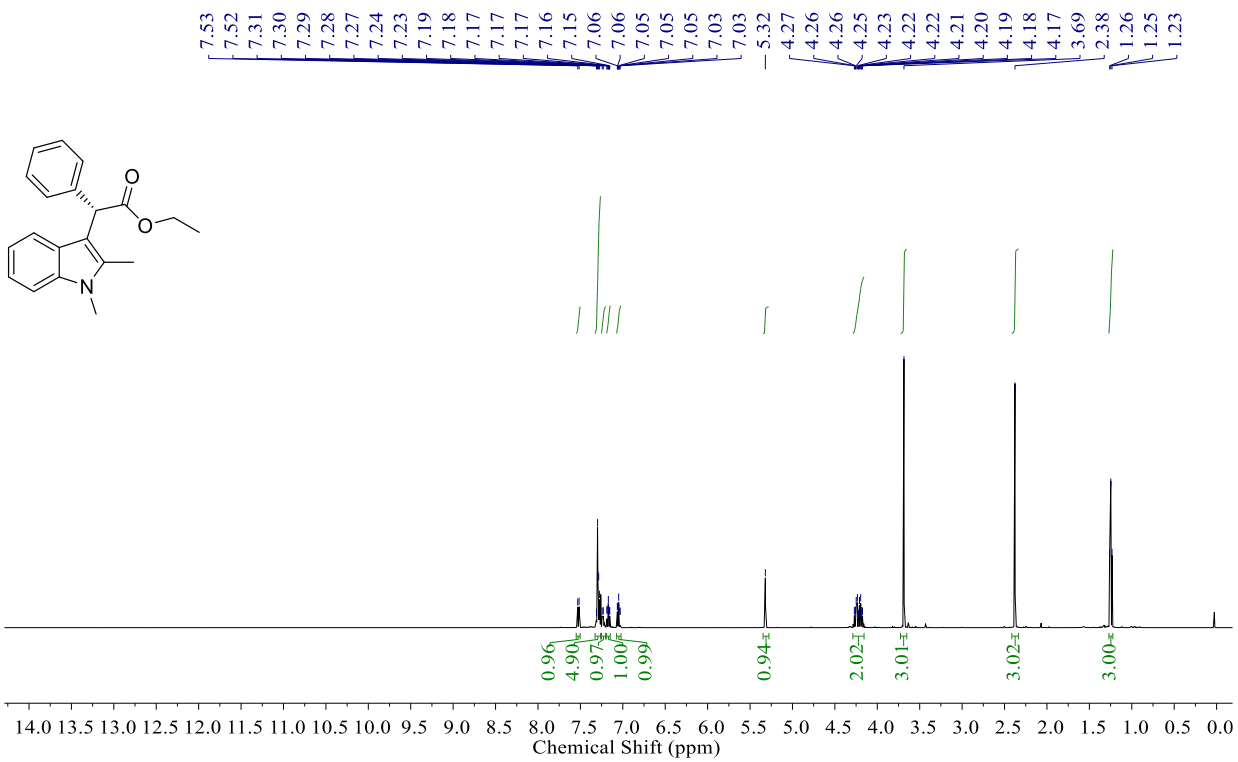

Figure S44. ^{1}H NMR, **3ca**

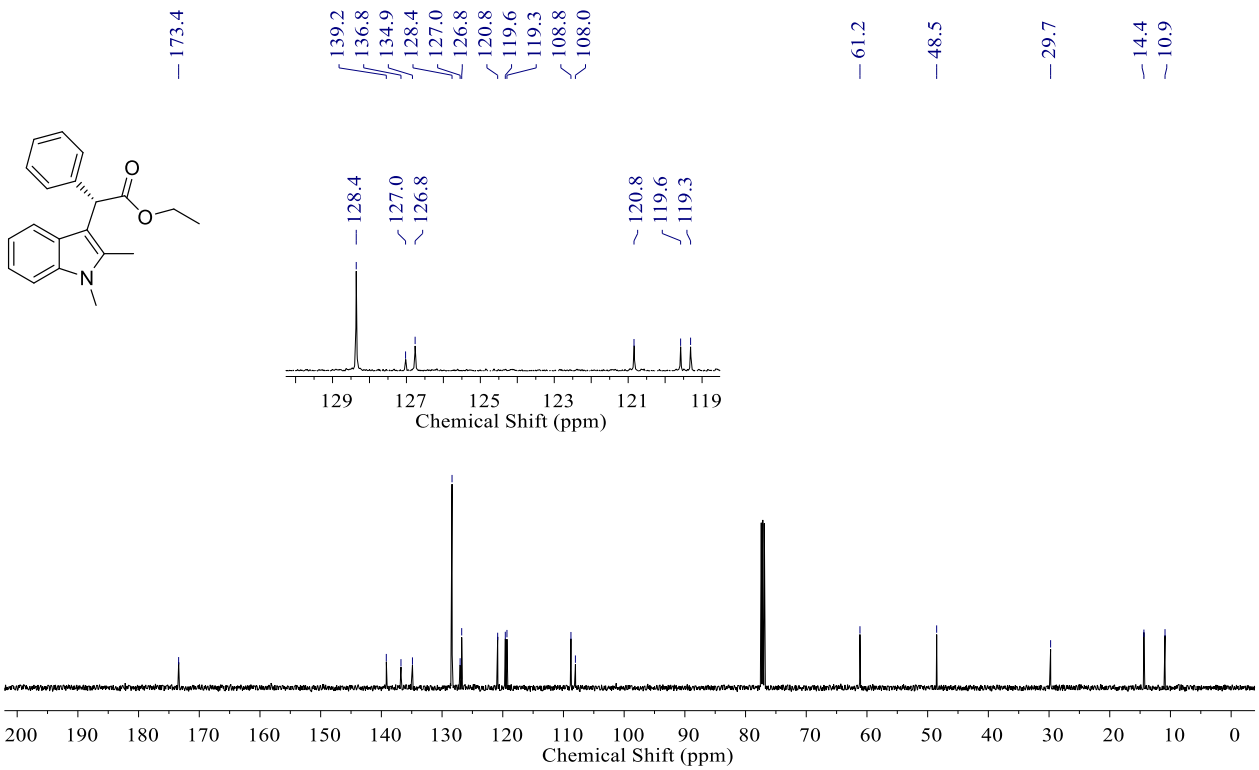

Figure S45. ^{13}C NMR, **3ca**

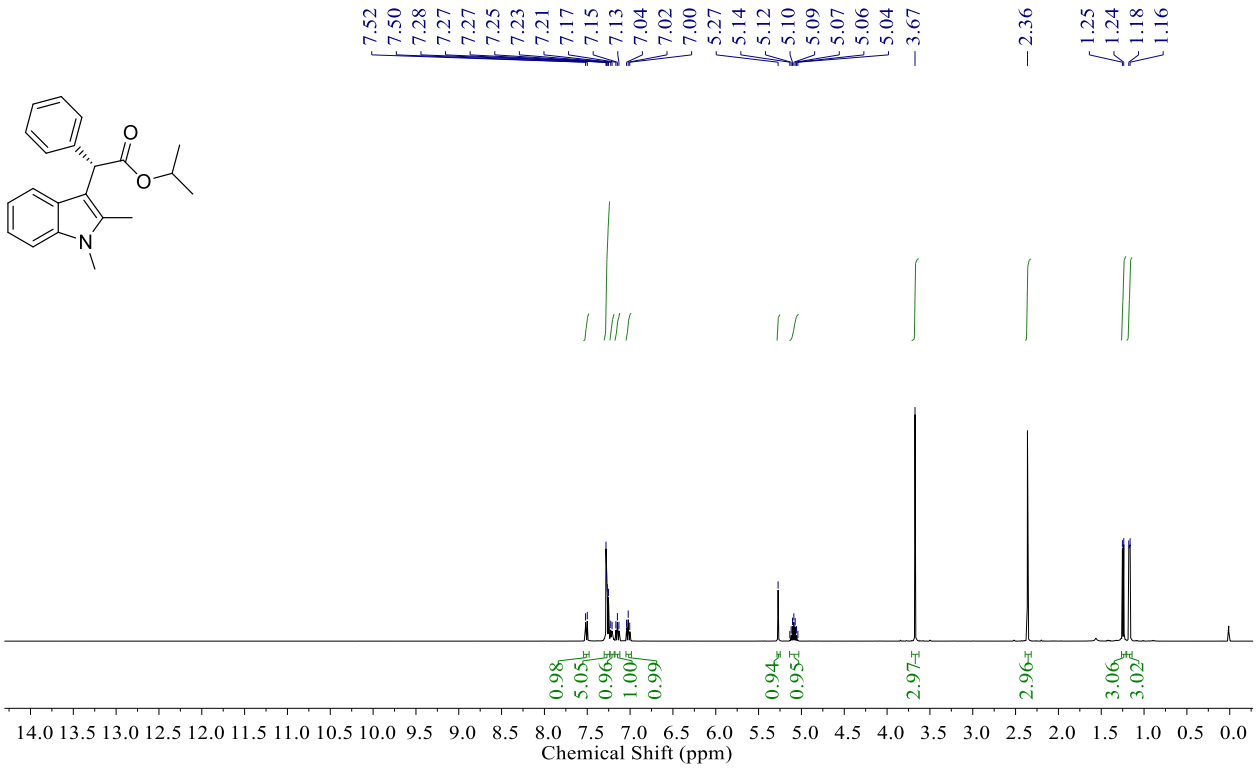

Figure S46. ^{1}H NMR, **3da**

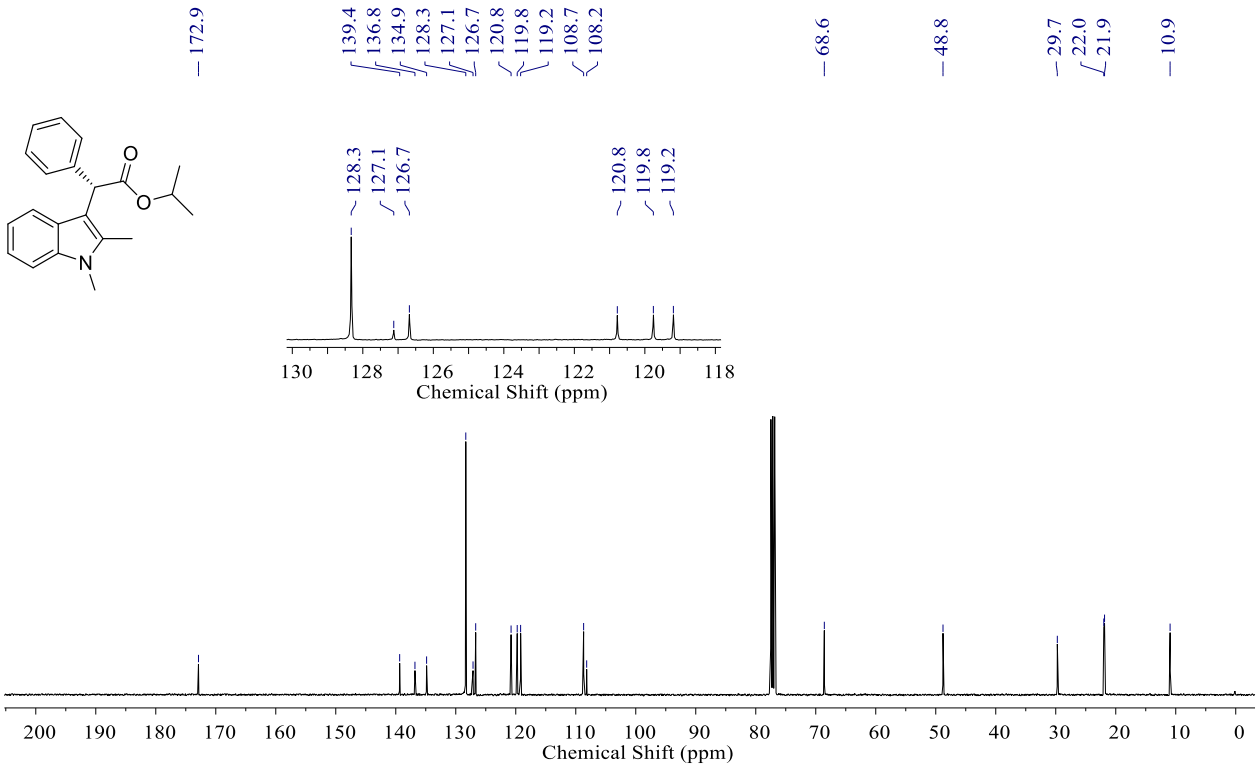

Figure S47. ^{13}C NMR, **3da**

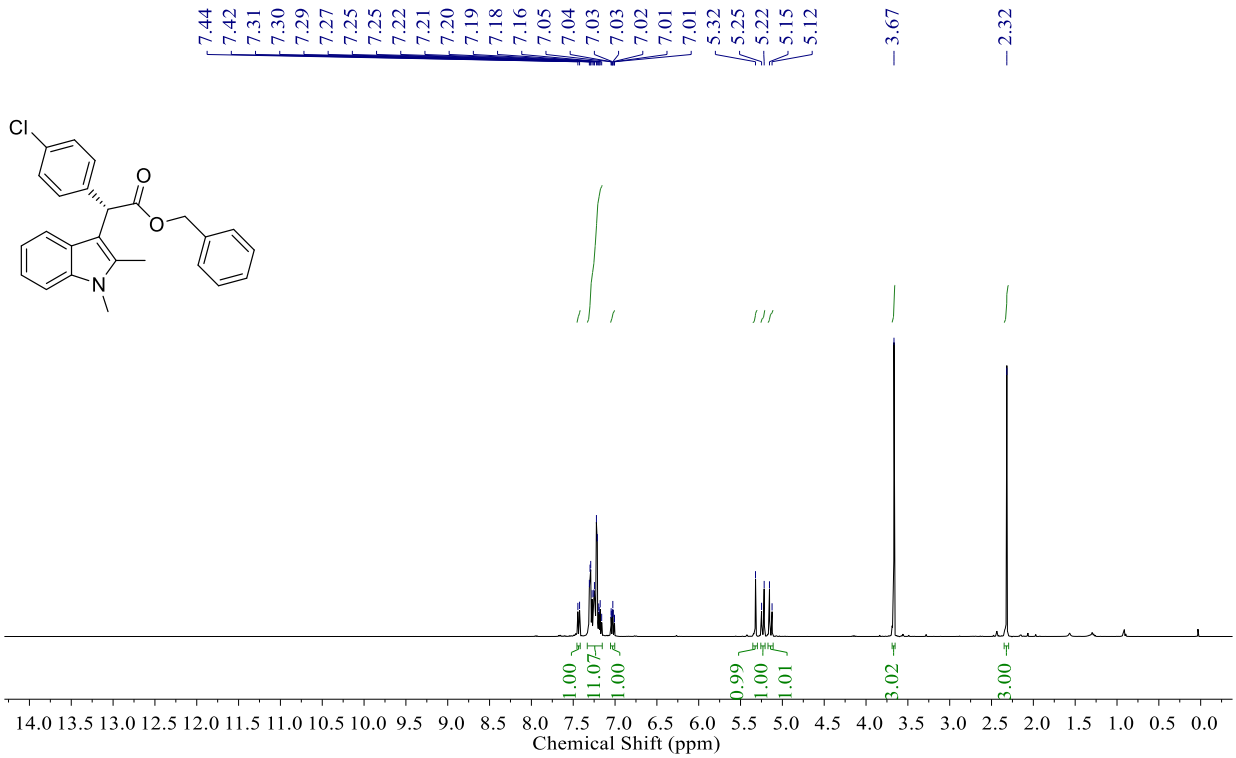

Figure S48. ^{1}H NMR, **3ea**

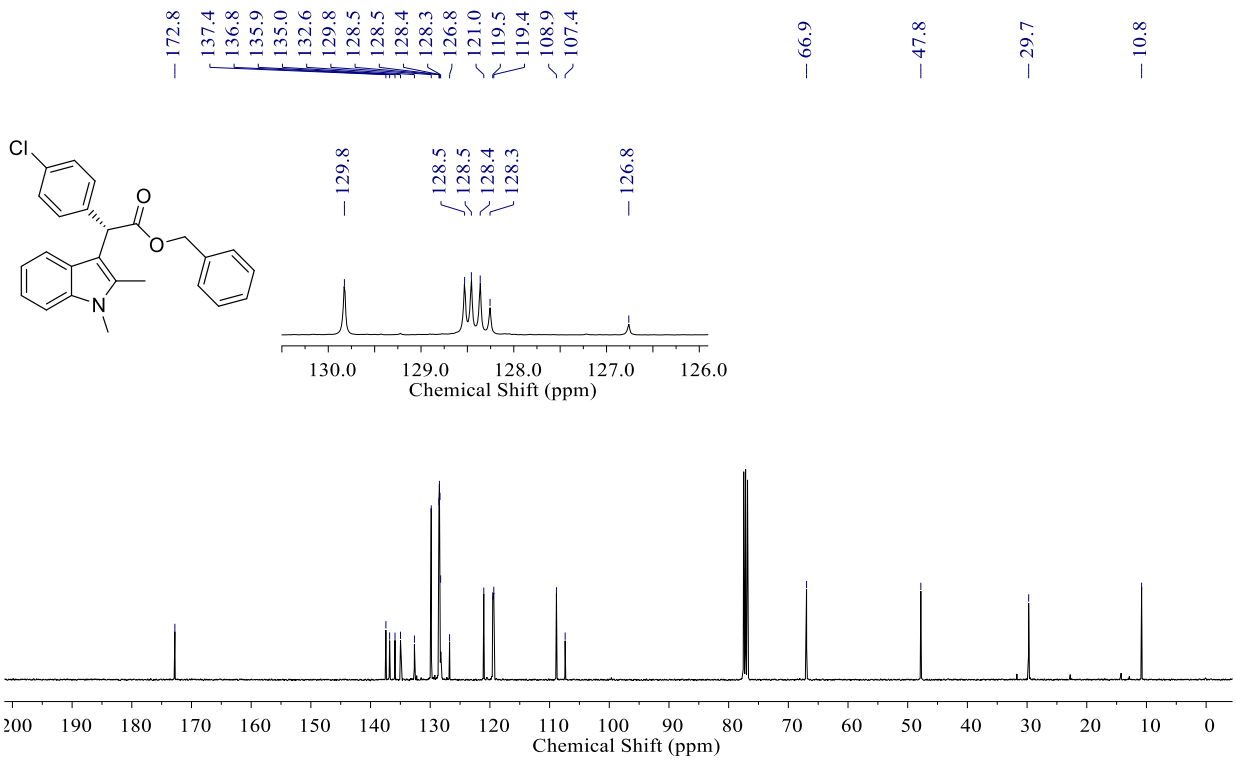

Figure S49. ^{13}C NMR, **3ea**

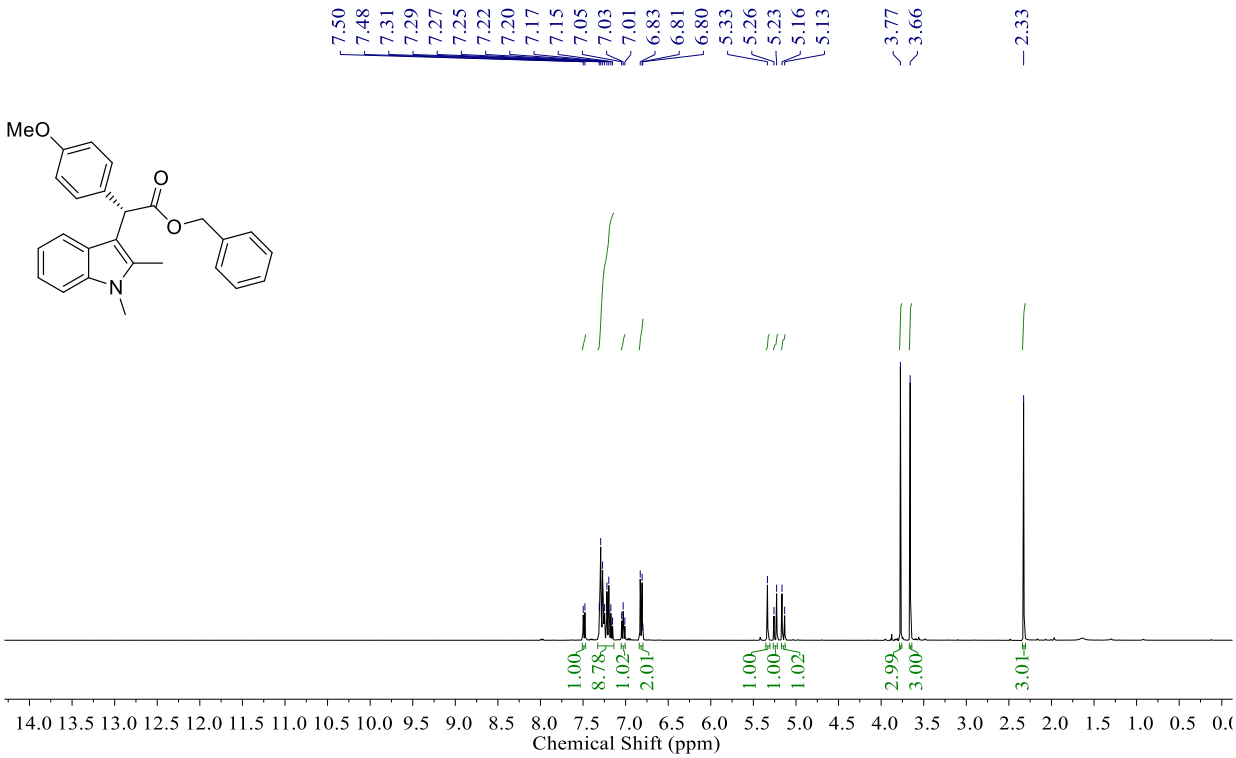

Figure S50. ^{1}H NMR, **3fa**

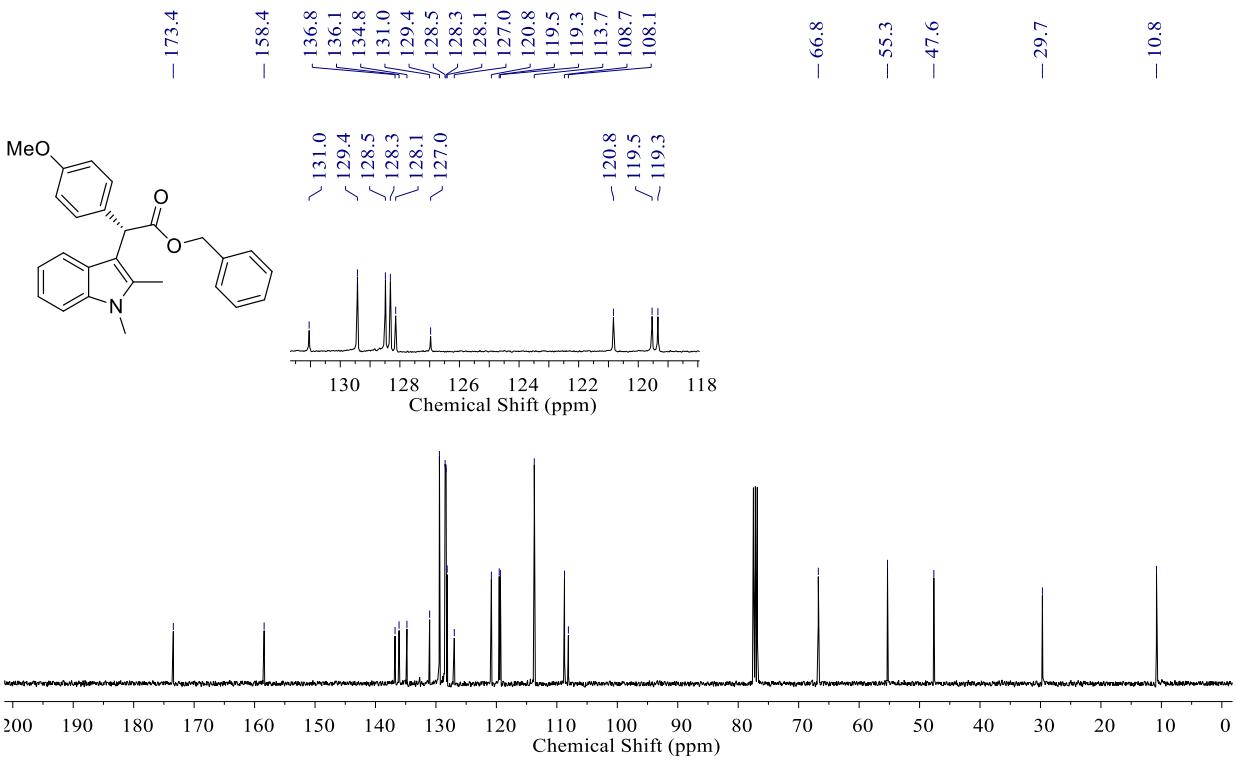

Figure S51. ^{13}C NMR, **3fa**

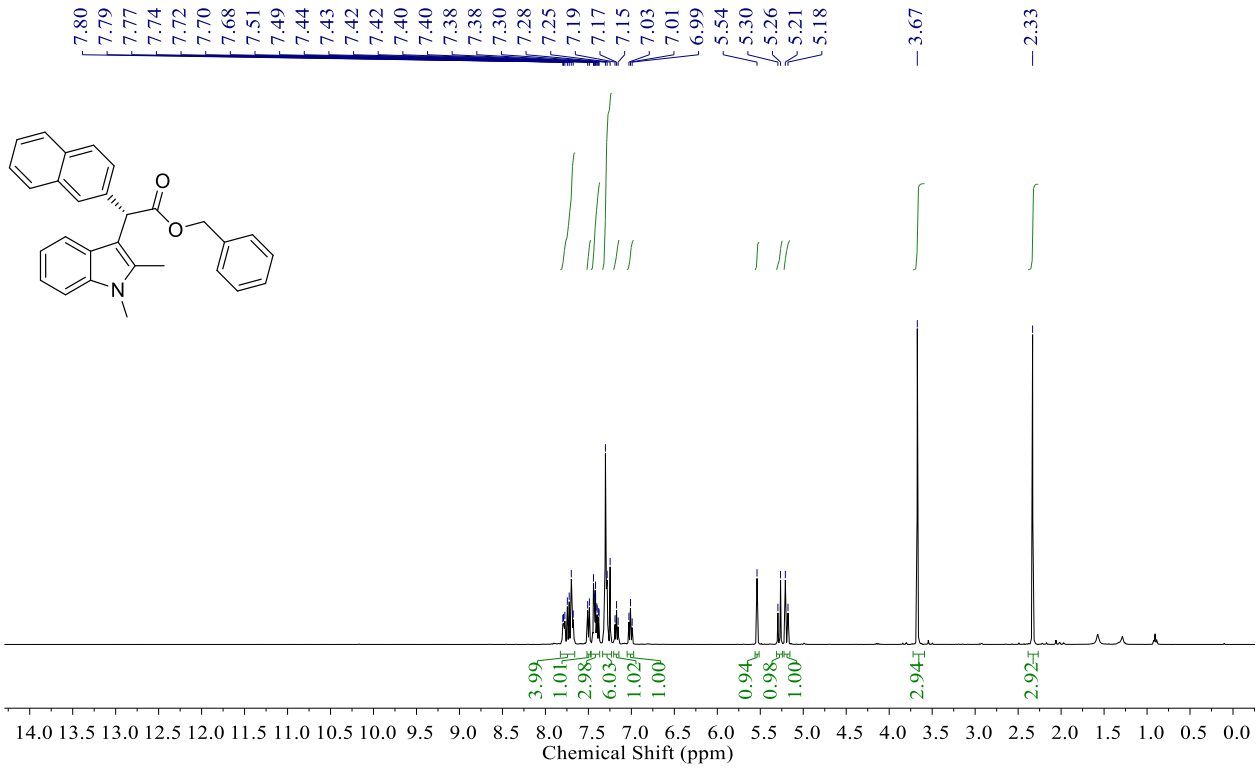

Figure S52. ^{1}H NMR, **3ga**

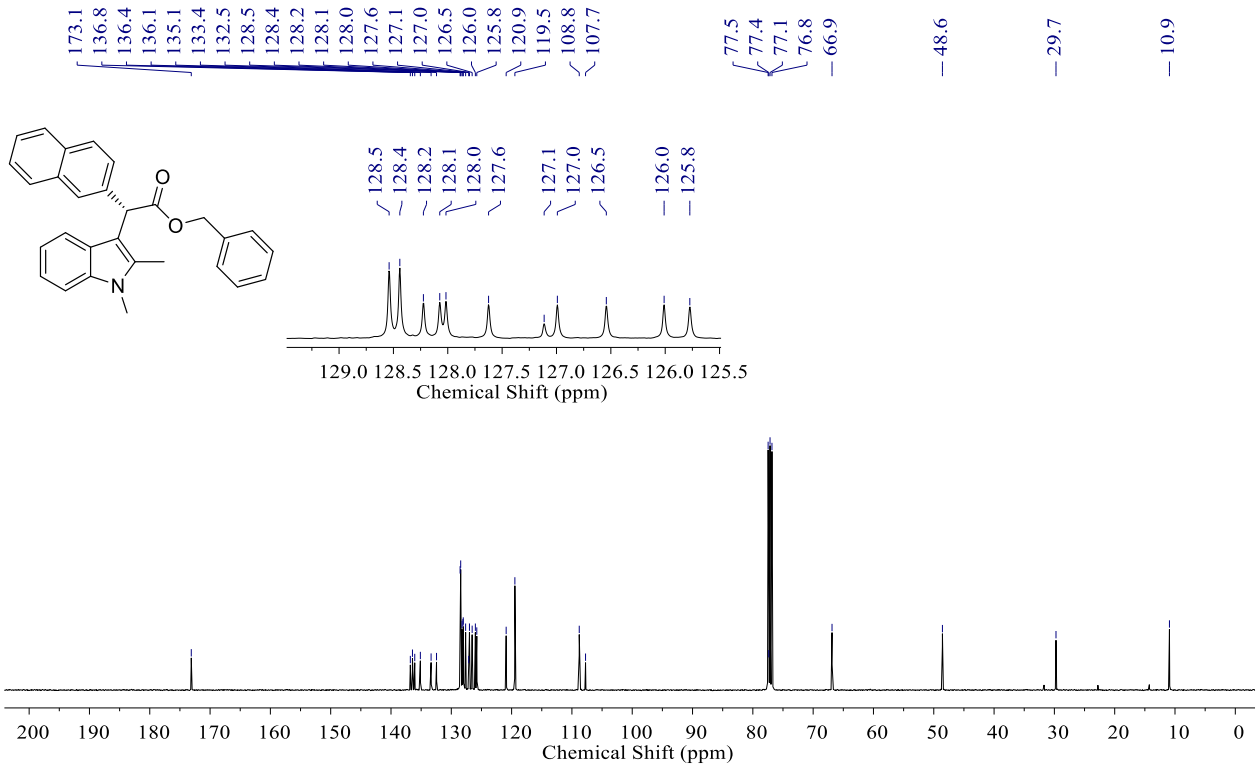

Figure S53. ^{13}C NMR, **3ga**

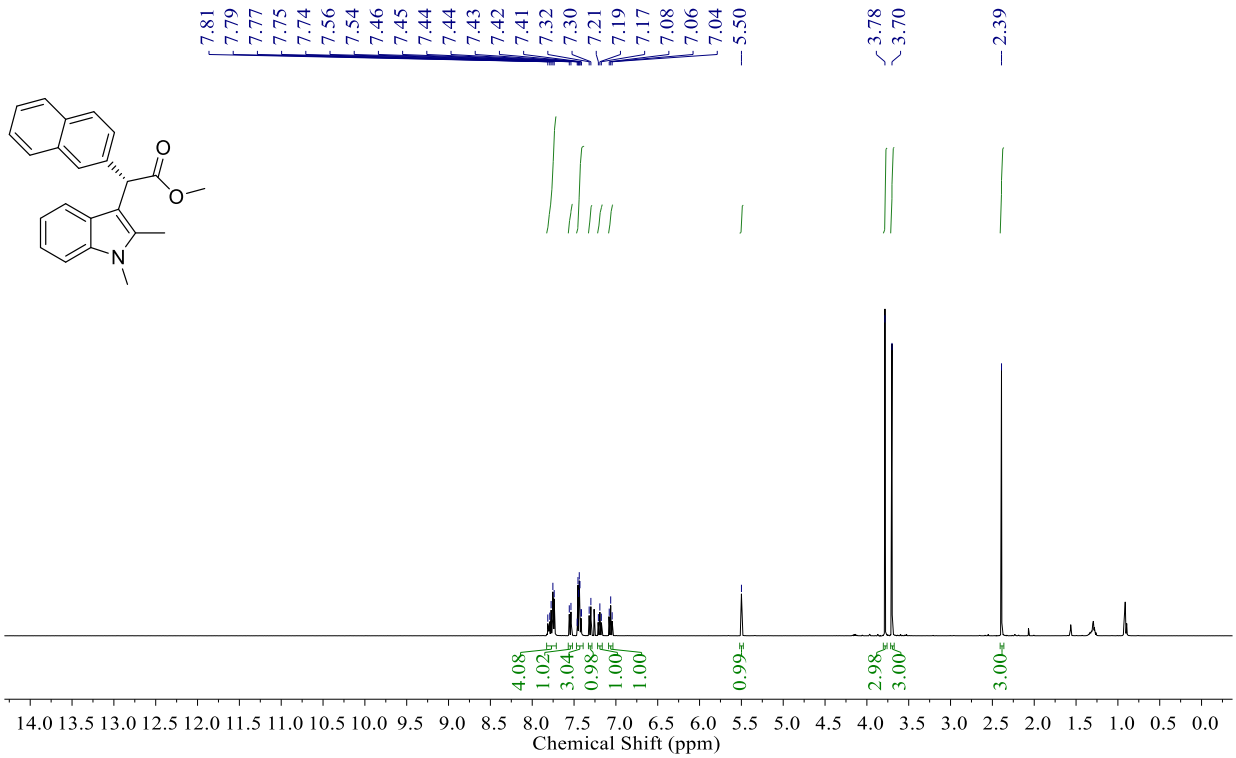

Figure S54. ^{1}H NMR, **3ha**

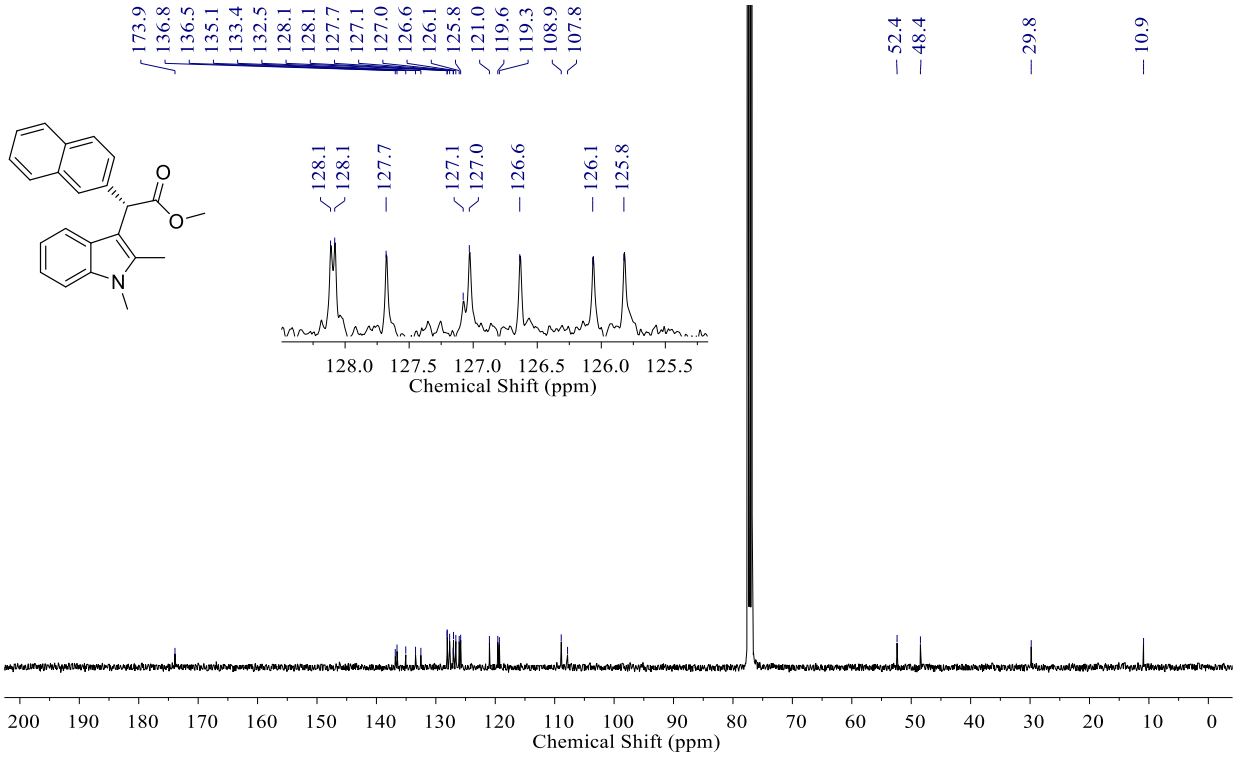

Figure S55. ^{13}C NMR, **3ha**

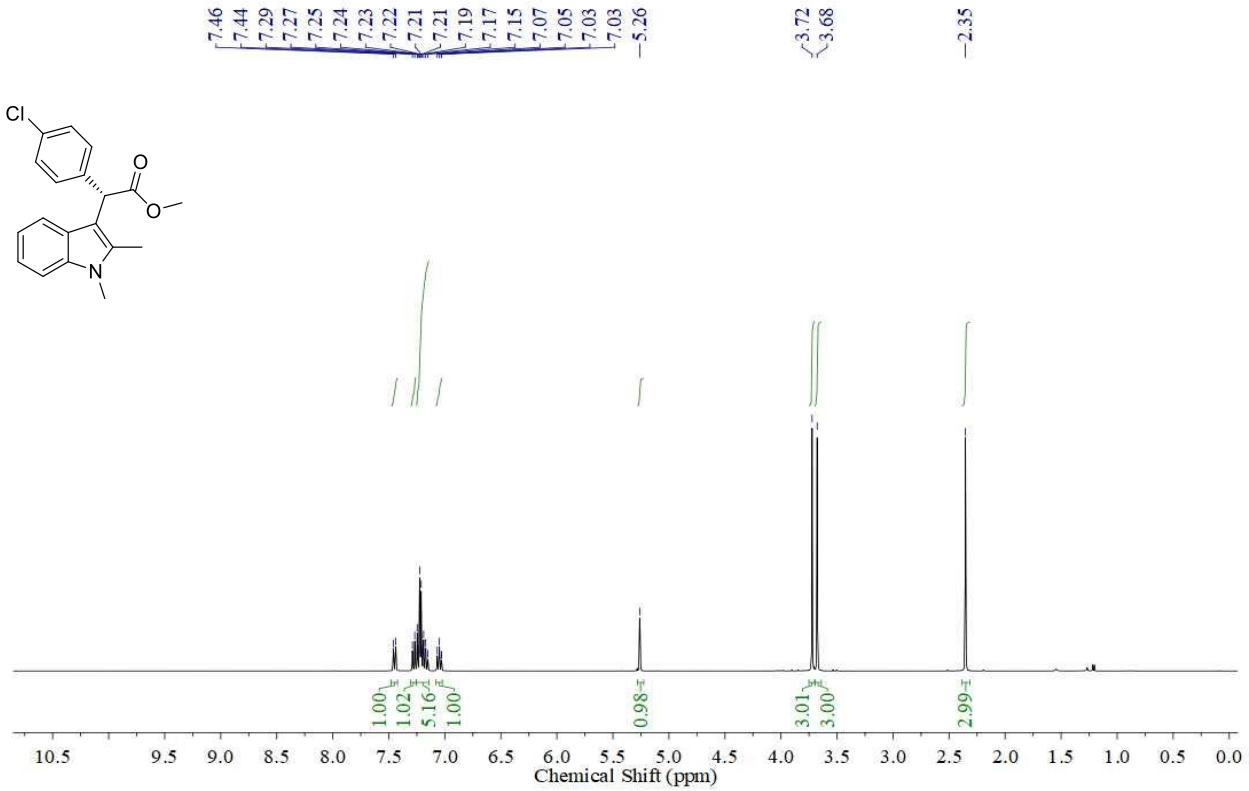

Figure S56. ^{1}H NMR, **3ia**

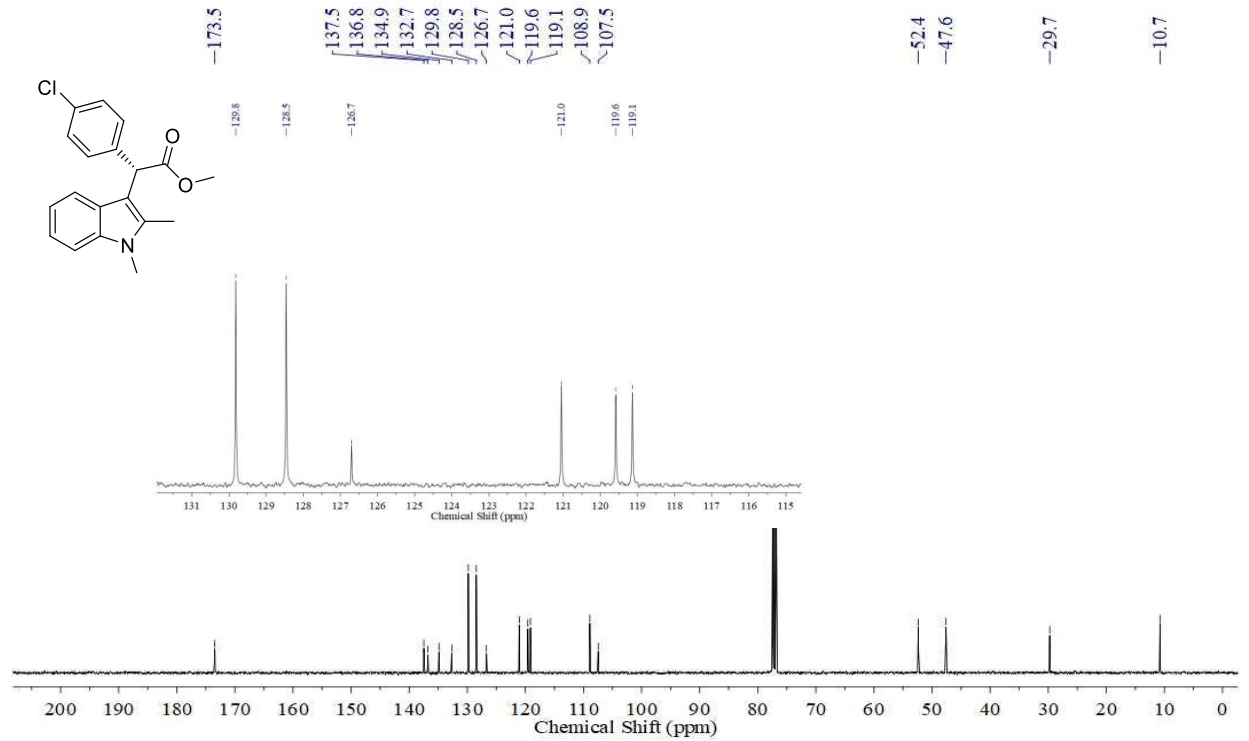

Figure S57. ^{13}C NMR, **3ia**

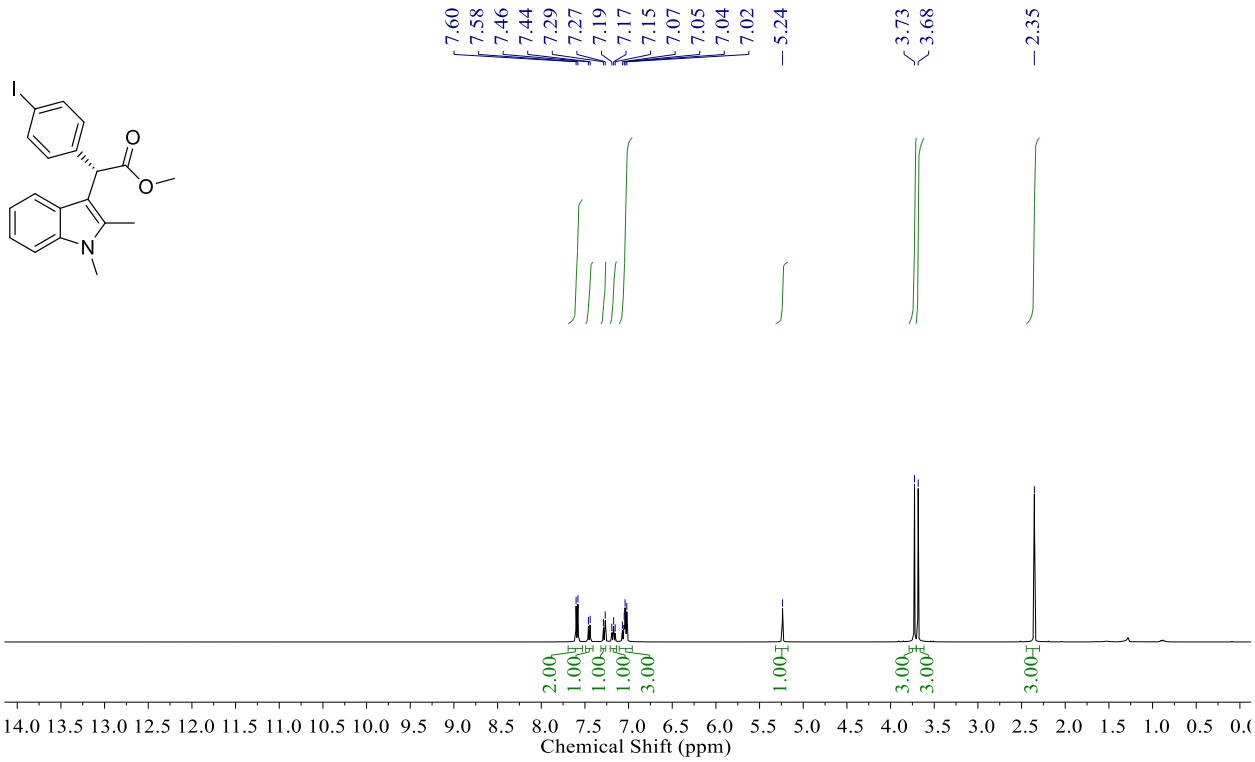

Figure S58. ^{1}H NMR, **3ka**

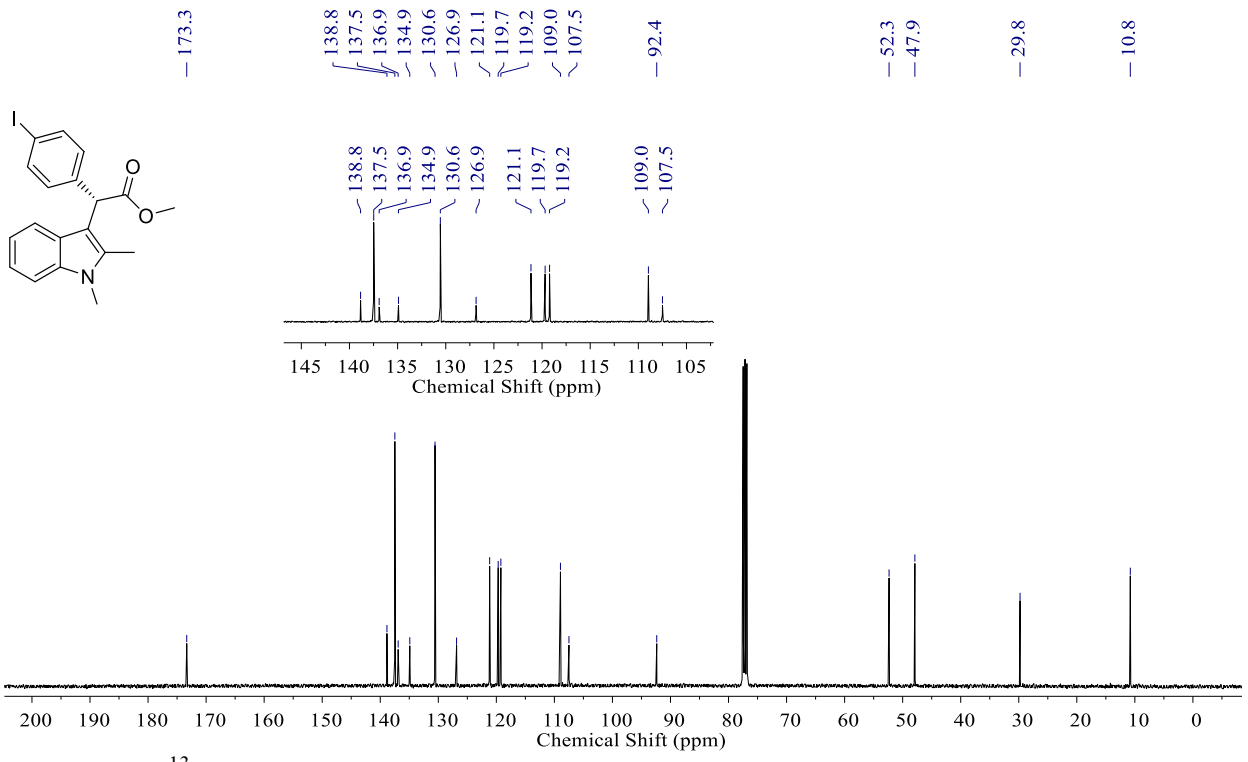

Figure S59. ^{13}C NMR, **3ka**

11. HPLC traces

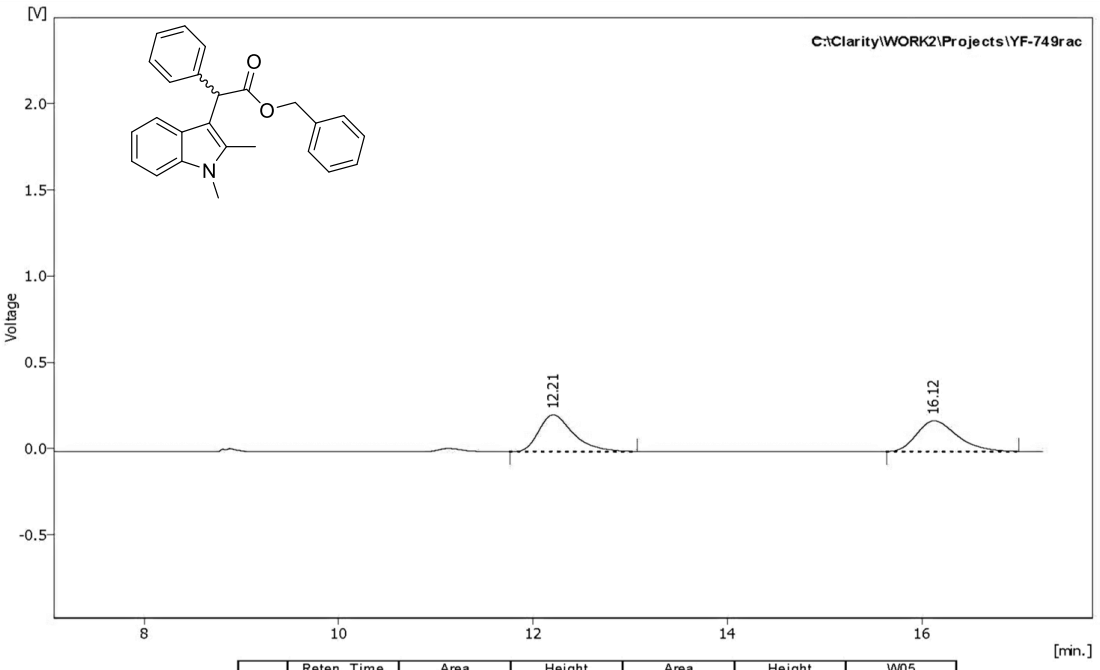

	Reten. Time [min]	Area [mV.s]	Height [mV]	Area [%]	Height [%]	W05 [min]
1	12.208	5266.154	213.229	50.3	54.4	0.37
2	16.124	5197.255	178.713	49.7	45.6	0.44
	Total	10463.409	391.943	100.0	100.0	

Figure S60. HPLC, racemic **3aa**

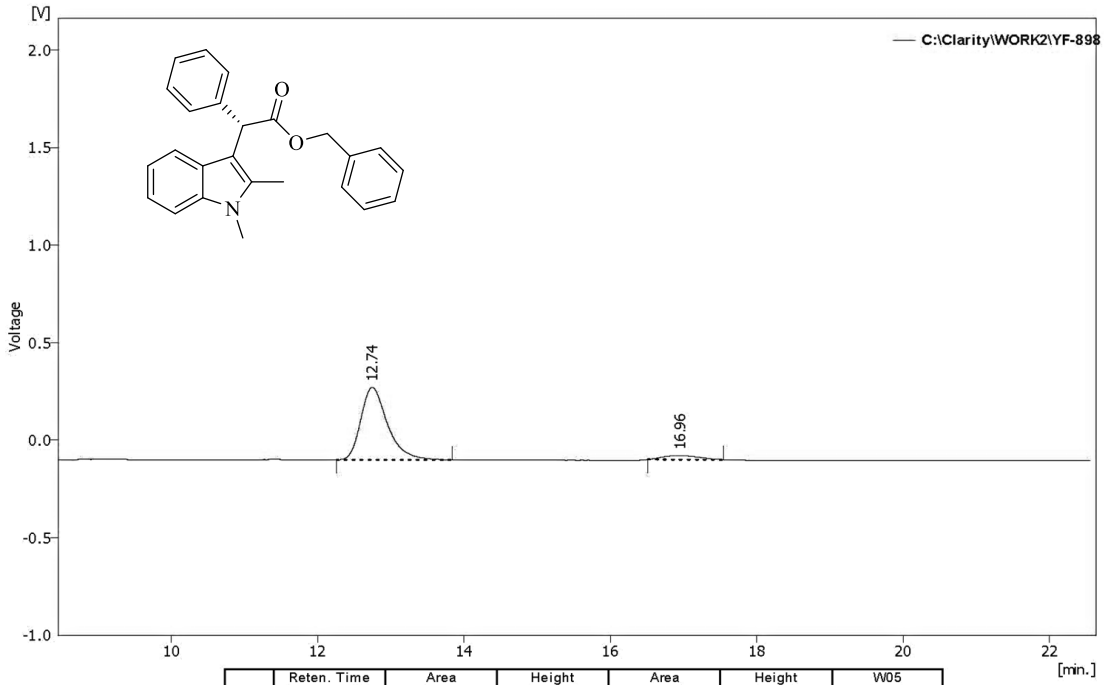

	Reten. Time [min]	Area [mV.s]	Height [mV]	Area [%]	Height [%]	W05 [min]
1	12.744	9410.501	371.523	93.2	94.9	0.38
2	16.956	691.628	20.158	6.8	5.1	0.58
	Total	10102.130	391.682	100.0	100.0	

Figure S61. HPLC, enantioenriched **3aa**

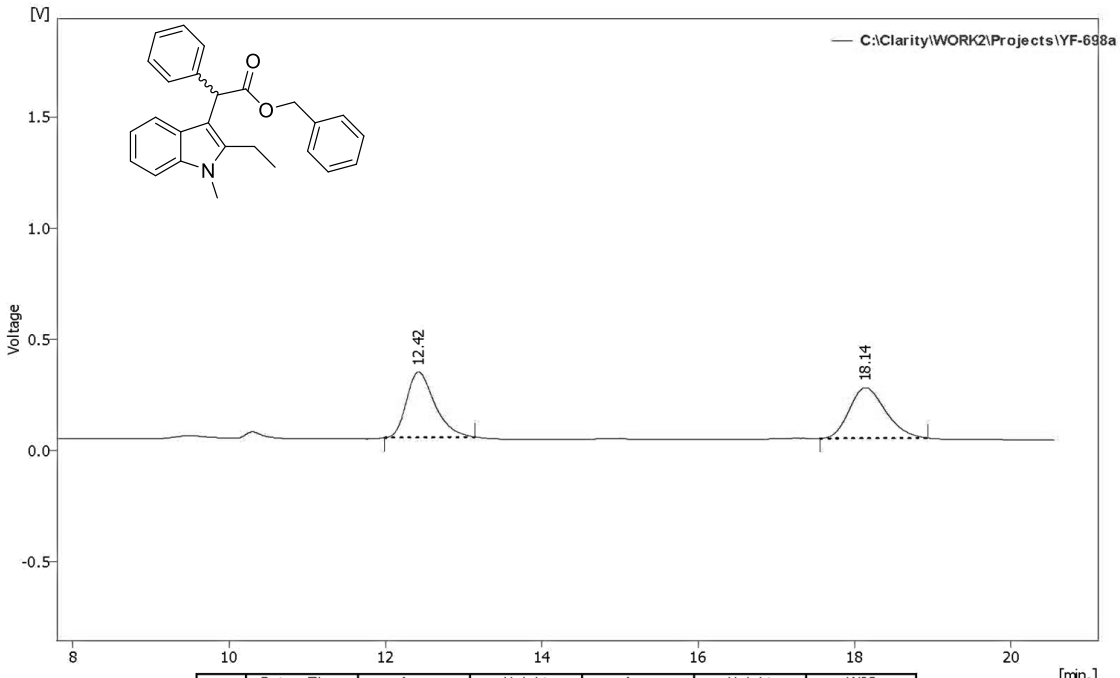

	Reten. Time [min]	Area [mV.s]	Height [mV]	Area [%]	Height [%]	W05 [min]
1	12.424	7371.724	295.013	50.1	56.4	0.38
2	18.144	7344.960	227.720	49.9	43.6	0.50
	Total	14716.684	522.733	100.0	100.0	

Figure S62. HPLC, racemic **3ab**

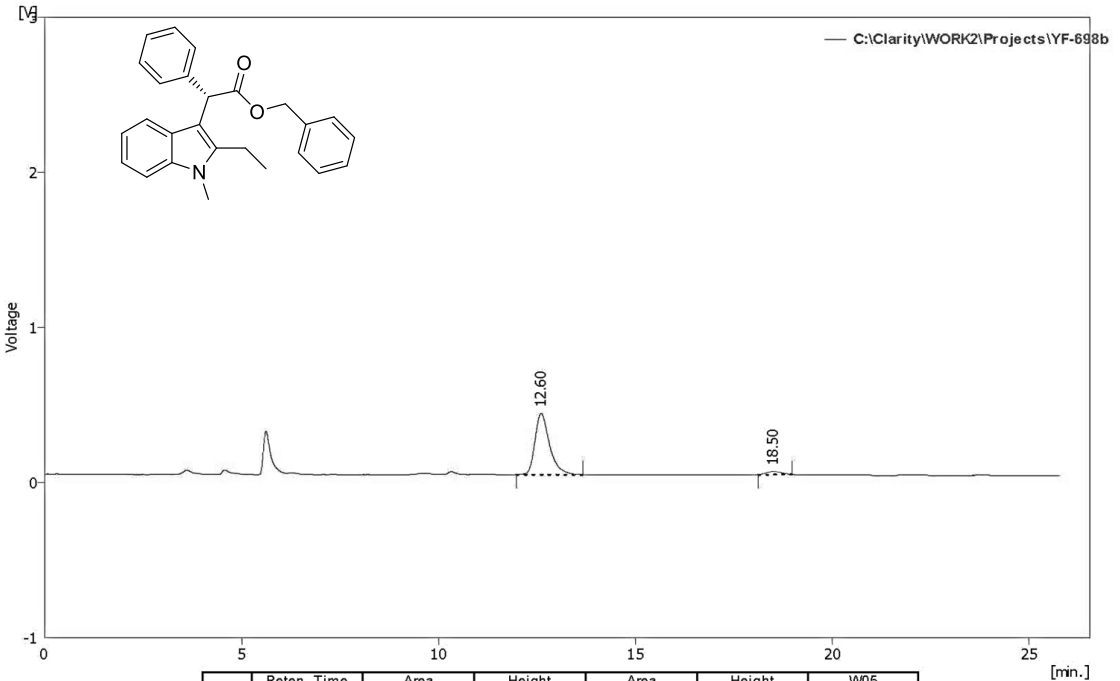

	Reten. Time [min]	Area [mV.s]	Height [mV]	Area [%]	Height [%]	W05 [min]
1	12.600	10205.403	395.319	95.0	95.2	0.38
2	18.496	542.587	20.046	5.0	4.8	0.46
	Total	10747.989	415.366	100.0	100.0	

Figure S63. HPLC, enantioenriched **3ab**

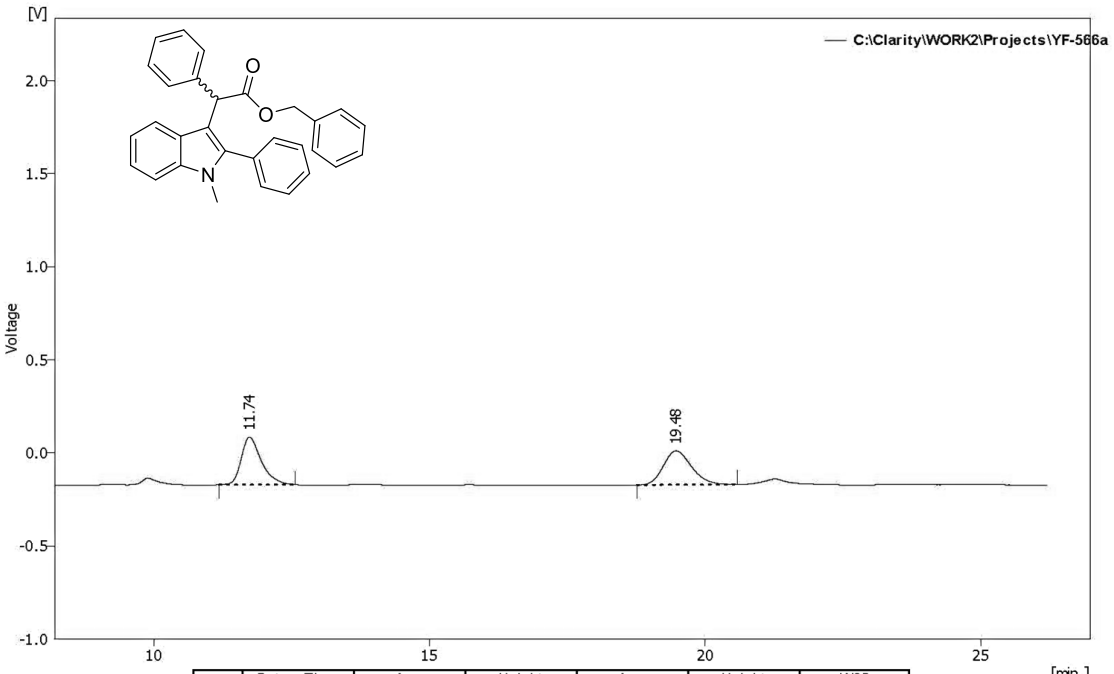

	Reten. Time [min]	Area [mV.s]	Height [mV]	Area [%]	Height [%]	W05 [min]
1	11.740	6461.487	255.500	50.0	58.4	0.38
2	19.476	6455.090	182.078	50.0	41.6	0.55
	Total	12916.577	437.578	100.0	100.0	

Figure S64. HPLC, racemic **3ac**

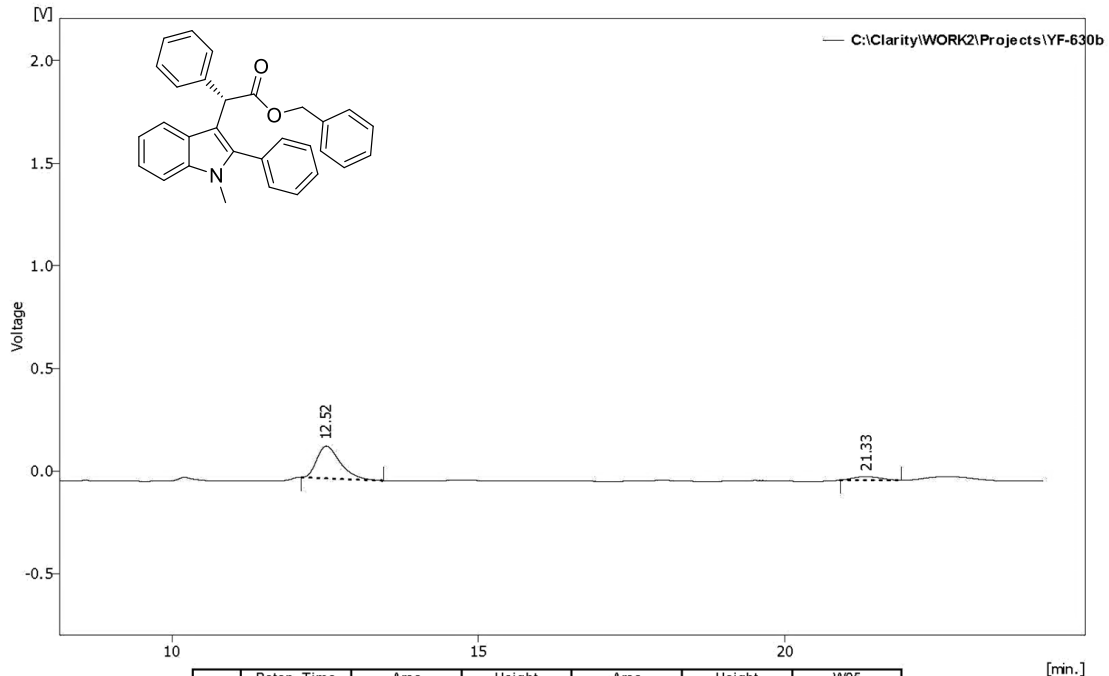

	Reten. Time [min]	Area [mV.s]	Height [mV]	Area [%]	Height [%]	W05 [min]
1	12.516	4148.997	156.936	88.4	89.9	0.40
2	21.332	542.924	17.565	11.6	10.1	0.52
	Total	4691.921	174.501	100.0	100.0	

Figure S65. HPLC, enantioenriched **3ac**

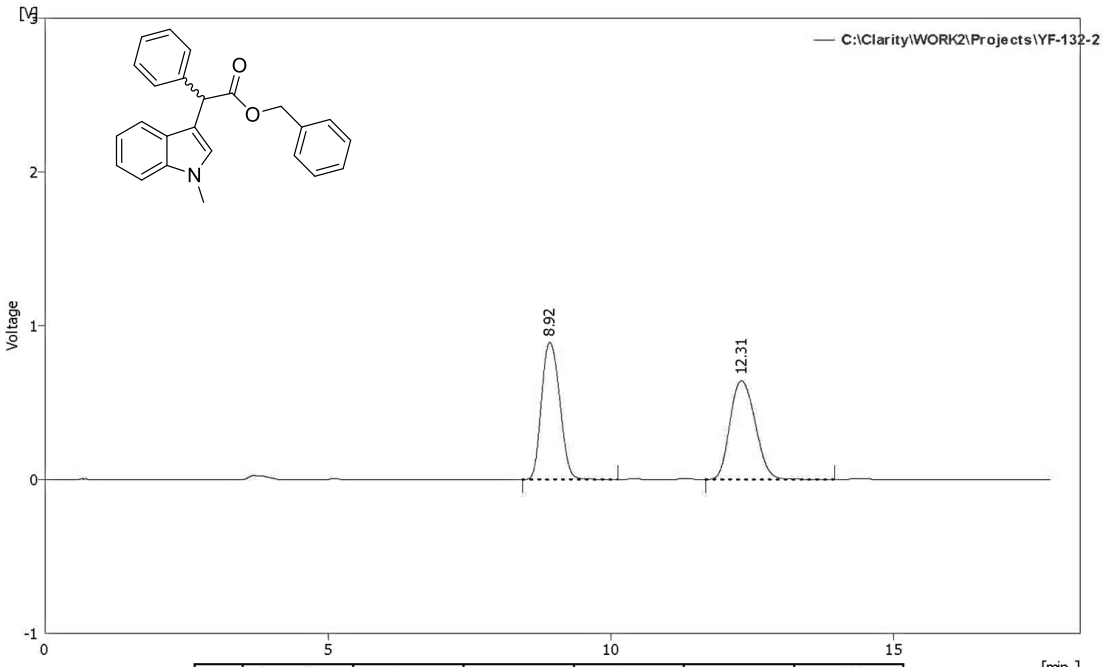

	Reten. Time [min]	Area [mV.s]	Height [mV]	Area [%]	Height [%]	W05 [min]
1	8.920	19950.469	891.758	50.1	58.1	0.36
2	12.308	19838.565	641.825	49.9	41.9	0.50
	Total	39789.034	1533.582	100.0	100.0	

Figure S66. HPLC, racemic **3ad**

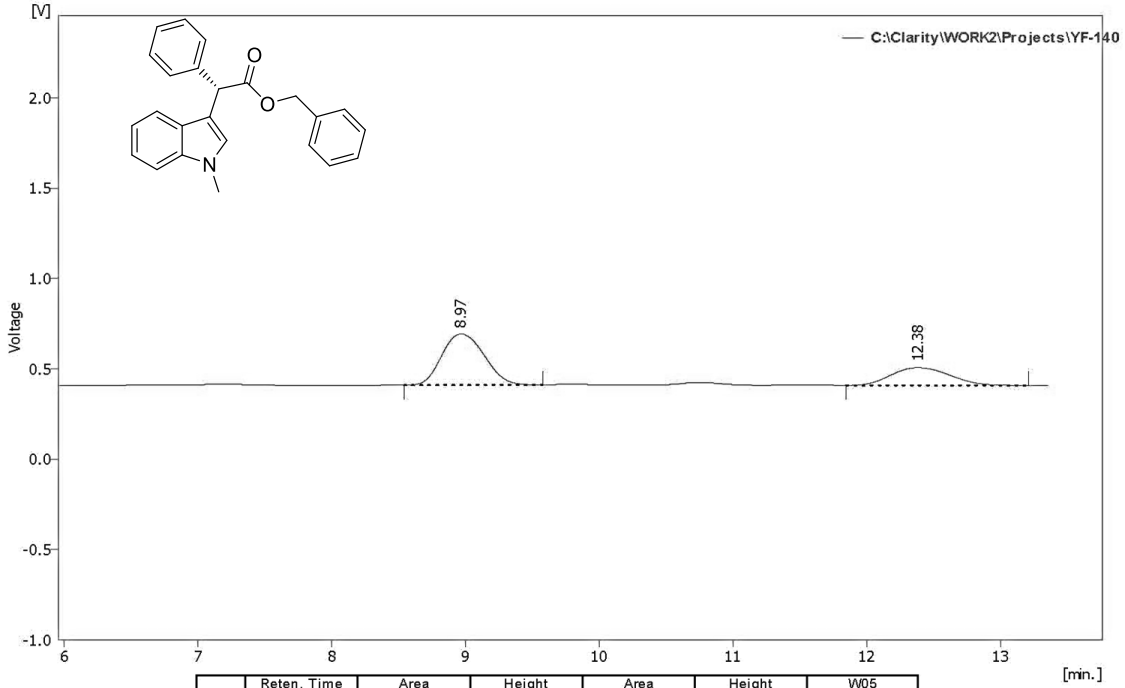

	Reten. Time [min]	Area [mV.s]	Height [mV]	Area [%]	Height [%]	W05 [min]
1	8.968	6213.999	282.825	67.7	74.3	0.36
2	12.384	2963.559	97.750	32.3	25.7	0.50
	Total	9177.558	380.575	100.0	100.0	

Figure S67. HPLC, enantioenriched **3ad**

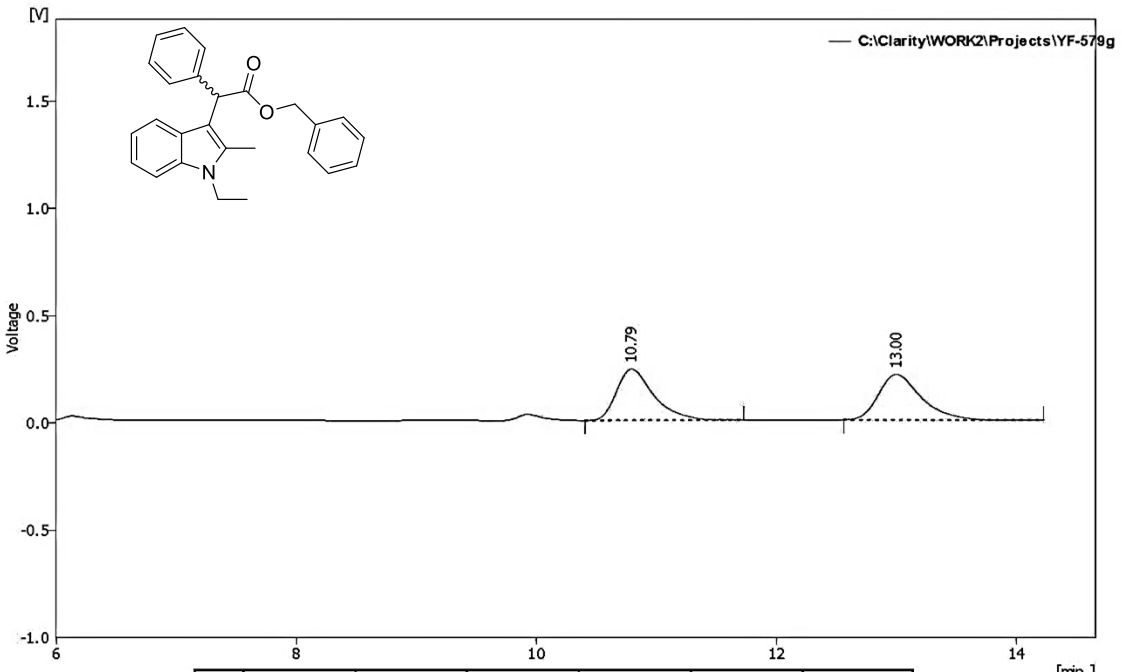

	Reten. Time [min]	Area [mV.s]	Height [mV]	Area [%]	Height [%]	W05 [min]
1	10.792	5146.733	239.169	49.5	53.0	0.32
2	12.996	5251.898	212.012	50.5	47.0	0.37
	Total	10398.631	451.182	100.0	100.0	

Figure S68. HPLC, racemic **3ae**

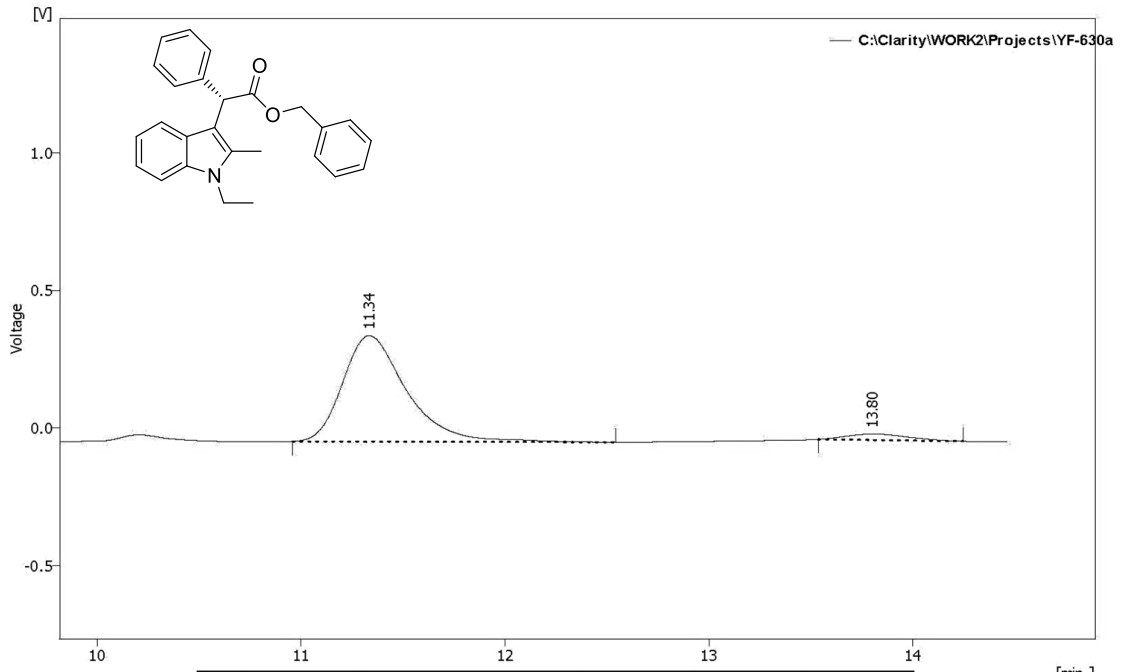

	Reten. Time [min]	Area [mV.s]	Height [mV]	Area [%]	Height [%]	W05 [min]
1	11.336	8337.329	385.242	94.8	94.6	0.32
2	13.804	461.583	21.784	5.2	5.4	0.34
	Total	8798.912	407.025	100.0	100.0	

Figure S69. HPLC, enantioenriched **3ae**

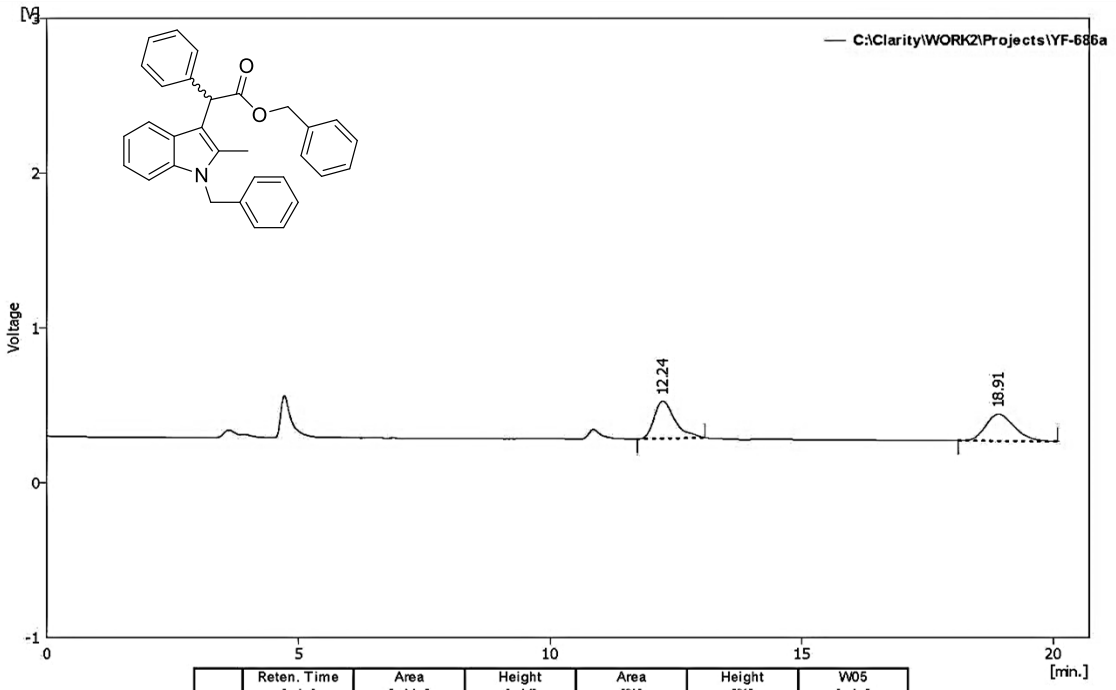

	Reten. Time [min]	Area [mV.s]	Height [mV]	Area [%]	Height [%]	W05 [min]
1	12.240	6928.381	241.982	50.1	58.2	0.42
2	18.908	6900.569	173.907	49.9	41.8	0.61
	Total	13828.950	415.890	100.0	100.0	

Figure S70. HPLC, racemic **3af**

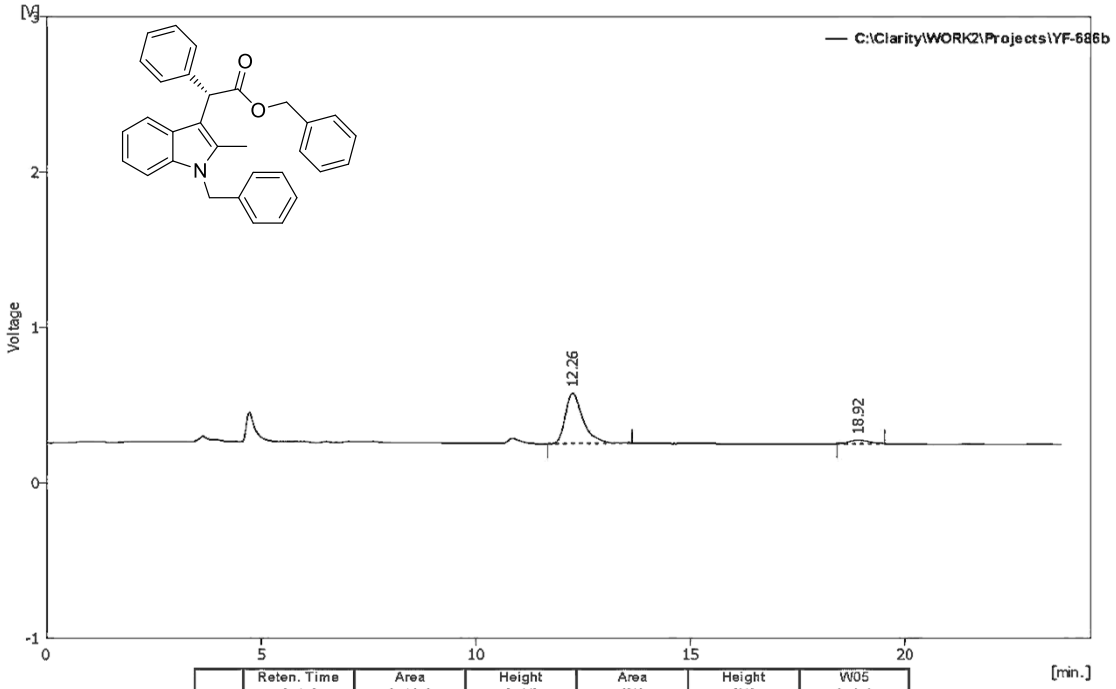

	Reten. Time [min]	Area [mV.s]	Height [mV]	Area [%]	Height [%]	W05 [min]
1	12.256	9235.943	324.953	92.5	93.6	0.42
2	18.916	745.534	22.214	7.5	6.4	0.56
	Total	9981.477	347.167	100.0	100.0	

Figure S71. HPLC, enantioenriched **3af**

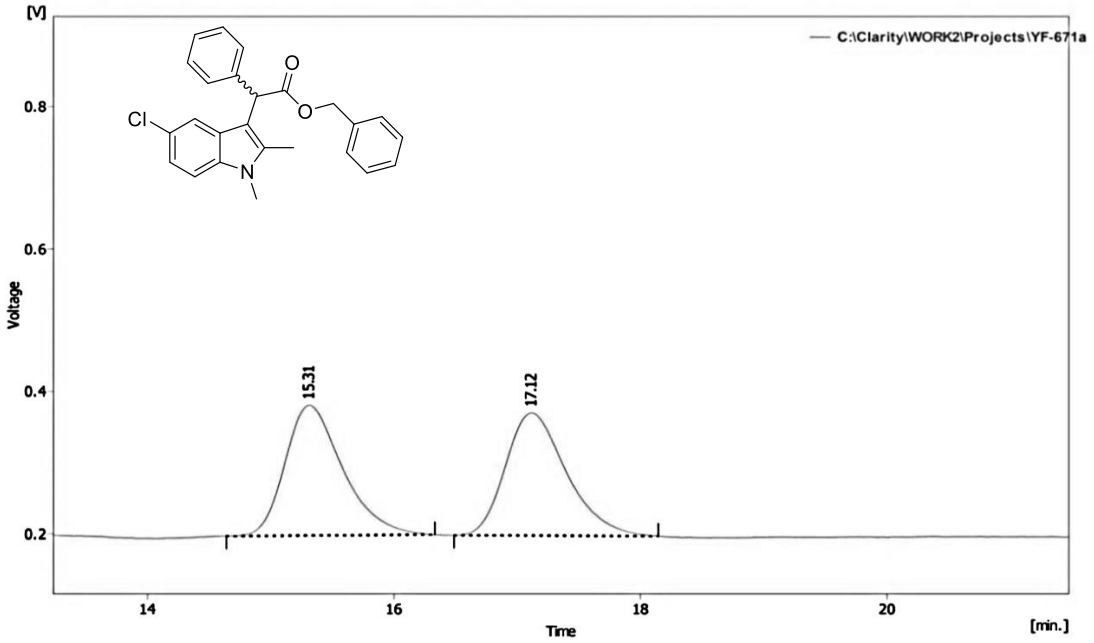

Result Table (Uncal - C:\Clarity\WORK2\Projects\YF-671a)

	Reten. Time [min]	Area [mV.s]	Height [mV]	Area [%]	Height [%]	W05 [min]
1	15.312	5955.928	183.099	50.1	51.5	0.50
2	17.116	5923.113	172.230	49.9	48.5	0.53
	Total	11879.041	355.329	100.0	100.0	

Figure S72. HPLC, racemic **3ag**

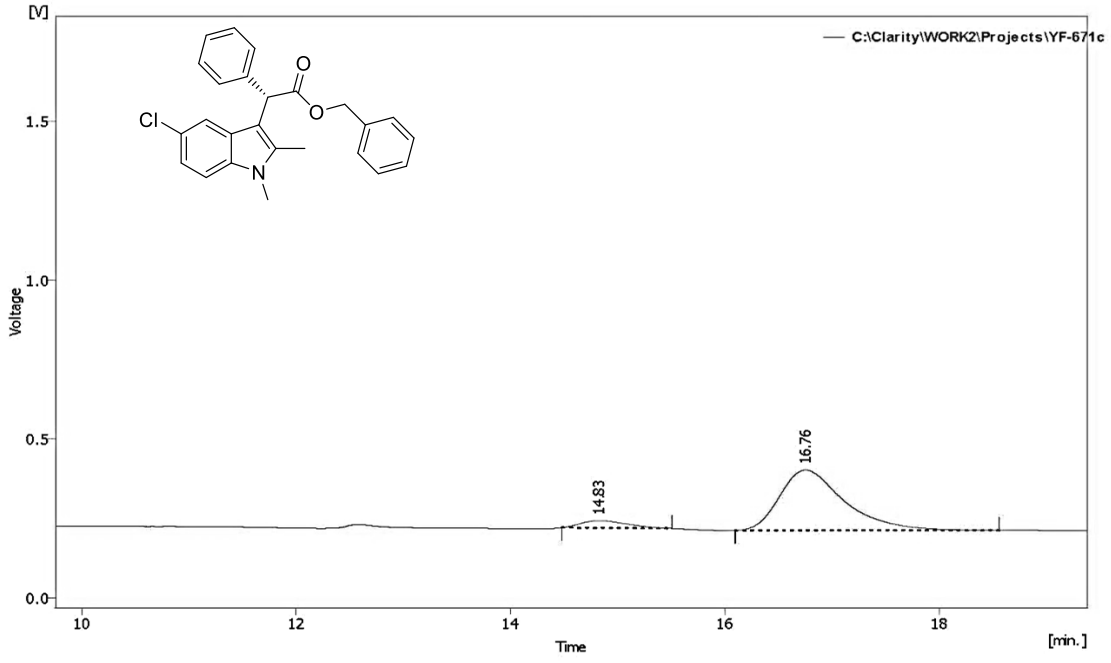

Result Table (Uncal - C:\Clarity\WORK2\Projects\YF-671c)

	Reten. Time [min]	Area [mV.s]	Height [mV]	Area [%]	Height [%]	W05 [min]
1	14.828	691.734	22.823	8.0	10.7	0.48
2	16.756	7962.948	190.161	92.0	89.3	0.62
	Total	8654.683	212.984	100.0	100.0	

Figure S73. HPLC, enantioenriched **3ag**

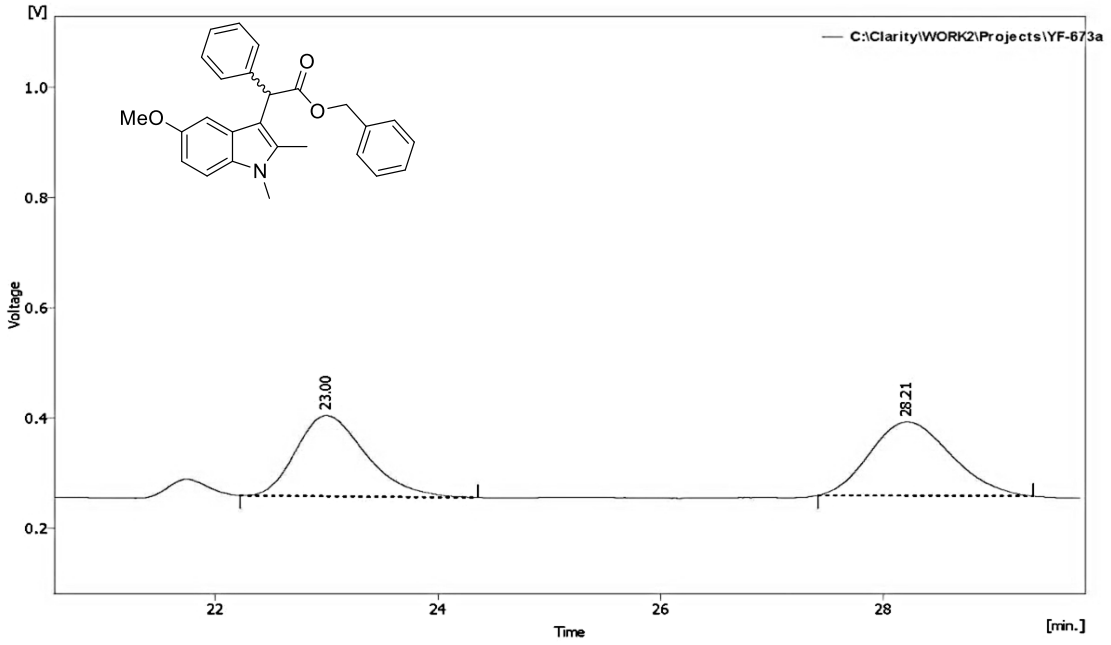

Result Table (Uncal - C:\Clarity\WORK2\Projects\YF-673a)

	Reten. Time [min]	Area [mV.s]	Height [mV]	Area [%]	Height [%]	W05 [min]
1	22.996	6397.337	146.691	48.5	52.3	0.67
2	28.208	6793.017	133.618	51.5	47.7	0.81
	Total	13190.354	280.309	100.0	100.0	

Figure S74. HPLC, racemic **3ah**

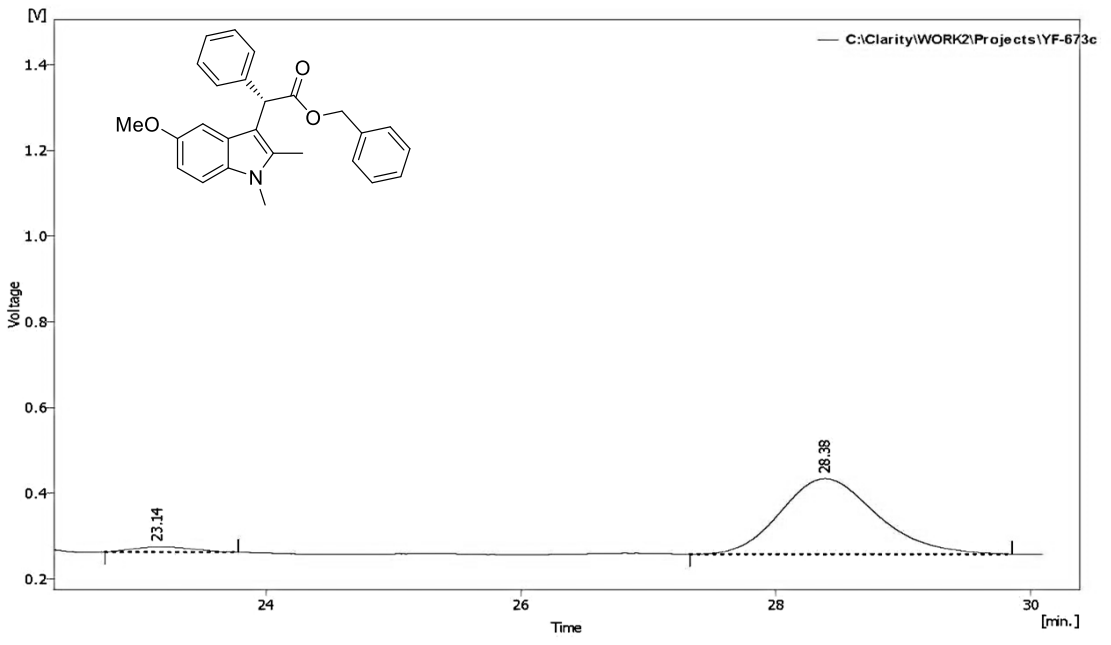

Result Table (Uncal - C:\Clarity\WORK2\Projects\YF-673c)

	Reten. Time [min]	Area [mV.s]	Height [mV]	Area [%]	Height [%]	W05 [min]
1	23.144	385.534	11.769	4.0	6.3	0.54
2	28.384	9193.656	175.642	96.0	93.7	0.81
	Total	9579.190	187.411	100.0	100.0	

Figure S75. HPLC, enantioenriched **3ag**

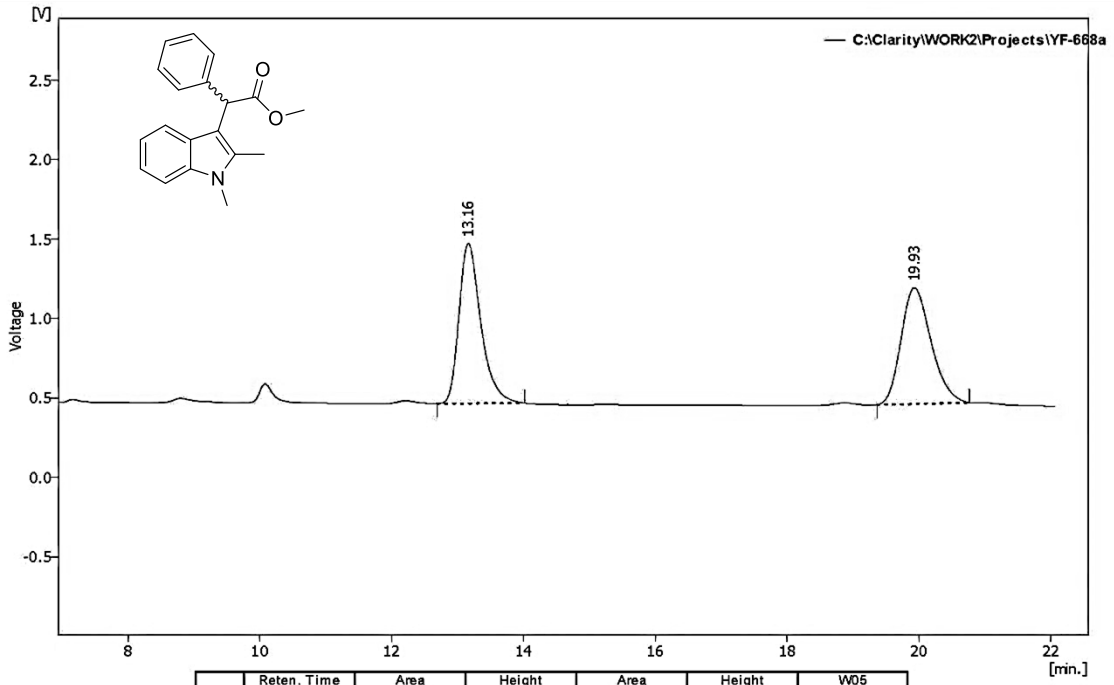

	Reten. Time [min]	Area [mV.s]	Height [mV]	Area [%]	Height [%]	W05 [min]
1	13.164	23181.909	1006.364	50.1	57.9	0.35
2	19.932	23107.837	730.965	49.9	42.1	0.50
	Total	46289.746	1737.328	100.0	100.0	

Figure S76. HPLC, racemic **3ba**

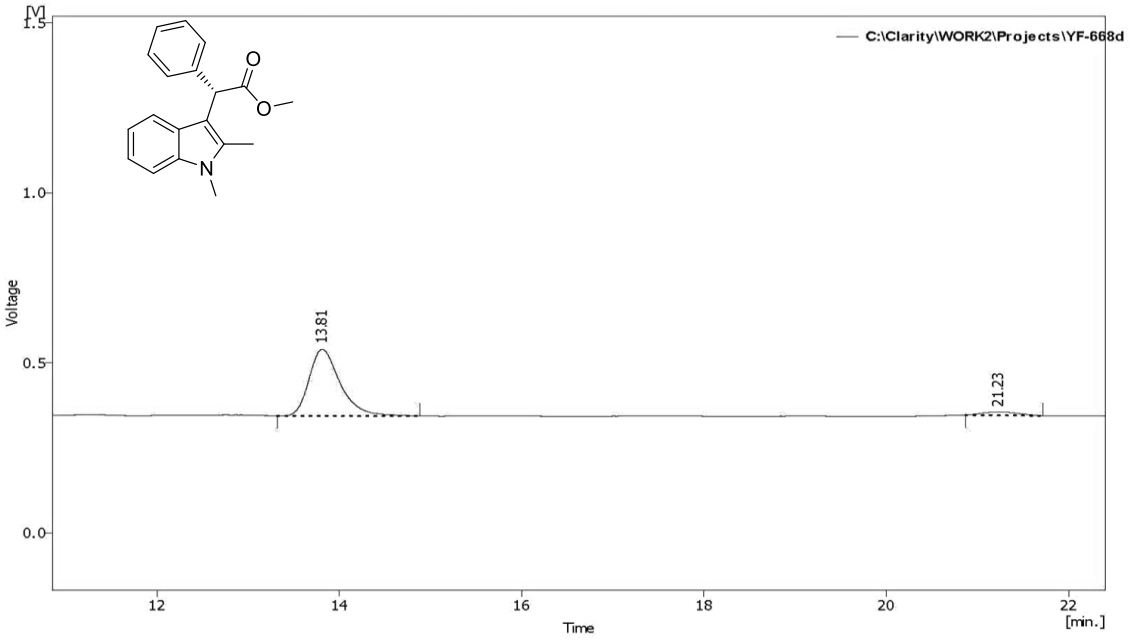

Result Table (Uncal - C:\Clarity\WORK2\Projects\YF-668d)

	Reten. Time [min]	Area [mV.s]	Height [mV]	Area [%]	Height [%]	W05 [min]
1	13.812	4644.624	196.287	94.4	95.1	0.35
2	21.232	274.657	10.158	5.6	4.9	0.44
	Total	4919.281	206.444	100.0	100.0	

Figure S77. HPLC, enantioenriched **3ba**

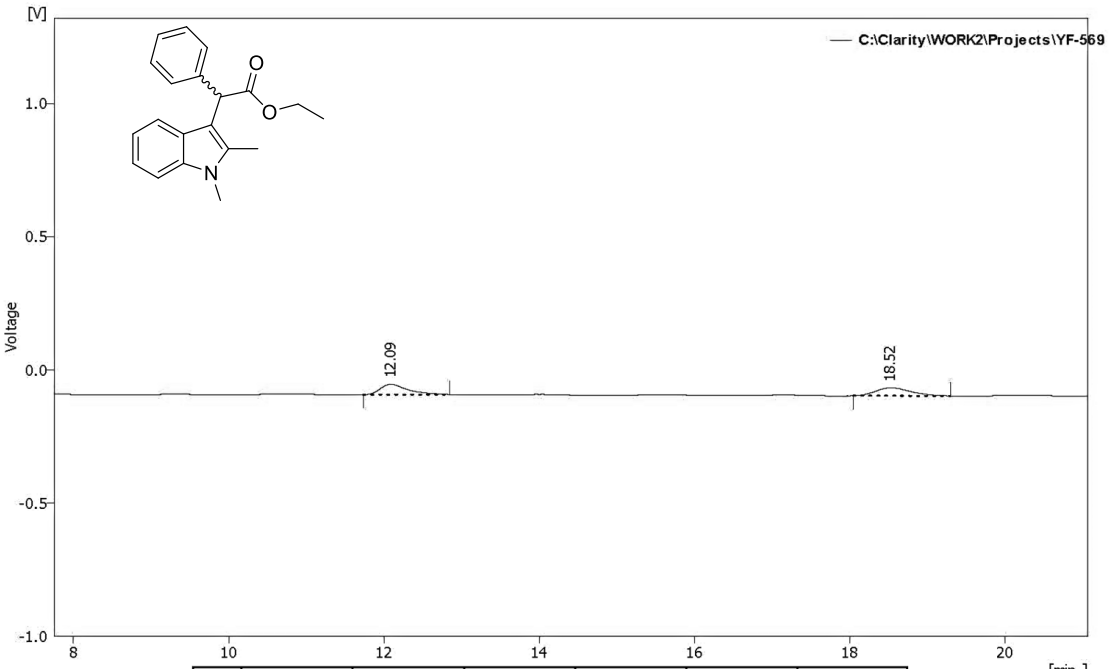

	Reten. Time [min]	Area [mV.s]	Height [mV]	Area [%]	Height [%]	W05 [min]
1	12.088	967.907	39.463	50.6	57.0	0.36
2	18.520	943.357	29.793	49.4	43.0	0.49
	Total	1911.263	69.256	100.0	100.0	

Figure S78. HPLC, racemic **3ca**

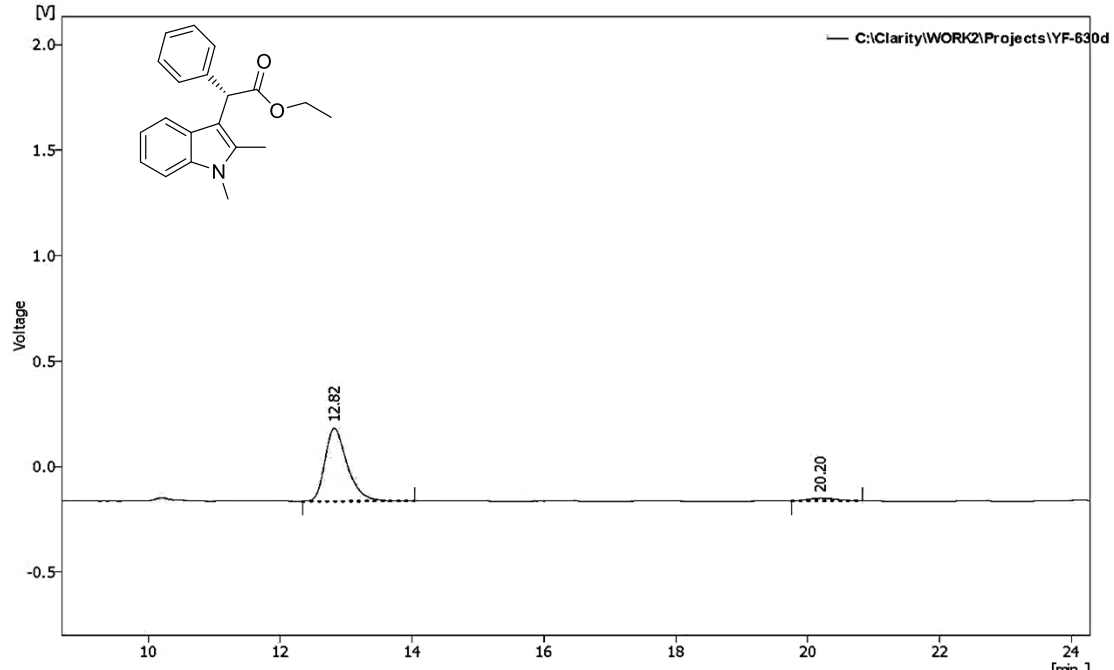

	Reten. Time [min]	Area [mV.s]	Height [mV]	Area [%]	Height [%]	W05 [min]
1	12.820	8097.186	345.656	96.0	96.6	0.36
2	20.200	337.751	12.024	4.0	3.4	0.46
	Total	8434.937	357.680	100.0	100.0	

Figure S79. HPLC, enantioenriched **3ca**

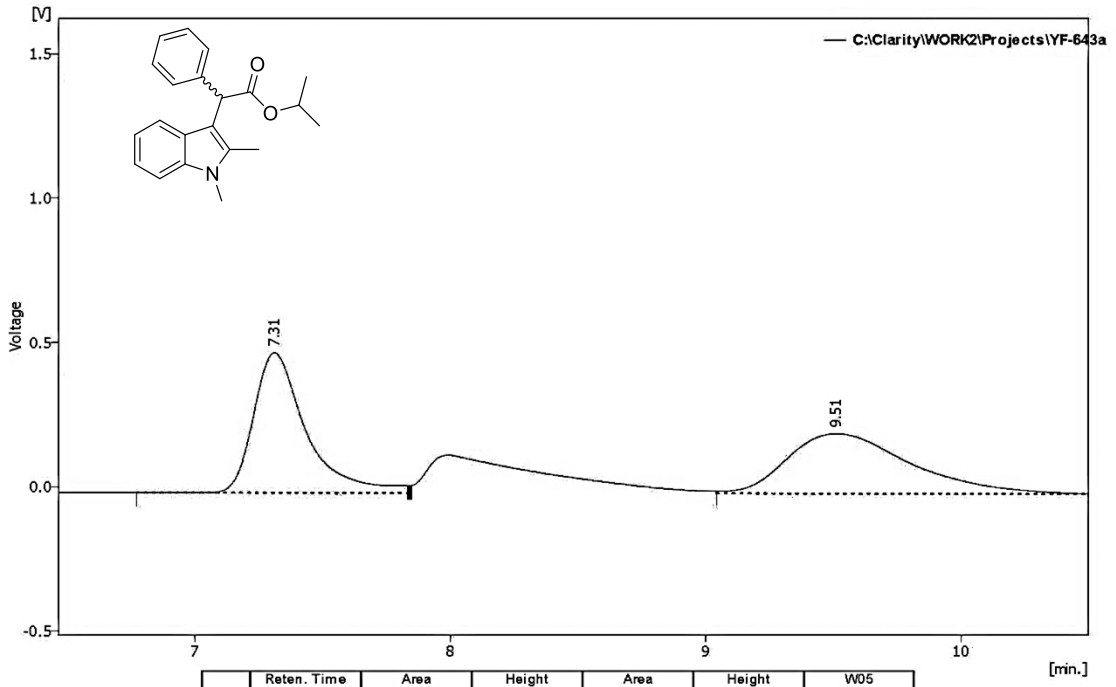

	Reten. Time [min]	Area [mV.s]	Height [mV]	Area [%]	Height [%]	W05 [min]
1	7.312	6919.802	484.913	49.8	70.0	0.20
3	9.512	6963.587	207.570	50.2	30.0	0.51
	Total	13883.389	692.483	100.0	100.0	

Figure S80. HPLC, racemic **3da**

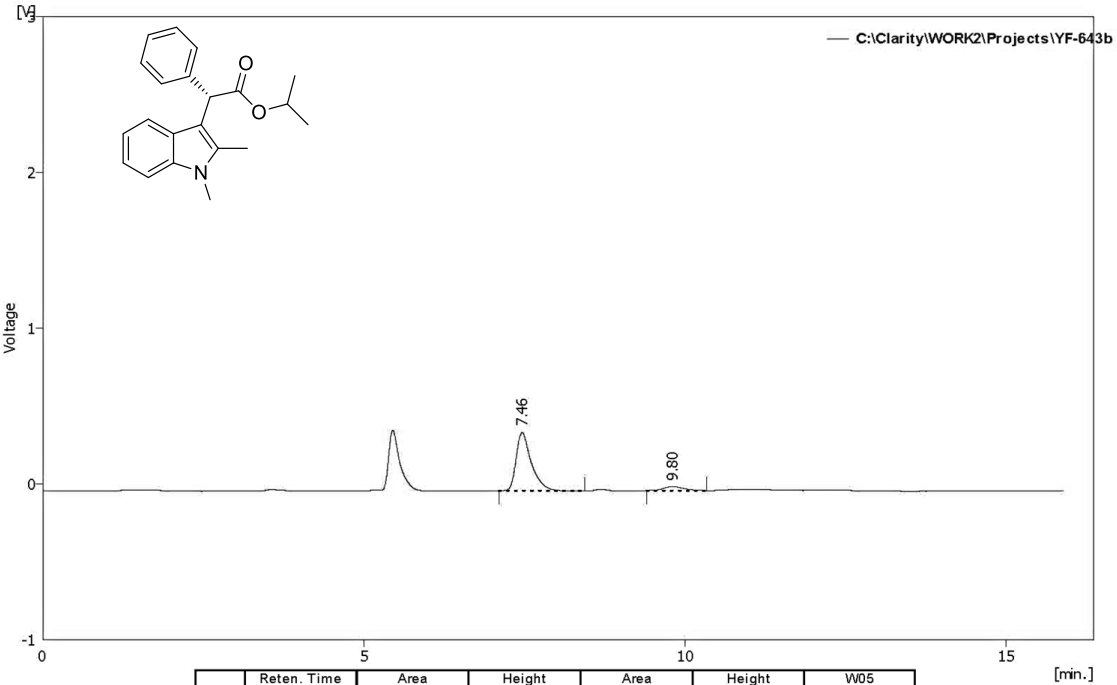

	Reten. Time [min]	Area [mV.s]	Height [mV]	Area [%]	Height [%]	W05 [min]
1	7.460	6124.602	373.638	91.5	93.4	0.24
2	9.804	568.415	26.305	8.5	6.6	0.33
	Total	6693.017	399.942	100.0	100.0	

Figure S81. HPLC, enantioenriched **3da**

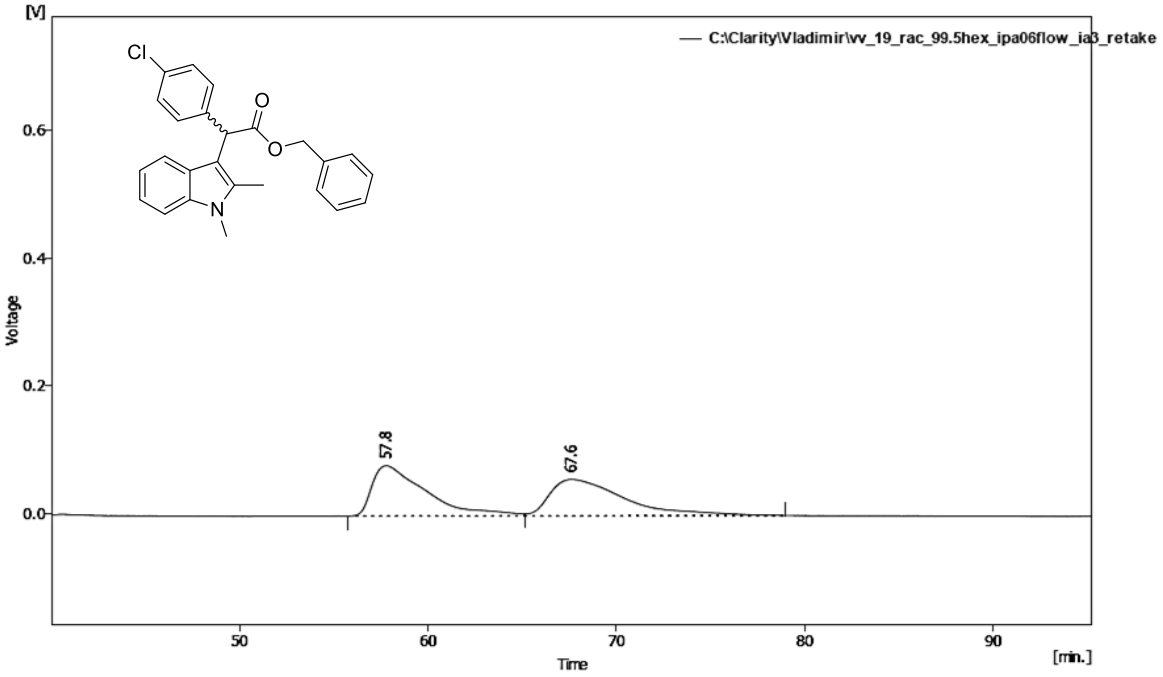

Result Table (Uncal - C:\Clarity\Vladimir\vv_19_rac_99.5hex_ipa06flow_ia3_retake)

	Reten. Time [min]	Area [mV.s]	Height [mV]	Area [%]	Height [%]	W05 [min]
1	57.768	15669.745	78.917	50.0	58.0	2.98
2	67.592	15641.008	57.212	50.0	42.0	4.03
	Total	31310.753	136.129	100.0	100.0	

Figure S82. HPLC, racemic **3ea**

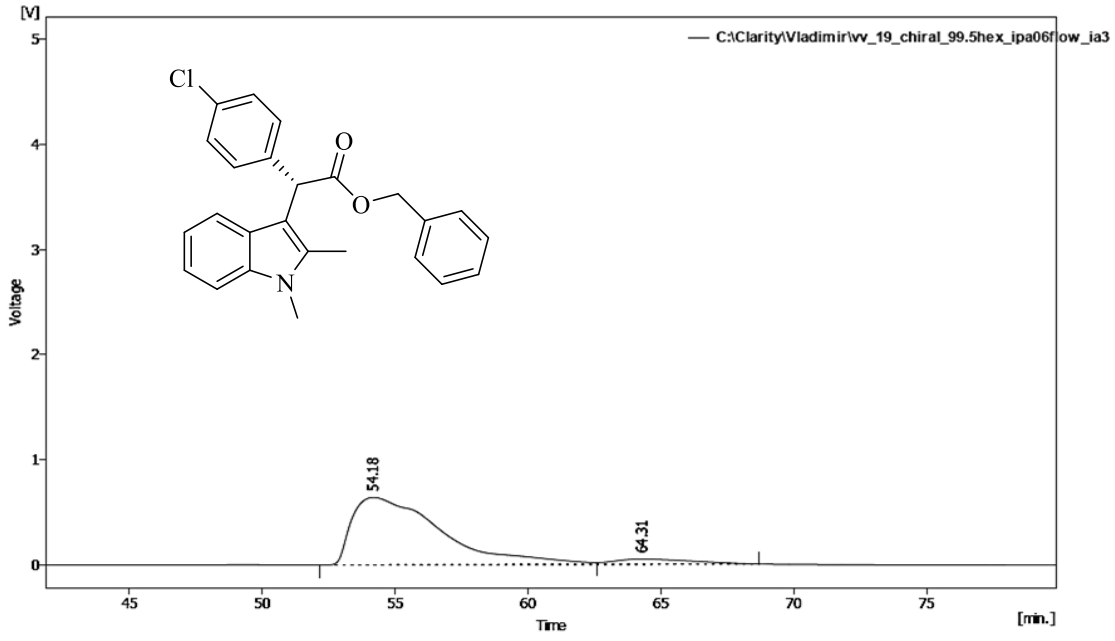

Result Table (Uncal - C:\Clarity\Vladimir\vv_19_chiral_99.5hex_ipa06flow_ia3)

	Reten. Time [min]	Area [mV.s]	Height [mV]	Area [%]	Height [%]	W05 [min]
1	54.180	150022.256	642.560	93.6	92.8	3.54
2	64.308	10199.576	49.791	6.4	7.2	3.51
	Total	160221.832	692.350	100.0	100.0	

Figure S83. HPLC, enantioenriched **3ea**

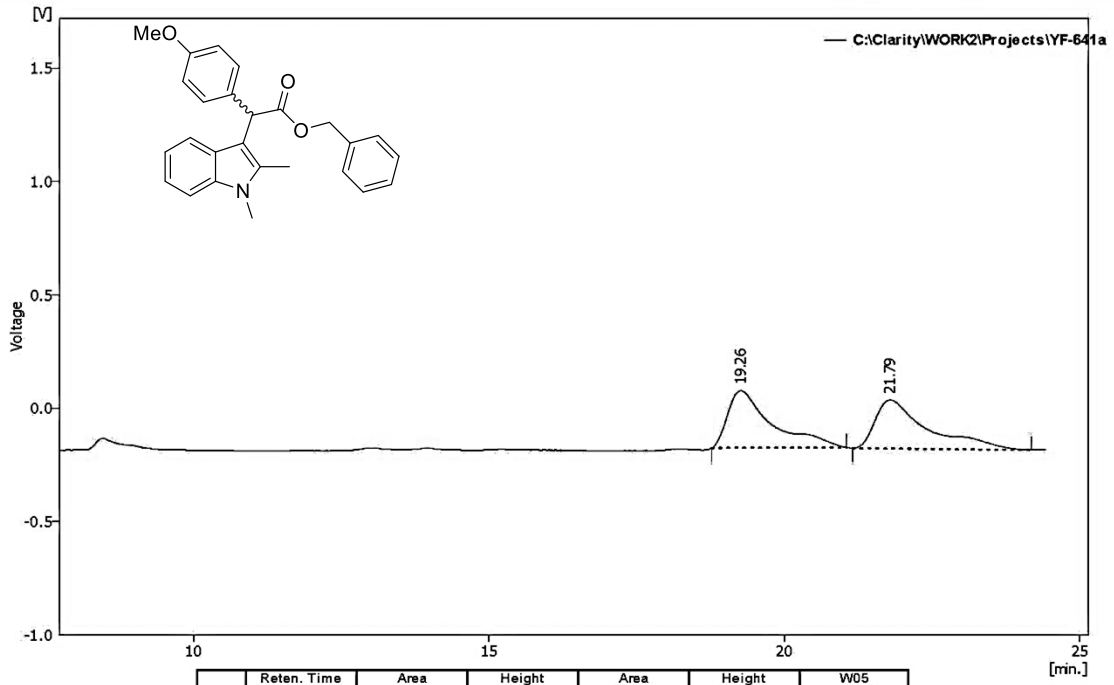

	Reten. Time [min]	Area [mV.s]	Height [mV]	Area [%]	Height [%]	W05 [min]
1	19.260	13135.437	252.504	49.8	54.0	0.67
2	21.788	13226.838	214.836	50.2	46.0	0.77
	Total	26362.274	467.340	100.0	100.0	

Figure S84. HPLC, racemic **3fa**

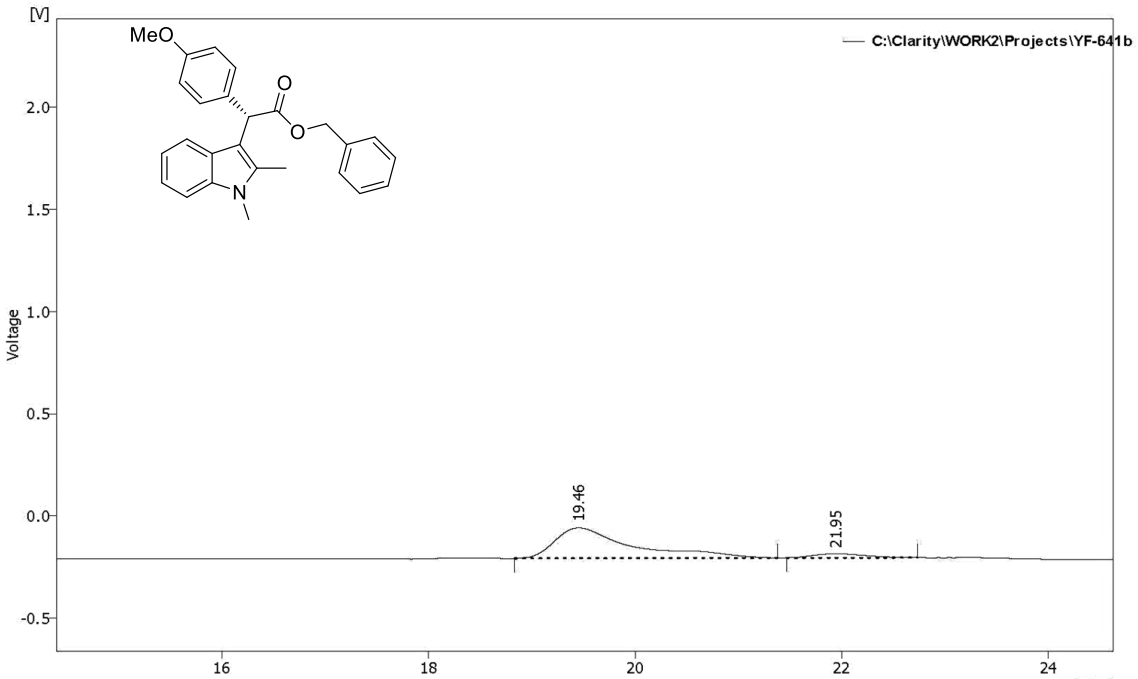

	Reten. Time [min]	Area [mV.s]	Height [mV]	Area [%]	Height [%]	W05 [min]
1	19.456	7749.139	148.959	91.8	88.3	0.66
2	21.948	690.497	19.679	8.2	11.7	0.57
	Total	8439.636	168.638	100.0	100.0	

Figure S85. HPLC, enantioenriched **3fa**

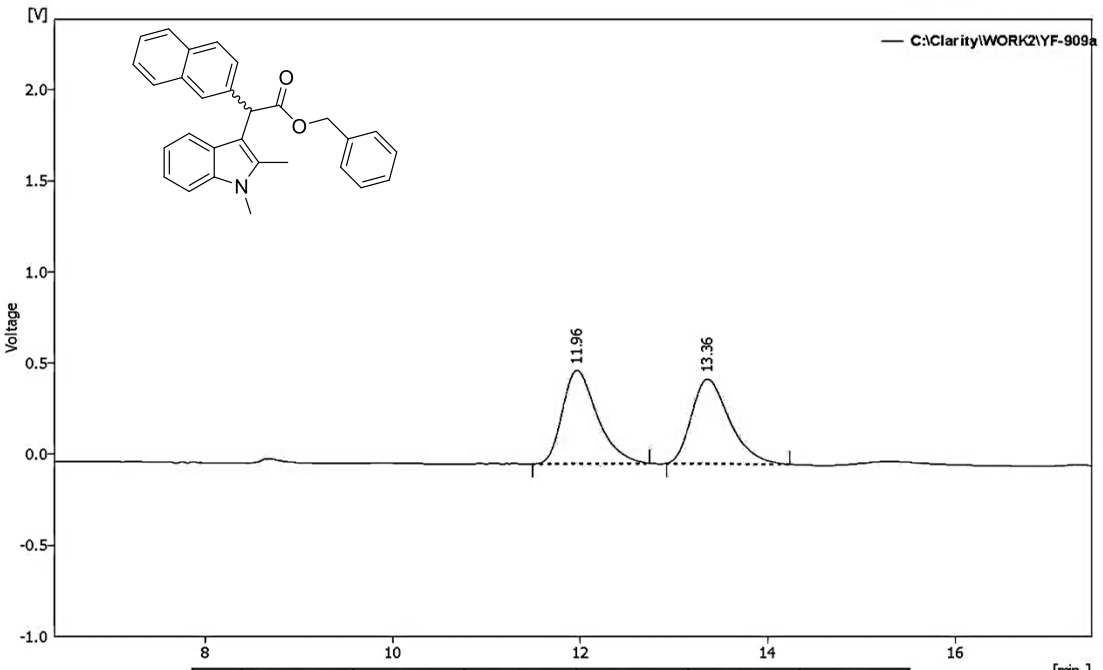

	Reten. Time [min]	Area [mV.s]	Height [mV]	Area [%]	Height [%]	W05 [min]
1	11.964	13212.446	511.847	50.2	52.5	0.40
2	13.356	13087.135	463.355	49.8	47.5	0.43
	Total	26299.581	975.202	100.0	100.0	

Figure S86. HPLC, racemic **3ga**

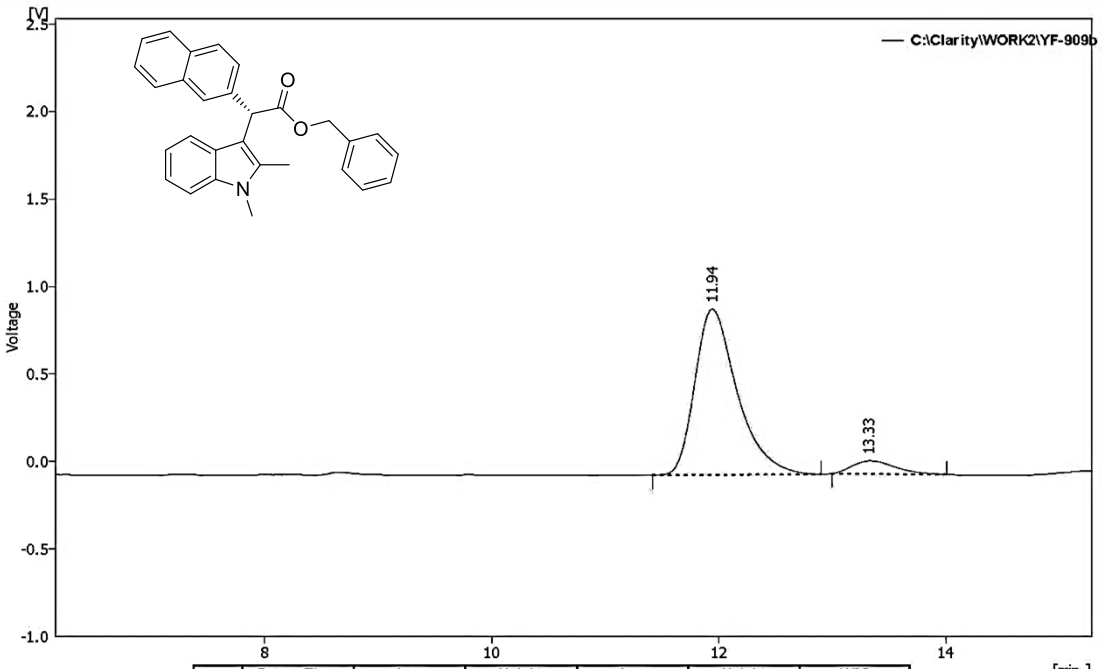

	Reten. Time [min]	Area [mV.s]	Height [mV]	Area [%]	Height [%]	W05 [min]
1	11.944	24537.494	948.099	92.6	92.7	0.39
2	13.328	1961.498	74.641	7.4	7.3	0.41
	Total	26498.992	1022.739	100.0	100.0	

Figure S87. HPLC, enantioenriched **3ga**

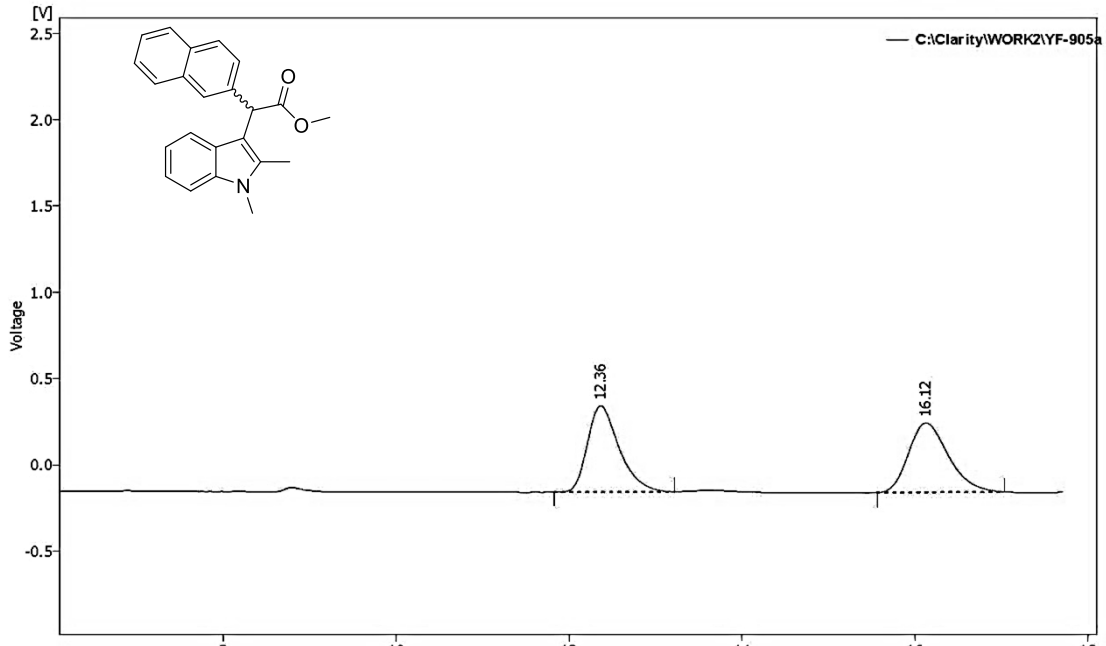

	Reten. Time [min]	Area [mV.s]	Height [mV]	Area [%]	Height [%]	W05 [min]
1	12.364	12733.371	499.552	49.7	55.4	0.39
2	16.124	12869.219	402.334	50.3	44.6	0.50
	Total	25602.589	901.886	100.0	100.0	

Figure S88. HPLC, racemic **3ha**

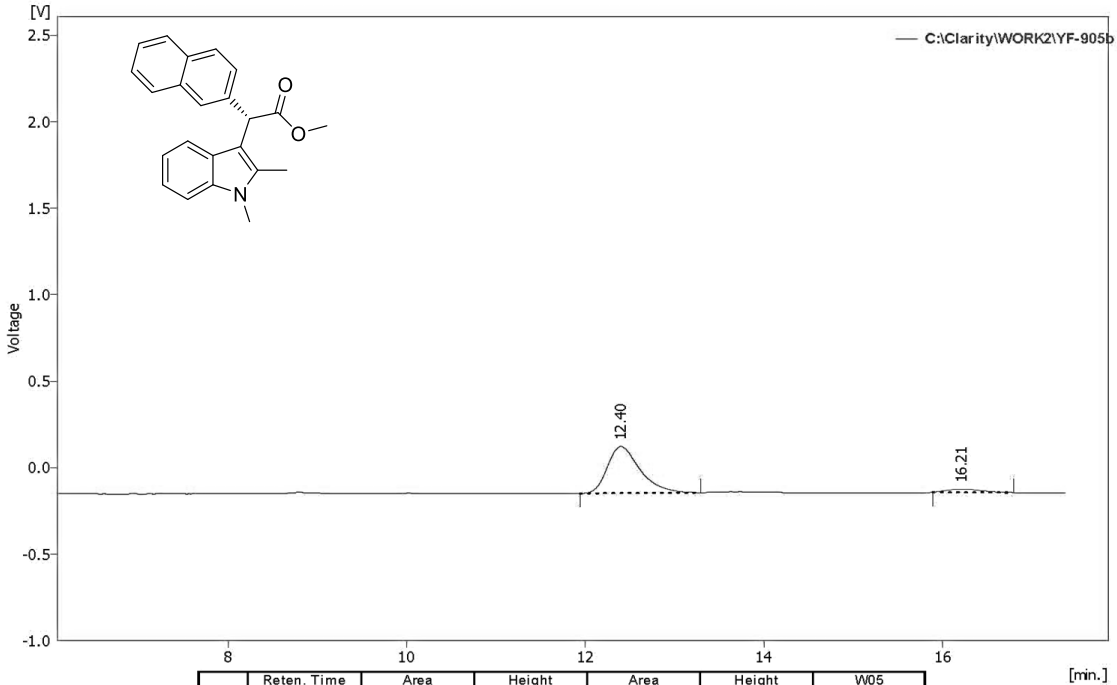

	Reten. Time [min]	Area [mV.s]	Height [mV]	Area [%]	Height [%]	W05 [min]
1	12.400	6853.300	269.982	93.0	93.3	0.38
2	16.212	516.362	19.302	7.0	6.7	0.44
	Total	7369.662	289.283	100.0	100.0	

Figure S89. HPLC, enantioenriched **3ha**

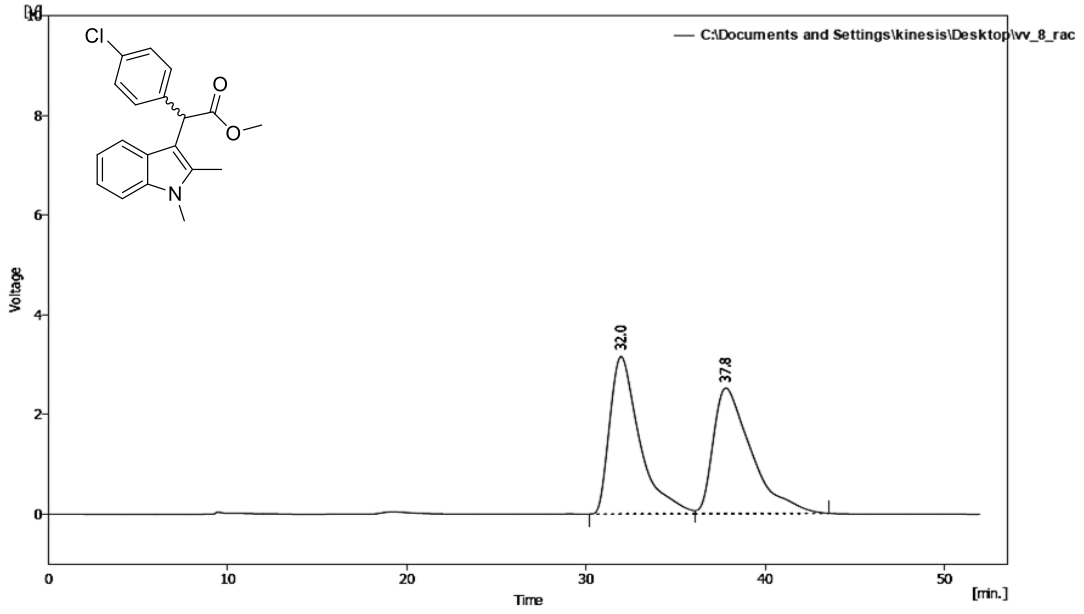

Result Table (Uncal - C:\Documents and Settings\kinesis\Desktop\vv_8_rac)

	Reten. Time [min]	Area [mV.s]	Height [mV]	Area [%]	Height [%]	W05 [min]
1	31.956	369121.147	3159.460	49.8	55.6	1.69
2	37.804	372442.473	2520.586	50.2	44.4	2.21
	Total	741563.620	5680.046	100.0	100.0	

Figure S90. HPLC, racemic **3ia**

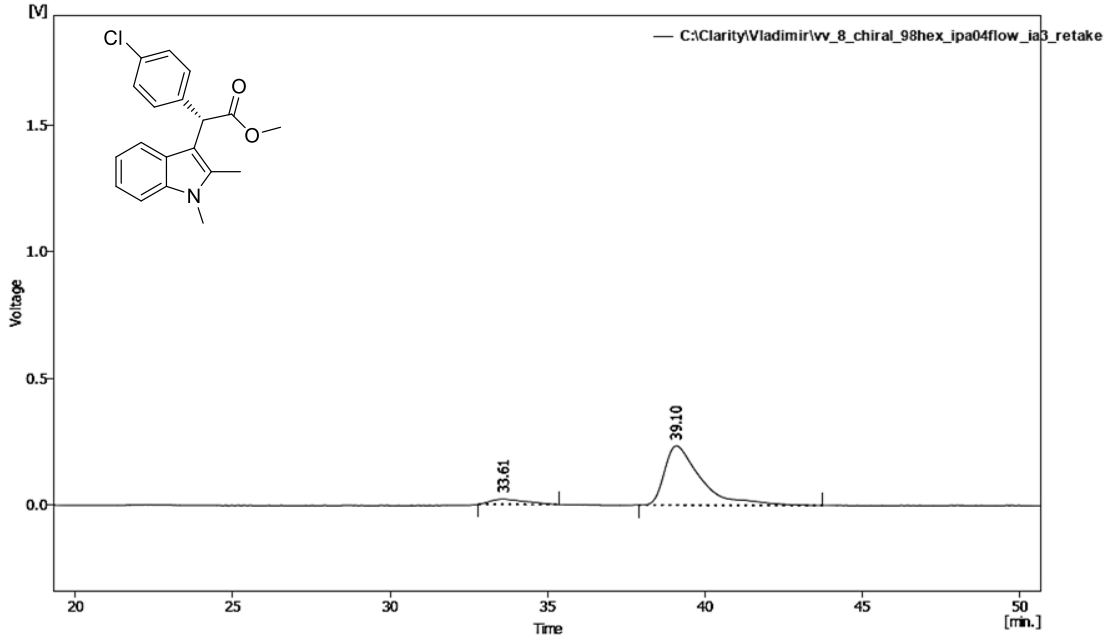

Result Table (Uncal - C:\Clarity\Vladimir\vv_8_chiral_98hex_ipa04flow_ia3_retake)

	Reten. Time [min]	Area [mV.s]	Height [mV]	Area [%]	Height [%]	W05 [min]
1	33.608	1548.404	20.142	7.6	7.9	1.27
2	39.104	18742.899	233.926	92.4	92.1	1.13
	Total	20291.303	254.068	100.0	100.0	

Figure S91. HPLC, enantioenriched **3ia**

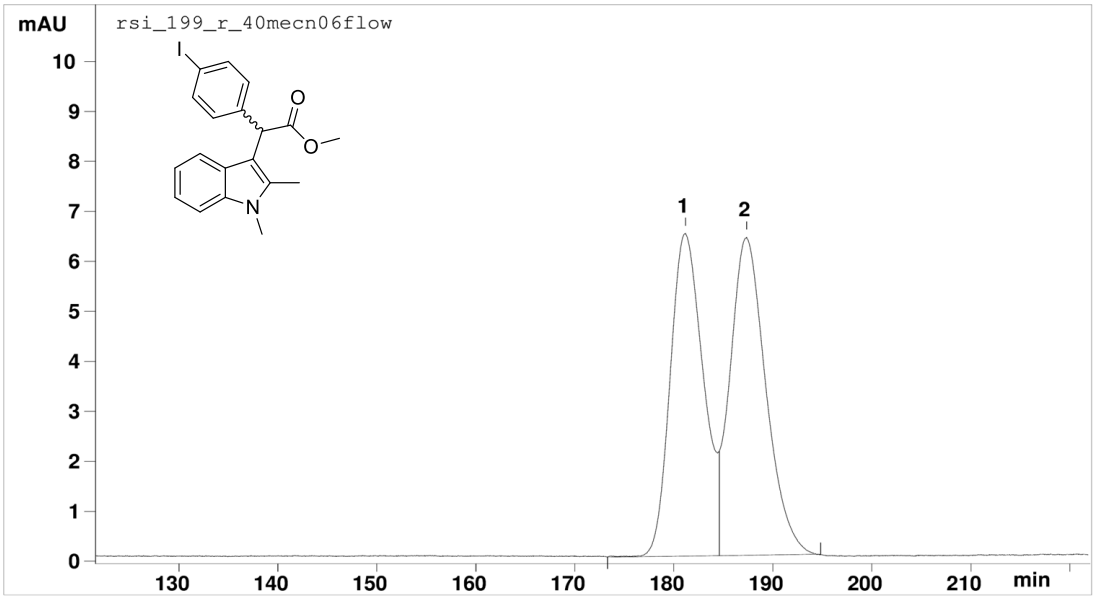

Quantitation method: Response normalization

Peak	Retention min	Area mAU*sec	Area %	Component
1	181.11	4875.858	48.54	
2	187.34	5170.119	51.46	
2	228.00	10045.978	100.00	

Figure S92. HPLC, racemic **3ka**

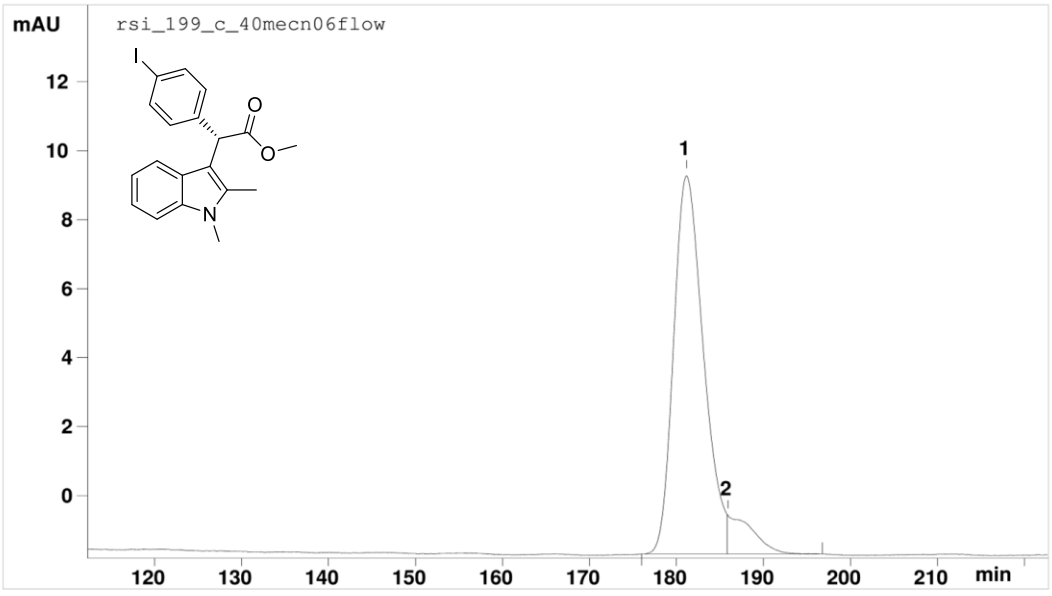

Quantitation method: Response normalization

Peak	Retention min	Area mAU*sec	Area %	Component
1	181.13	8316.250	93.37	
2	185.91	590.627	6.63	
2	228.00	8906.877	100.00	

Figure S93. HPLC, enantioenriched **3ka**

12. ESI-MS spectra

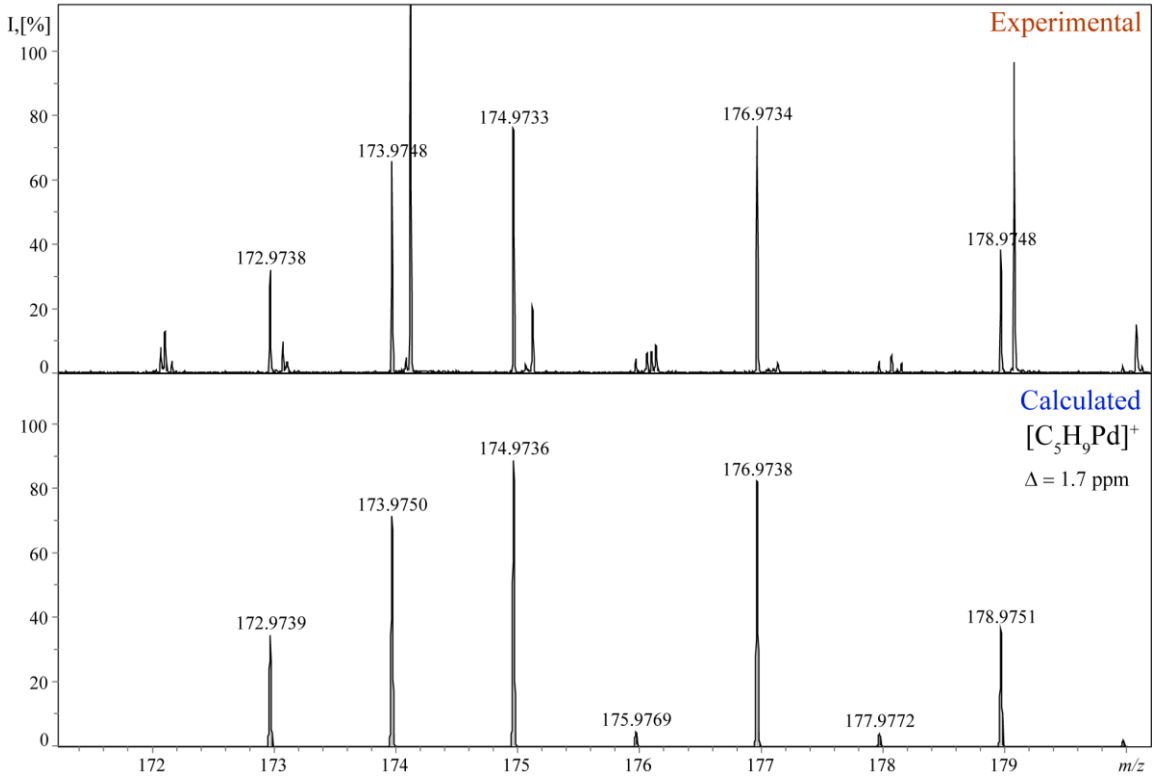

Figure S94. Experimentally detected and theoretical ESI-MS (+) spectrum of palladium complex Pd (C_5H_9) from the reaction mixture with ligand **7g** under online monitoring; experimental peak $[M]^+$=174.9733 Da, calculated for PdC_5H_9 = 174.9736 Da, Δ = 1.7 ppm.

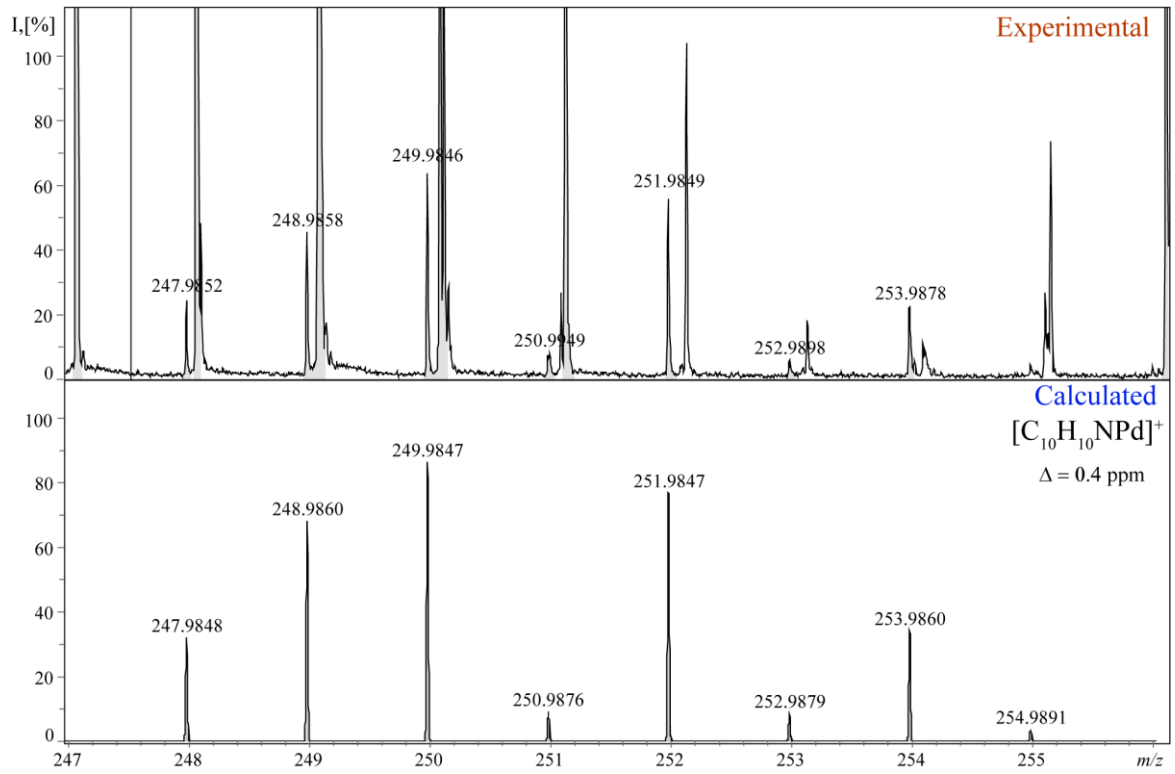

Figure S95. Experimentally detected and theoretical ESI-MS (+) spectrum of palladium complex Pd(2) from reaction mixture with ligand **7g** under online monitoring; experimental peak $[M]^+$=249.9846 Da, calculated for $PdC_{10}H_{10}N$ = 249.9847 Da, Δ = 0.4 ppm

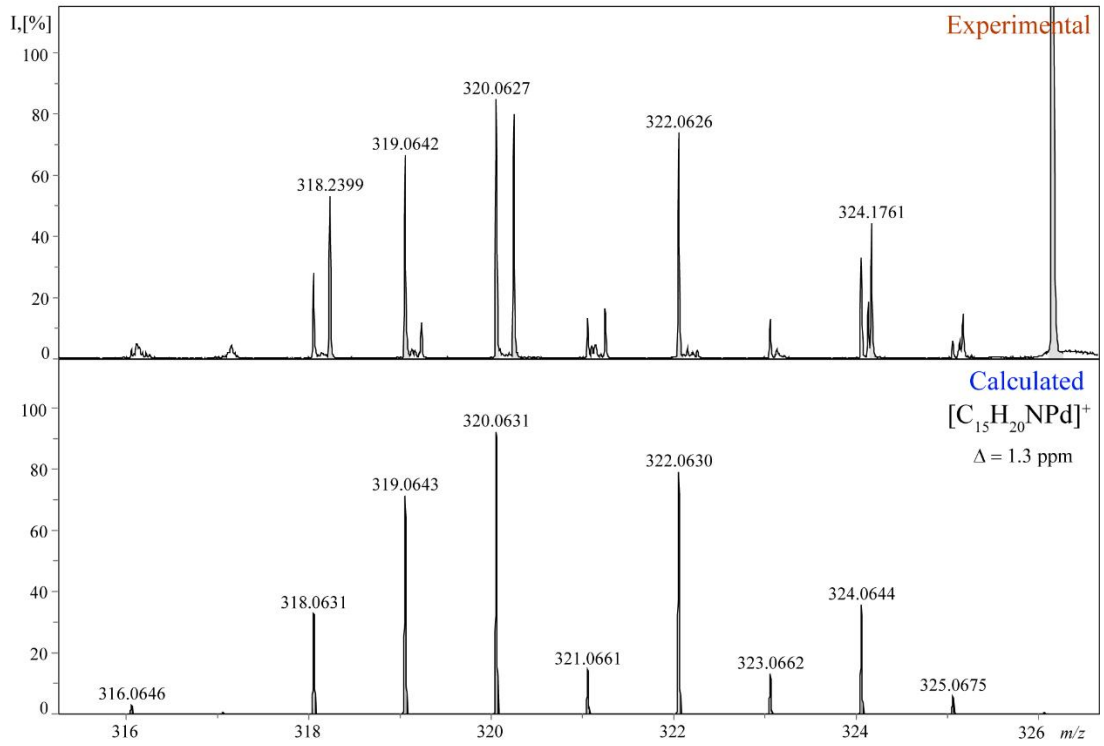

Figure S96. Experimentally detected and theoretical ESI-MS (+) spectrum of palladium complex Pd(**2**)C_5H_9+H from the reaction mixture with ligand **7g** under online monitoring; experimental peak $[M]^+$=320.0627 Da, calculated for $PdC_{15}H_{20}N$ = 320.0631 Da, Δ = 1.3 ppm.

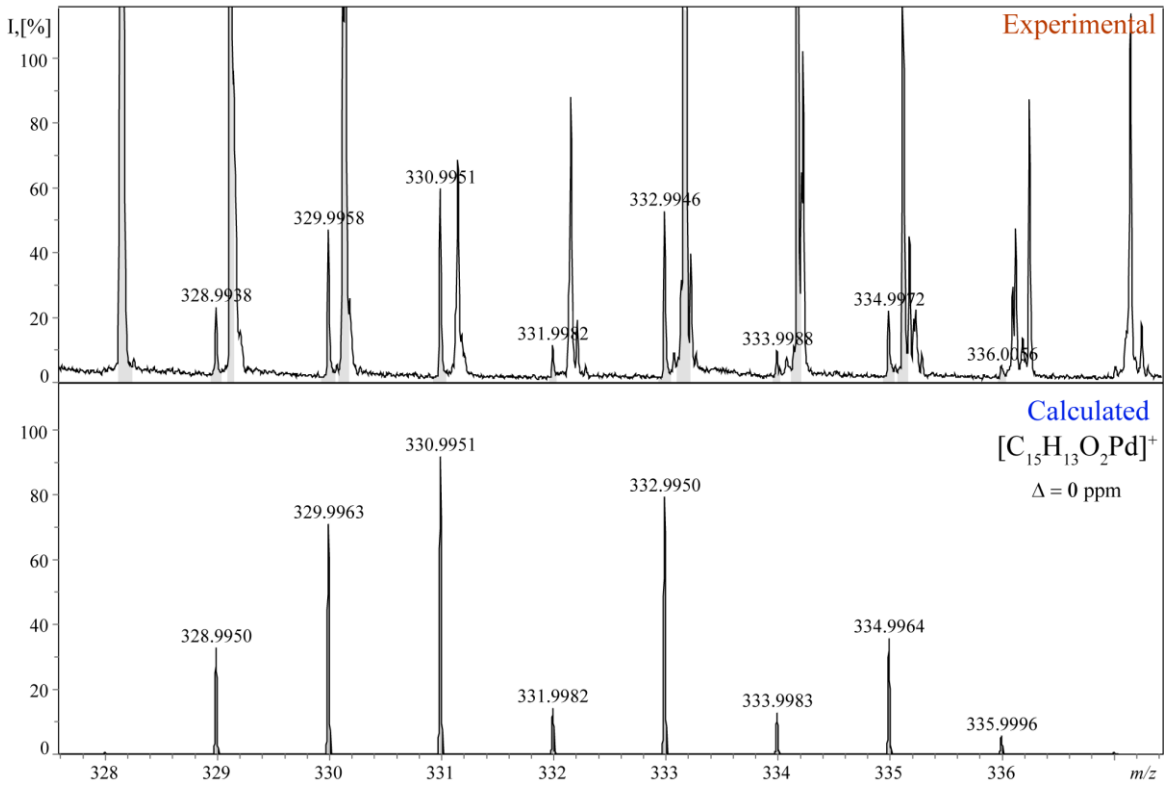

Figure S97. Experimentally detected and theoretical ESI-MS (+) spectrum of palladium complex Pd(**1**)+H from reaction mixture with ligand **7g** under online monitoring; experimental peak $[M]^+$=330.9951 Da, calculated for $PdC_{15}H_{13}O_2$ = 330.9951 Da, Δ = 0 ppm

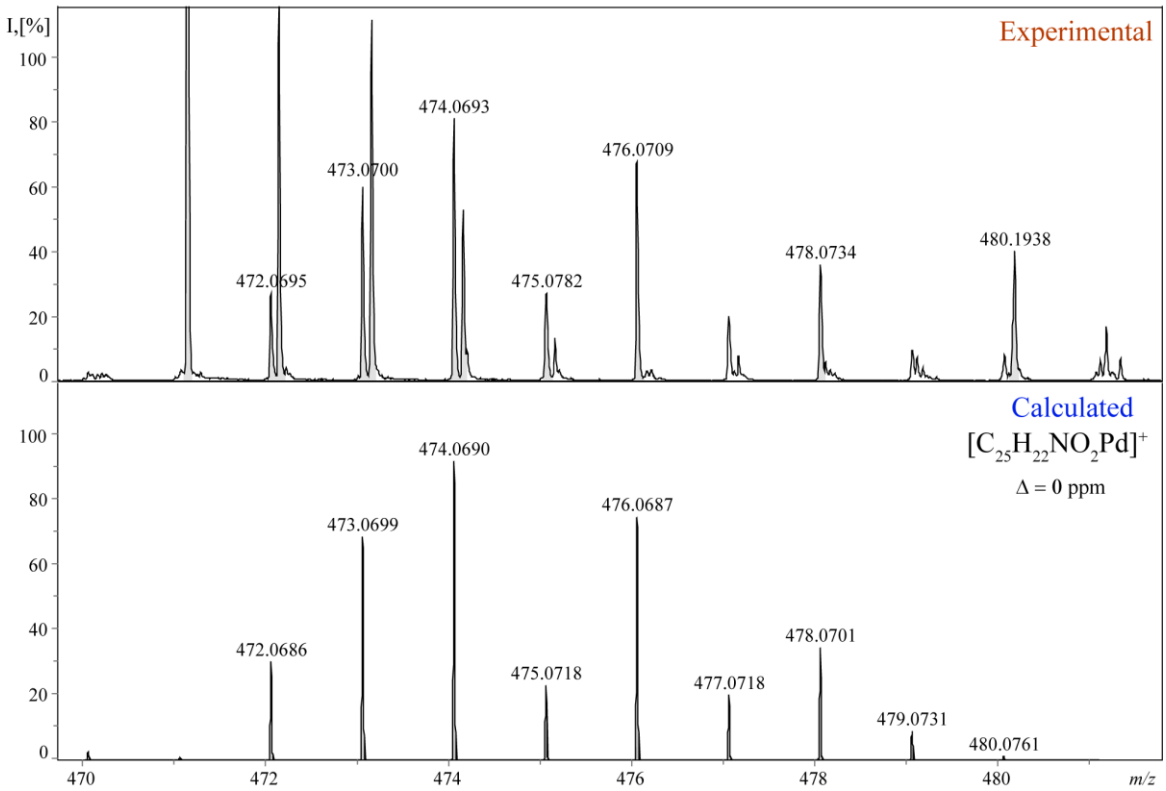

Figure S98. Experimentally detected and theoretical ESI-MS (+) spectrum of palladium complex Pd(3) from the reaction mixture with ligand **7g** under online monitoring; experimental peak $[M]^+$=474.0693 Da, calculated for $PdC_{25}H_{22}NO_2$ = 474.0690 Da, Δ = 0 ppm.

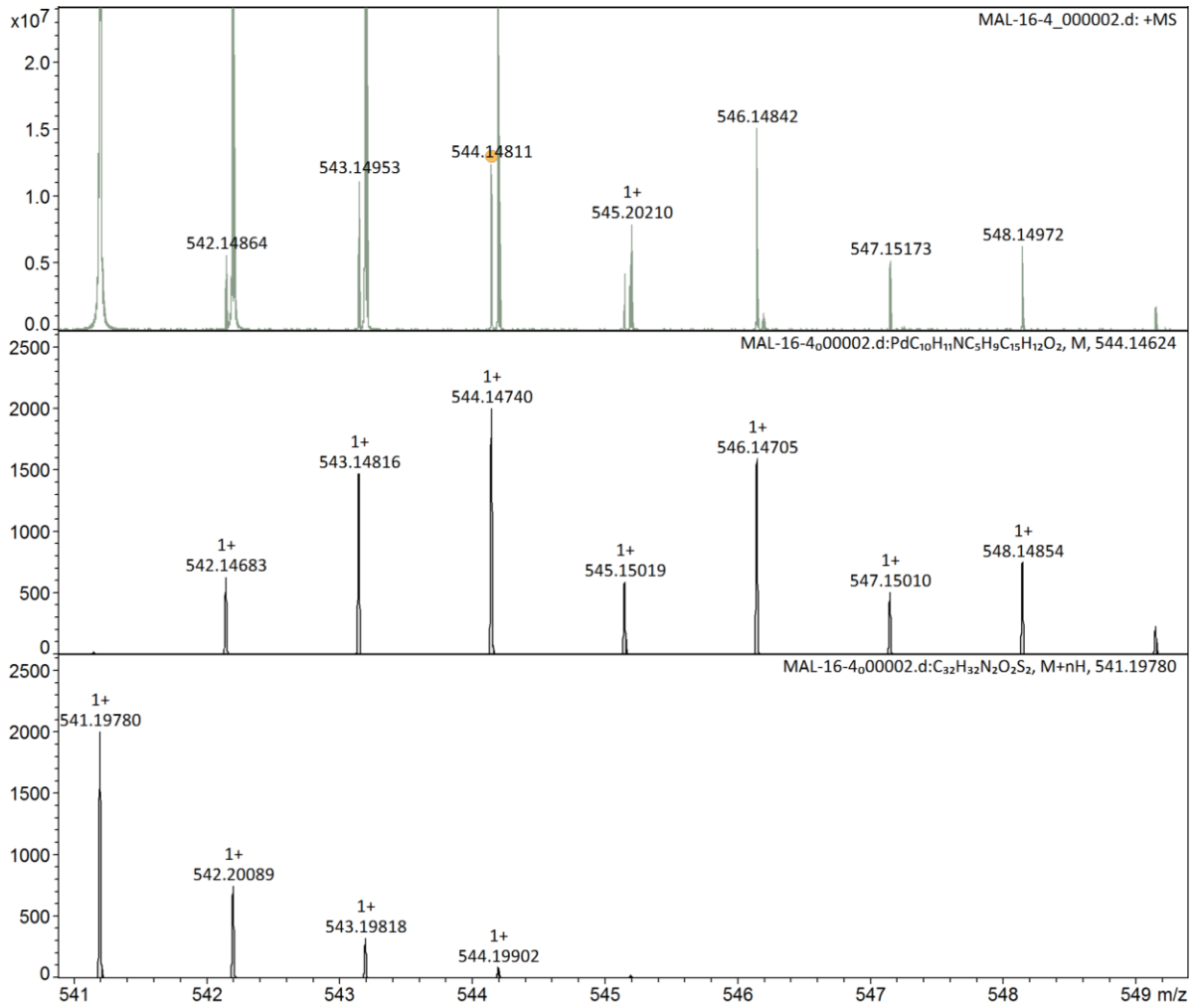

Figure S99. Experimentally detected and theoretical ESI-MS (+) spectrum of palladium complex Pd(**3**)(C_5H_9) from the reaction mixture under online monitoring; experimental peak $[M]^+$=544.14811 Da, calculated for $PdC_{30}H_{32}O_2N$= 544.14740 Da, Δ = 1.3 ppm. The main experimental peak corresponds to ligand $C_{32}H_{33}O_2N_2S_2$

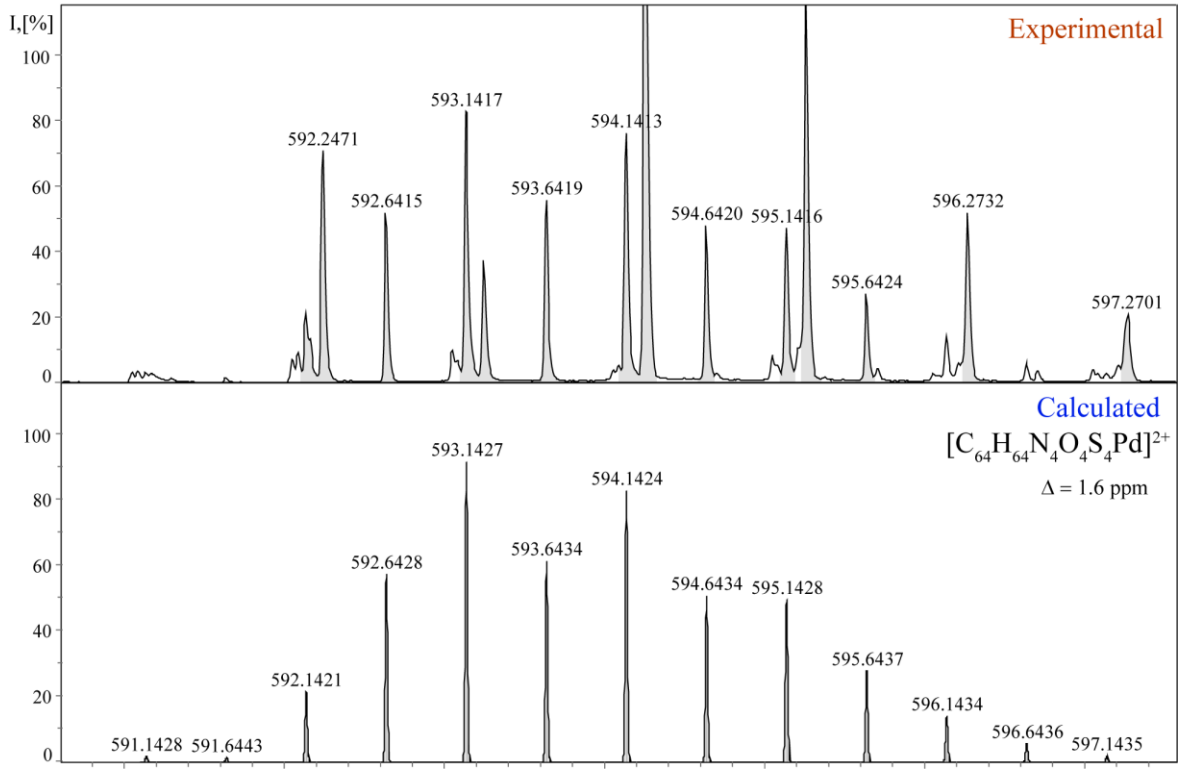

Figure S100. Experimentally detected and theoretical ESI-MS (+) spectrum of palladium complex Pd(**7g**)$_2$ from the reaction mixture with ligand **7g** under online monitoring; experimental peak $[M]^{2+}$=593.1417 Da, calculated for $PdC_{64}H_{64}N_4O_4S_4$ = 593.1427 Da, Δ = 1.6 ppm.

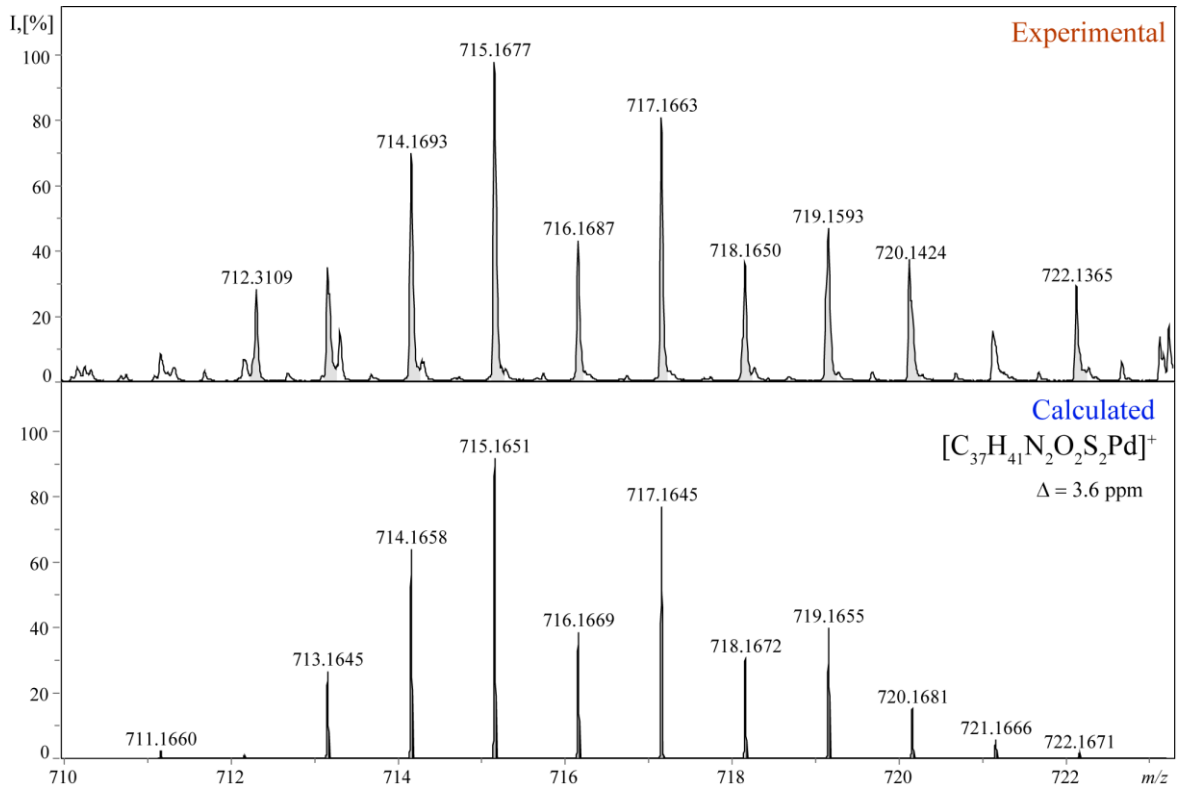

Figure S101. Experimentally detected and theoretical ESI-MS (+) spectrum of palladium complex Pd(**7g**)(C_5H_9) from the reaction mixture with ligand **7g** under online monitoring; experimental peak $[M]^+$ =715.1677 Da, calculated for $PdC_{37}H_{41}N_2O_2S_2$= 715.1677 Da, Δ = 3.6 ppm.

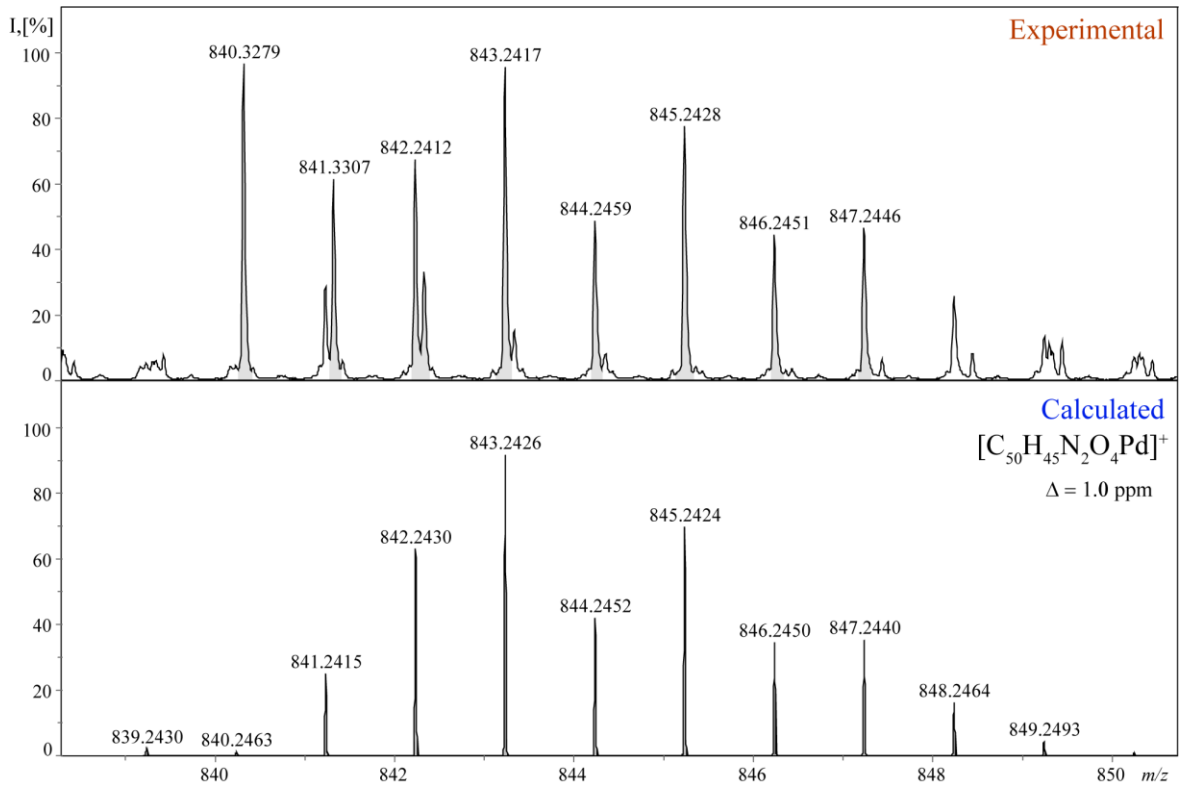

Figure S102. Experimentally detected and theoretical ESI-MS (+) spectrum of palladium complex Pd(**3**)$_2$-H from the reaction mixture with ligand **7g** under online monitoring; experimental peak $[M]^+$ =843.2417 Da, calculated for $PdC_{50}H_{45}N_2O_4$= 843.2426 Da, Δ = 1.0 ppm.

References

S1. Liu, Y.; Yao, B.; Deng, C. L.; Tang, R. Y.; Zhang, X. G.; Li, J. H., Palladium-catalyzed selective heck-type diarylation of allylic esters with aryl halides involving a beta-OAc elimination process. *Org. Lett.* **2011,** *13* (5), 1126-9.

S2. Nemoto, K.; Tanaka, S.; Konno, M.; Onozawa, S.; Chiba, M.; Tanaka, Y.; Sasaki, Y.; Okubo, R.; Hattori, T., Me2AlCl-mediated carboxylation, ethoxycarbonylation, and carbamoylation of indoles. *Tetrahedron* **2016,** *72* (5), 734-745.

S3. Maier, A. F.; Tussing, S.; Schneider, T.; Florke, U.; Qu, Z. W.; Grimme, S.; Paradies, J., Frustrated Lewis Pair Catalyzed Dehydrogenative Oxidation of Indolines and Other Heterocycles. *Angew. Chem., Int. Ed.* **2016,** *55* (40), 12219-23.

S4. Ferrer, S.; Naughton, D. P.; Threadgill, M. D., 1H NMR studies on the reductively triggered release of heterocyclic and steroid drugs from 4,7-dioxoindole-3-methyl prodrugs. *Tetrahedron* **2003,** *59* (19), 3445-3454.

S5. Zhang, Y.; Yao, Y.; He, L.; Liu, Y.; Shi, L., Rhodium(II)/Chiral Phosphoric Acid-Cocatalyzed Enantioselective O-H Bond Insertion of α-Diazo Esters. *Adv. Synth. Catal.* **2017,** *359* (16), 2754-2761.

S6. Davis, O. A.; Croft, R. A.; Bull, J. A., Synthesis of diversely functionalised 2,2-disubstituted oxetanes: fragment motifs in new chemical space. *Chem. Commun.* **2015,** *51* (84), 15446-9.

S7. Gao, X.; Wu, B.; Huang, W. X.; Chen, M. W.; Zhou, Y. G., Enantioselective palladium-catalyzed C-H functionalization of indoles using an axially chiral 2,2'-bipyridine ligand. *Angew. Chem., Int. Ed.* **2015,** *54* (41), 11956-60.

S8. Gu, P.; Su, Y.; Wu, X. P.; Sun, J.; Liu, W.; Xue, P.; Li, R., Enantioselective preparation of cis-beta-azidocyclopropane esters by cyclopropanation of azido alkenes using a chiral dirhodium catalyst. *Org. Lett.* **2012,** *14* (9), 2246-9.

S9. Fukazawa, Y.; Vaganov, V. Y.; Shipilovskikh, S. A.; Rubtsov, A. E.; Malkov, A. V., Stereoselective Synthesis of Atropisomeric Bipyridine N,N'-Dioxides by Oxidative Coupling. *Organic letters* **2019,** *21* (12), 4798-4802.

S10. Jayaraman, A.; Misal Castro, L. C.; Fontaine, F.-G., Practical and Scalable Synthesis of Borylated Heterocycles Using Bench-Stable Precursors of Metal-Free Lewis Pair Catalysts. *Org. Process Res. Dev.* **2018,** *22* (11), 1489-1499.

S11. Rochette, E.; Desrosiers, V.; Soltani, Y.; Fontaine, F. G., Isodesmic C-H Borylation: Perspectives and Proof of Concept of Transfer Borylation Catalysis. *J. Am. Chem. Soc.* **2019,** *141* (31), 12305-12311.

S12. Iniesta, E.; Vidal-Ferran, A., Supramolecularly regulated copper-bisoxazoline catalysts for the efficient insertion of carbenoid species into hydroxyl bonds. *Chem. Commun.* **2020,** *56* (47), 6364-6367.

S13. Wu, L. P.; Suenaga, Y.; Kuroda-Sowa, T.; Maekawa, M.; Furuichi, K.; Munakata, M., Syntheses, structures and properties of palladium (II) complexes with photochromic 4-methoxyazobenzene. *Inorg. Chim. Acta* **1996,** *248* (2), 147-152.

S14. Li, N.; Zhu, W.-J.; Huang, J.-J.; Hao, X.-Q.; Gong, J.-F.; Song, M.-P., Chiral NCN Pincer Iridium(III) Complexes with Bis(imidazolinyl)phenyl Ligands: Synthesis and Application in Enantioselective C–H Functionalization of Indoles with α-Aryl-α-diazoacetates. *Organometallics* **2020,** *39* (12), 2222-2234.

S15. Gao, X.; Wu, B.; Yan, Z.; Zhou, Y. G., Copper-catalyzed enantioselective C-H functionalization of indoles with an axially chiral bipyridine ligand. *Organic & biomolecular chemistry* **2016,** *14* (35), 8237-40.

S16. Nag, E.; Gorantla, S.; Arumugam, S.; Kulkarni, A.; Mondal, K. C.; Roy, S., Tridentate Nickel(II)-Catalyzed Chemodivergent C-H Functionalization and Cyclopropanation: Regioselective and Diastereoselective Access to Substituted Aromatic Heterocycles. *Org. Lett.* **2020,** *22* (16), 6313-6318.

S17. Delgado-Rebollo, M.; Prieto, A.; Pérez, P. J., Catalytic Functionalization of Indoles by Copper-Mediated Carbene Transfer. *ChemCatChem* **2014,** *6* (7), 2047-2052.

S18. Dasgupta, A.; Babaahmadi, R.; Slater, B.; Yates, B. F.; Ariafard, A.; Melen, R. L., Borane-Catalyzed Stereoselective C–H Insertion, Cyclopropanation, and Ring-Opening Reactions. *Chem* **2020,** *6* (9), 2364-2381.

S19. Dolomanov, O. V.; Bourhis, L. J.; Gildea, R. J.; Howard, J. A. K.; Puschmann, H., OLEX2: a complete structure solution, refinement and analysis program. *J. Appl. Crystallogr.* **2009,** *42* (2), 339-341.

S20. Sheldrick, G., A short history of SHELX. *Acta Crystallogr., Sect. A: Found. Adv.* **2008,** *64* (1), 112-122.

21. Tao, J.; Perdew, J. P.; Staroverov, V. N.; Scuseria, G. E., Climbing the density functional ladder: nonempirical meta-generalized gradient approximation designed for molecules and solids. *Phys. Rev. Lett.* **2003,** *91* (14), 146401.

22. Weigend, F.; Ahlrichs, R., Balanced basis sets of split valence, triple zeta valence and quadruple zeta valence quality for H to Rn: Design and assessment of accuracy. *Phys. Chem. Chem. Phys.* **2005,** *7* (18), 3297-305.

S23. Andrae, D.; Häußermann, U.; Dolg, M.; Stoll, H.; Preuß, H., Energy-adjustedab initio pseudopotentials for the second and third row transition elements. *Theor. Chim. Acta* **1990,** *77* (2), 123-141.

S24. Grimme, S.; Ehrlich, S.; Goerigk, L., Effect of the damping function in dispersion corrected density functional theory. *J. Comput. Chem.* **2011,** *32* (7), 1456-65.

S25. Marenich, A. V.; Cramer, C. J.; Truhlar, D. G., Universal solvation model based on solute electron density and on a continuum model of the solvent defined by the bulk dielectric constant and atomic surface tensions. *J. Phys. Chem. B.* **2009,** *113* (18), 6378-96.

S26. Peverati, R.; Truhlar, D. G., M11-L: A Local Density Functional That Provides Improved Accuracy for Electronic Structure Calculations in Chemistry and Physics. *J. Phys. Chem. Lett.* **2011,** *3* (1), 117-124.

S27. Epifanovsky, E.; Gilbert, A. T. B.; Feng, X.; Lee, J.; Mao, Y.; Mardirossian, N.; Pokhilko, P.; White, A. F.; Coons, M. P.; Dempwolff, A. L.; Gan, Z.; Hait, D.; Horn, P. R.; Jacobson, L. D.; Kaliman, I.; Kussmann, J.; Lange, A. W.; Lao, K. U.; Levine, D. S.; Liu, J.; McKenzie, S. C.; Morrison, A. F.; Nanda, K. D.; Plasser, F.; Rehn, D. R.; Vidal, M. L.; You, Z. Q.; Zhu, Y.; Alam, B.; Albrecht, B. J.; Aldossary, A.; Alguire, E.; Andersen, J. H.; Athavale, V.; Barton, D.; Begam, K.; Behn, A.; Bellonzi, N.; Bernard, Y. A.; Berquist, E. J.; Burton, H. G. A.; Carreras, A.; Carter-Fenk, K.; Chakraborty, R.; Chien, A. D.; Closser, K. D.; Cofer-Shabica, V.; Dasgupta, S.; de Wergifosse, M.; Deng, J.; Diedenhofen, M.; Do, H.; Ehlert, S.; Fang, P. T.; Fatehi, S.; Feng, Q.; Friedhoff, T.; Gayvert, J.; Ge, Q.; Gidofalvi, G.; Goldey, M.; Gomes, J.; Gonzalez-Espinoza, C. E.; Gulania, S.; Gunina, A. O.; Hanson-Heine, M. W. D.; Harbach, P. H. P.; Hauser, A.; Herbst, M. F.; Hernandez Vera, M.; Hodecker, M.; Holden, Z. C.; Houck, S.; Huang, X.; Hui, K.; Huynh, B. C.; Ivanov, M.; Jasz, A.; Ji, H.; Jiang, H.; Kaduk, B.; Kahler, S.; Khistyaev, K.; Kim, J.; Kis, G.; Klunzinger, P.; Koczor-Benda, Z.; Koh, J. H.; Kosenkov, D.; Koulias, L.; Kowalczyk, T.;

Krauter, C. M.; Kue, K.; Kunitsa, A.; Kus, T.; Ladjanszki, I.; Landau, A.; Lawler, K. V.; Lefrancois, D.; Lehtola, S.; Li, R. R.; Li, Y. P.; Liang, J.; Liebenthal, M.; Lin, H. H.; Lin, Y. S.; Liu, F.; Liu, K. Y.; Loipersberger, M.; Luenser, A.; Manjanath, A.; Manohar, P.; Mansoor, E.; Manzer, S. F.; Mao, S. P.; Marenich, A. V.; Markovich, T.; Mason, S.; Maurer, S. A.; McLaughlin, P. F.; Menger, M.; Mewes, J. M.; Mewes, S. A.; Morgante, P.; Mullinax, J. W.; Oosterbaan, K. J.; Paran, G.; Paul, A. C.; Paul, S. K.; Pavosevic, F.; Pei, Z.; Prager, S.; Proynov, E. I.; Rak, A.; Ramos-Cordoba, E.; Rana, B.; Rask, A. E.; Rettig, A.; Richard, R. M.; Rob, F.; Rossomme, E.; Scheele, T.; Scheurer, M.; Schneider, M.; Sergueev, N.; Sharada, S. M.; Skomorowski, W.; Small, D. W.; Stein, C. J.; Su, Y. C.; Sundstrom, E. J.; Tao, Z.; Thirman, J.; Tornai, G. J.; Tsuchimochi, T.; Tubman, N. M.; Veccham, S. P.; Vydrov, O.; Wenzel, J.; Witte, J.; Yamada, A.; Yao, K.; Yeganeh, S.; Yost, S. R.; Zech, A.; Zhang, I. Y.; Zhang, X.; Zhang, Y.; Zuev, D.; Aspuru-Guzik, A.; Bell, A. T.; Besley, N. A.; Bravaya, K. B.; Brooks, B. R.; Casanova, D.; Chai, J. D.; Coriani, S.; Cramer, C. J.; Cserey, G.; DePrince, A. E., 3rd; DiStasio, R. A., Jr.; Dreuw, A.; Dunietz, B. D.; Furlani, T. R.; Goddard, W. A., 3rd; Hammes-Schiffer, S.; Head-Gordon, T.; Hehre, W. J.; Hsu, C. P.; Jagau, T. C.; Jung, Y.; Klamt, A.; Kong, J.; Lambrecht, D. S.; Liang, W.; Mayhall, N. J.; McCurdy, C. W.; Neaton, J. B.; Ochsenfeld, C.; Parkhill, J. A.; Peverati, R.; Rassolov, V. A.; Shao, Y.; Slipchenko, L. V.; Stauch, T.; Steele, R. P.; Subotnik, J. E.; Thom, A. J. W.; Tkatchenko, A.; Truhlar, D. G.; Van Voorhis, T.; Wesolowski, T. A.; Whaley, K. B.; Woodcock, H. L., 3rd; Zimmerman, P. M.; Faraji, S.; Gill, P. M. W.; Head-Gordon, M.; Herbert, J. M.; Krylov, A. I., Software for the frontiers of quantum chemistry: An overview of developments in the Q-Chem 5 package. *The Journal of chemical physics* **2021,** *155* (8), 084801.